



HAL
open science

Computational approach for the diagnosis of mycetoma causative agents using histopathological microscopic images

Hyam Omar Abbass Ali

► **To cite this version:**

Hyam Omar Abbass Ali. Computational approach for the diagnosis of mycetoma causative agents using histopathological microscopic images. Medical Imaging. Université d'Orléans; University of Khartoum, 2023. English. NNT : 2023ORLE1006 . tel-04244540

HAL Id: tel-04244540

<https://theses.hal.science/tel-04244540>

Submitted on 16 Oct 2023

HAL is a multi-disciplinary open access archive for the deposit and dissemination of scientific research documents, whether they are published or not. The documents may come from teaching and research institutions in France or abroad, or from public or private research centers.

L'archive ouverte pluridisciplinaire **HAL**, est destinée au dépôt et à la diffusion de documents scientifiques de niveau recherche, publiés ou non, émanant des établissements d'enseignement et de recherche français ou étrangers, des laboratoires publics ou privés.

ÉCOLE DOCTORALE : Mathématiques, informatique, physique théorique et ingénierie
des systèmes (MITPIS):
Institut Denis Poisson, Université d'Orléans, Orléans, France.
UMR U1253, iBrain, INSERM, Université de Tours, Tours, France
Centre de Recherche sur le Mycétome (MRC), Université de Khartoum, Khartoum, Soudan

THÈSE EN COTUTELLE INTERNATIONALE présentée par :

Hyam OMAR ABBASS ALI

soutenue le : 14 Mars 2023

pour obtenir le grade de :

**Docteur de Université d'Orléans
et de l'Université de Khartoum**

Discipline/ Spécialité : Mathématiques

Computational Approach for the Diagnosis of Mycetoma Causative Agents Using Histopathological Microscopic Images

THÈSE dirigée par :

M. ABRAHAM Romain
M. TAUBER Clovis
M. FAHAL Ahmed

Professeur, Université d'Orléans
Maître de conférences (HDR), Université de Tours
Professeur, Université de Khartoum

RAPPORTEURS :

M. SPITERI Pierre
M. RODIN Vincent

Professeur, Université de Toulouse, IRIT
Professeur, Université de Bretagne Occidentale, STICC.

JURY :

Mme. DELON Julie
M. SPITERI Pierre
M. RODIN Vincent
M. ABRAHAM Romain
M. TAUBER Clovis
M. FAHAL Ahmed

Professeure, Université Paris-Cité, MAP5, Président du jury.
Professeur, Université de Toulouse, IRIT
Professeur, Université de Bretagne Occidentale, STICC.
Professeur, Université d'Orléans
Maître de conférences, Université de Tours
Professeur, Université de Khartoum

INVITES :

M. DESOUBEAUX Guillaume

Professeur, Université de Tours

Hyam OMAR ABBASS ALI

Méthodes d'Analyse d'Images Histopathologiques pour le Diagnostic Automatique du Mycétome

Résumé

Le mycétome est une maladie infectieuse chronique négligée dans les régions tropicales et subtropicales qui peut entraîner une invalidité grave. En considérant les agents responsables, le mycétome est classé en eumycétome (champignon) et actinomycétome (bactérie). La stratégie diagnostique repose sur la présentation clinique et l'identification des agents responsables du mycétome. L'identification précise des agents responsables est une priorité pour le diagnostic du mycétome. Les outils d'identification actuels comprennent les techniques moléculaires, la cytologie, l'histologie et la culture des grains qui est l'outil de référence. Les techniques moléculaires sont l'outil le plus fiable, mais il est coûteux et donc peu utilisé dans les zones endémiques, tandis que la culture est longue, difficile et nécessite un personnel expert. La cytologie et l'histologie sont des outils simples, rapides et bon marché. Cependant, la cytologie est loin d'être satisfaisante en termes de performances car elle a tendance à donner des résultats faussement positifs. Bien que l'histopathologie soit considérée comme l'outil optimal à utiliser dans les zones endémiques, elle nécessite un pathologiste expert pour une identification concluante qui fait défaut dans les zones rurales endémiques.

Avec l'avènement des approches numériques, des algorithmes automatisés d'analyse d'images peuvent être utilisés comme solution à ce problème. L'objectif principal de cette thèse est de développer une nouvelle méthode diagnostique de calcul pour le diagnostic du mycétome à l'aide d'images microscopiques histopathologiques. Premièrement, nous créons la première base de données d'images microscopiques de mycétomes. Cette contribution découle de la nécessité d'un ensemble de données pour le développement de modèles de calcul. Ensuite, nous présentons une nouvelle méthode de calcul pour discriminer semi-automatiquement les agents responsables du mycétome. La méthode est basée sur l'analyse radiomique de grains de mycétomes segmentés manuellement et l'analyse de discrimination des moindres carrés partiels (PLS-DA). Le modèle présenté peut jouer un rôle fondamental dans un centre clinique non spécialisé car il atteint une précision comparable à celle des pathologistes experts. Enfin, nous introduisons une méthode de segmentation automatisée pour les grains de mycétome. La méthode de segmentation est un modèle de type Convolution Neural Network (CNN) basé sur l'architecture U-net. Il permet l'automatisation et la rapidité des méthodes de discrimination. En conclusion, cette thèse présente à la fois une méthode automatisée de diagnostic des images microscopiques histopathologiques du mycétome et une méthode semi-automatisée de différenciation des grains de mycétome.

Mots-clés: Diagnostic du mycétome, Histopathologie numérique, Images microscopiques, Analyse d'images, Intelligence artificielle et Radiomique.

Computational Approach for the Diagnosis of Mycetoma Causative Agents Using Histopathological Microscopic Images

Abstract:

Mycetoma is a chronic, neglected infectious disease endemic in tropical and subtropical areas that may lead to severe disability. By considering the causative agents, mycetoma is classified into eumycetoma (fungus) and actinomycetoma (bacteria). The diagnosis strategy relies on the clinical presentation and the identification of mycetoma causative agents. Accurate identification of the causative agents is a priority for mycetoma diagnosis.

The current identification tools include molecular techniques, cytology, histology and grain culturing which is the gold standard tool. Molecular techniques are the most reliable tool, but it is expensive to be used in endemic areas, while culture is time-consuming, difficult and requires expert personnel. Cytology and histology are simple, rapid, and cheap tools. However, cytology is far from being satisfactory in terms of performance because it tends to give false positive results. Although histopathology is considered to be the optimal tool to be used in endemic areas, it requires expert pathologists for conclusive identification, which are lacking in endemic rural areas.

With the advent of digital pathology, automated image analysis algorithms can be used to solve this issue. The main aim of this thesis is to develop a novel computational diagnostic method for mycetoma diagnostic using histopathological microscopic images. Firstly, we create the first database for mycetoma microscopic images. This issue arises from the need for a dataset to develop a computation model. Then, we present a novel computation method to semi-automatically discriminate the mycetoma causative agents. The method is based on the radiomics analysis of manually segmented mycetoma grains and Partial Least Square-Discrimination Analysis (PLS-DA). The presented model can play a fundamental role in the non-specialised clinical centres because it reaches an accuracy comparable to expert pathologists. Lastly, we introduce an automated segmentation method for mycetoma grains. The segmentation method is Convolution Neural Network (CNN) model based on U-net architecture. It allows the full automation of the discrimination approach. In conclusion, this thesis presents both automated diagnostic methods for mycetoma histopathological microscopic images and semi-automated differentiate methods for mycetoma grains.

Keywords: Mycetoma diagnosis, Digital Histopathology, Microscopic Images, Image Analysis, Artificial Intelligence and Radiomics.



Résumé Substantiel

Le mycétome est une maladie tropicale négligée reconnue par l'OMS. Il s'agit d'un problème majeur de santé publique qui affecte fréquemment les jeunes adultes et les enfants des zones rurales reculées, provoquant des malformations, des handicaps et parfois la mort. Le mycétome est causé par certains types de bactéries ou de champignons, et est donc classé respectivement en actinomycétome et en eumycétome. L'identification de l'agent pathogène est un élément fondamental du diagnostic pour adapter le traitement.

La recherche sur le mycétome s'est principalement concentrée sur les aspects cliniques et de laboratoire de la maladie. Bien que l'identification moléculaire de l'agent causal du mycétome soit la plus précise, les méthodes de culture restent les techniques de référence dans le diagnostic en laboratoire du mycétome. La plupart des études diagnostiques ont été menées pour proposer de nouvelles techniques, alors que peu ont été menées pour améliorer les techniques existantes. Avec toutes les études, l'analyse informatisée des méthodes de diagnostic utilisées a pris du retard. Cela pourrait s'expliquer par le fait que le mycétome est une maladie négligée, sa prévalence est concentrée dans les régions peu développées et chez les personnes à faible statut socio-économique. En outre, la progression indolore et lente et la nature non contagieuse de cette maladie pourraient être une cause supplémentaire pour laquelle le mycétome ne reçoit pas beaucoup d'attention en termes de recherche sur le diagnostic assisté par ordinateur (CAD).

Pour suivre l'ère moderne de la CAD et, en même temps, faciliter le processus de diagnostic tout en conservant la technique la plus simple pouvant être utilisée dans les zones rurales endémiques, nous avons étudié la possibilité de proposer un modèle de diagnostic automatisé pour le mycétome. Étant donné que les techniques d'imagerie arrivent à la deuxième étape du diagnostic, nous explorons les techniques de laboratoire avec leurs avantages et leurs inconvénients et dans quelle mesure elles sont précieuses et utiles ou précises dans le diagnostic.

Cette thèse a porté sur l'analyse d'images microscopiques histopathologiques. Bien que l'histologie ne soit pas la méthode de référence pour le diagnostic, elle reste un outil optimal dans les environnements à ressources limitées et/ou les zones rurales.

L'automatisation de l'analyse histopathologique du mycétome pourrait affecter de manière significative le temps, le coût et la qualité du diagnostic.

Jusqu'en 2013, le mycétome avait été négligé pendant des années avant d'être inclus dans la liste des maladies tropicales négligées de l'OMS. Bien que cela attire l'attention des médias et des communautés scientifiques, cette reconnaissance est principalement limitée aux zones endémiques et au personnel intéressé par la médecine tropicale. C'est la raison pour laquelle [Chapitre 2](#) fournit un manuel d'informations générales et essentielles sur le mycétome, son diagnostic et sa prise en charge. En outre, il dresse l'état de l'art pour la recherche sur le mycétome et les lacunes dans les connaissances et la motivation pour proposer la méthode de calcul pour le diagnostic du mycétome.

Puisque nous sommes les pionniers d'une méthode automatisée pour le diagnostic du mycétome, dans [Chapitre 3](#), nous avons passé en revue les études CAD d'images histopathologiques. Les études examinées se concentrent sur les principales étapes impliquées dans le développement de méthodes d'histologie du mycétome, à savoir l'amélioration de l'image, la segmentation, les caractéristiques et la reconnaissance des formes. La partie la plus difficile consistait à étudier le choix d'une catégorie de caractéristiques appropriée qui pourrait être discriminante pour les images de tissus de mycétome. Les fonctionnalités de Radiomics semblent prometteuses car elles combinent plusieurs catégories dans trois grandes classes de fonctionnalités. Nous explorons également de manière approfondie les méthodes d'apprentissage automatique et de réseaux de neurones artificiels.

La création de la base de données sur les mycétomes était l'objectif principal du [Chapitre 4](#). Le chapitre a présenté la création de la première base de données d'images microscopiques histopathologiques de mycétomes, appelée MyData. Il a également fourni des informations détaillées sur les échantillons utilisés pour créer cette base de données. MyData constitue la première étape vers la proposition de méthodes de diagnostic automatisées utilisant certaines des méthodes et techniques passées en revue dans le chapitre précédent. En outre, cela pourrait être très bénéfique pour de nombreux chercheurs intéressés par l'étude de cette maladie négligée et l'amélioration des soins de santé. La base de données est collectée, préparée, analysée et étiquetée selon un protocole précis et adapté. Les échantillons de tissus ont été prélevés sur des patients confirmés atteints de mycétome vus et pris

en charge au Centre de recherche sur le mycétome (MRC), un centre collaborateur de l'OMS pour la recherche sur le mycétome. Les blocs de paraffine ont été préparés et envoyés à l'hôpital Bretonneau en France. Après une coupe uniforme et une procédure de coloration H&E, nous avons préparé les lames histopathologiques pour 142 patients. Plusieurs lames histopathologiques contenant des grains différents ont été préparées pour chaque patient, avec une moyenne de six grains par patient. Parce que les grains sont la caractéristique unique de l'infection par le mycétome, il était nécessaire de segmenter manuellement les grains (ROI) pour chaque lame histopathologique.

La base de données était composée de 864 images microscopiques de grains de mycétomes avec leur grain segmenté (vérité terrain). Il comprend 80 échantillons d'eumycétomes et 62 d'actinomycétomes et couvre quatre des cinq espèces de mycétomes les plus courantes signalées dans le monde. MyData est acquis avec un protocole d'acquisition reproductible homogène et unique. Pour cette raison, nous pensons que cette base de données est la première étape vers la création d'une base de données de plus en plus large avec diverses espèces du monde entier, d'autant plus qu'un protocole de préparation et d'acquisition spécifique est fourni.

Bien que la base de données comprenne 142 patients de la MRC avec les deux types de mycétomes, elle ne comprend pas toutes les espèces de mycétomes. Actuellement, il existe plus de 80 espèces causales différentes avec une répartition géographique inégale. Les patients du CRM sont soit soudanais, soit originaires des pays voisins où *Madurella mycetomatis*, *Actinomadura madurae*, *Streptomyces somaliensis* et *Actinomadura pelletierii* sont les espèces les plus courantes. Par conséquent, notre base de données s'est concentrée sur ces espèces pour les actinomycétomes ainsi que sur le genre *Madurella* en général et *Madurella mycetomatis* en particulier. pour eumycétome.

Selon les agents responsables du mycétome, quelle que soit l'espèce, le traitement nécessite l'administration prolongée d'antifongiques ou d'antibiotiques. Cette phase de traitement reste éprouvante, difficile et décevante. Par conséquent, l'identification des agents responsables du mycétome joue un rôle important dans le processus de traitement. Une identification incorrecte peut sérieusement affecter les patients ainsi que le pronostic et l'issue de la maladie. En conséquence, [Chapitre 5](#) est principalement concentré sur la proposition d'un modèle de classification des

eumycétomes et des actinomycétomes correctement appelés cétome m *AI* . Nous avons cherché à diminuer ou à éliminer toutes les sources qui pourraient affecter la précision. Comme nous ne savions pas comment l'auto-segmentation ou la variation dans la préparation des échantillons pouvait avoir un impact sur le modèle, nous avons introduit un modèle qui a été formé et validé à l'aide de la base de données de mycétomes avec les grains segmentés manuellement. Le modèle formé a obtenu des résultats prometteurs avec une précision de 91,89 %, ce qui est comparable au résultat des pathologistes experts (92,8 %) lors de l'utilisation d'une analyse manuelle.

Même si le modèle de classification a montré des performances significatives, ces performances sont probablement limitées par les espèces de mycétomes qui étaient représentées dans la base de données et utilisées pour la formation du modèle. Pour cette raison, notre modèle identifiera probablement à tort toute autre espèce. Et il devrait mieux performer en Europe et en Afrique qu'en Amérique du Sud et en Asie. Ainsi, cette limitation devrait être étudiée avec soin dans les études futures compte tenu de la répartition géographique des autres espèces.

L'un des objectifs de ce travail était de fournir un ensemble de caractéristiques quantitatives décrivant les deux types de mycétomes et d'essayer de les corrélérer avec les caractéristiques qualitatives utilisées par les pathologistes. Nous explorons les trois principaux groupes de caractéristiques utilisées par les pathologistes pour diagnostiquer le mycétome : la forme, la couleur et la texture des grains. Par conséquent, 102 caractéristiques radiomiques ont été étudiées et examinées pour leur capacité de discrimination dans la classification de type mycétome. Cela a montré que les caractéristiques de forme n'étaient pas pertinentes pour les tâches de discrimination, tandis que les caractéristiques de texture étaient importantes.

Les résultats prometteurs du modèle de classification ainsi que le fait que la segmentation manuelle des grains de mycétome nécessitait du temps et de l'expérience, nous ont incités à proposer une méthode automatique pour segmenter les grains à partir de coupes de tissus et à la combiner avec notre modèle de classification. [Chapitre 6](#) présenté un réseau CNN inspiré de l'architecture Unet pour automatiser la segmentation des grains. Selon nos expériences et nos résultats, le cadre proposé, GrUnet, démontre des performances significatives sur les images microscopiques d'histopathologie du mycétome, conduisant à une précision de 93,8 % sur la tâche de segmentation et un coefficient de Dice de 0,7843.

Nous avons intégré les modèles de classification et de segmentation pour automatiser entièrement le processus de diagnostic de manière à ce que l'utilisateur n'ait qu'à fournir l'image sans effectuer la segmentation manuelle. La précision de la classification était de 88 % et de 90,8 % pour l'identification automatisée et manuelle des grains. Avec les grains segmentés automatisés, les performances du modèle ont légèrement diminué mais restent proches de celles avec les grains segmentés manuellement. Nous pensons que cela se produit parce que le modèle de segmentation détecte de faux grains et les attribue au modèle de classification pour la différenciation.

Nous avons développé un outil qui offre une méthode de diagnostic différentiel semi-automatisé pour le mycétome. Il peut être utilisé à la fois pour la segmentation manuelle et la classification. Nous pensons que cet outil est plus fiable pour une version que les modèles combinés. En effet, ce modèle combiné peut faussement segmenter d'autres composants en tant que grains conduisant à un diagnostic incorrect, tandis que l'outil guide le diagnostic différentiel des cas confirmés de mycétome.

Perspective future

1. Base de données sur les mycétomes

Cette thèse vise à proposer une méthode de diagnostic automatisé du mycétome utilisable à l'échelle mondiale (car le fardeau global est inconnu) et en particulier dans les zones d'endémie. Cependant, la base de données construite dans ce travail est attribuée aux espèces de mycétomes du Soudan et d'autres régions géographiques avec une distribution similaire. Comme mentionné, ce problème pourrait affecter la précision de nos modèles, de sorte que l'exposition du modèle à certaines espèces, qui n'étaient pas incluses dans l'ensemble de données, ne pourrait pas être correctement classée. Par conséquent, plus d'échantillons doivent être collectés pour élargir la base de données existante avec de nouvelles espèces et plus d'échantillons des espèces existantes. L'échantillon doit être prélevé dans différents pays et continents car la répartition géographique des espèces varie considérablement.

De plus, les images de vérité au sol des grains segmentés manuellement devaient être mises à jour et inclure tous les grains dans chaque image. Ensuite, la base de données

doit être modifiée en conséquence. Nous avons observé la nécessité de cette modification lors de l'évaluation du modèle de segmentation car l'inclusion de tous les grains dans la vérité terrain donne des résultats différents par rapport au grain unique.

2. Le modèle de segmentation

Le GrUnet a été formé à l'aide de la base de données sur les mycétomes avec un seul grain par image comme vérité terrain. Comme mentionné ci-dessus, l'évaluation a démontré des performances différentes sur les différents ensembles de données. Pour cette raison, nous pensons que le ré-entraînement du modèle avec la base de données mise à jour pourrait améliorer la capacité du modèle à segmenter les grains de mycétome. Une autre possibilité est de ré-entraîner le modèle avec les grains de mycétome prédits.

Pour développer davantage la méthode de diagnostic automatisé, le modèle de segmentation présenté doit être couplé à une technique de détection. En effet, nous avons observé une dégradation de la précision des modèles combinés qui est principalement attribuée à la détection et à la segmentation de faux grains. Ce problème est considéré comme une limitation de notre modèle de diagnostic automatisé. Pour surmonter cela, nous devons proposer un modèle de détection à utiliser pour la détection des grains de mycétome. Le modèle devrait être la première étape dans le pipeline de la méthode de diagnostic automatisé. À cette fin, un ensemble de données de faux grains est nécessaire pour développer et entraîner le modèle.

3. Le modèle de classification

La classification du genre et/ou de l'espèce des agents responsables peut être explorée. Actuellement, tous les patients atteints de mycétome reçoivent le même schéma thérapeutique antifongique ou antibactérien, quelle que soit l'espèce. Cependant, il existe une corrélation entre les résultats du traitement et l'identification des espèces. Pour cette raison, la classification au niveau de l'espèce pourrait aider au suivi et au pronostic.

Cette classification a été examinée dans le cadre du modèle radiomique proposé. Cependant, nous pensons que le nombre limité d'images pour ces classes affecte fortement les performances du modèle étendu. En conséquence, nous suggérons

d'augmenter le nombre d'images des différentes classes pour le modèle étendu dans les travaux à venir. En outre, une autre perspective est le développement d'un modèle de classement qui examine l'espèce d'agent causal.

De plus, une attention particulière doit être portée à la classification négative de *Madurella mycetomatis* et *Madurella mycetomatis*. Cette classe de classification présente un intérêt particulier car *Madurella mycetomatis* est l'organisme causal le plus courant dans le monde et son traitement est difficile et problématique. En outre, la plupart des patients touchés ne répondent pas au traitement médical seul et nécessitent une intervention chirurgicale. Il est intéressant de savoir que l'histopathologie seule ne peut pas faire cette classification et n'est possible que par des techniques moléculaires. Nous avons testé notre modèle de classification à cette fin, mais les performances n'étaient pas satisfaisantes. Par conséquent, nous examinons les transformées de diffusion en ondelettes. Le modèle a atteint une précision de classification de 71 %. Des échantillons supplémentaires pour *Madurella mycetomatis* négatif sont nécessaires pour conclure que cette précision est fiable. Nous pensons que notre échantillon négatif de *Madurella mycetomatis* pourrait contenir peu d'espèces d'eumycétomes par rapport aux 40 espèces réellement signalées. Par conséquent, davantage d'échantillons négatifs de *Madurella mycetomatis* doivent être collectés compte tenu de leur espèce.

Enfin, un modèle d'apprentissage profond devrait être envisagé après avoir élargi et modifié la base de données. Le modèle pourrait être capable d'effectuer toutes les tâches de segmentation et de classification des grains de mycétome à la fois.

Table of Contents

List of Figures	13
List of Tables	17
List of Abbreviation	18
Abstract	19
Résumé	20
Chapter 1: Introduction.....	22
1.1 Context and Challenges.....	23
1.2 Contributions.....	25
1.3 Thesis Outlines	26
Chapter 2: Mycetoma	28
2.1 Introduction	28
2.1.1 Historical Background.....	28
2.1.2 Overview.....	29
2.2 Mycetoma Diagnosis.....	32
2.2.1 Imaging techniques.....	33
2.2.2 Identification of causative organisms' techniques	34
2.3 Mycetoma Treatment and Management:	40
2.3.1 Why is mycetoma a public health dilemma and a unique neglected tropical disease?.....	41
2.4 Motivation.....	43
2.5 Conclusion	44
Chapter 3: Microscopic Image Analysis and Related Work.....	45
3.1 Computer-Aided Diagnostics Models.....	45
3.2 Microscopic Image enhancement.....	46
3.3 Segmentation.....	48
3.4 Microscopic Image Features	50
3.4.1 Features Extraction and Categories:.....	50
3.4.1.1 Radiomics Features.....	52
3.4.2 Feature Reduction:	53
3.5 Pattern Recognition.....	55
3.6 Machine Learning.....	59

3.6.1 Learning Strategies.....	60
3.6.2 Hyperparameters tuning	61
3.6.3 Popular machine-learning models	62
3.7 Artificial Neural Network.....	63
3.7.1 Feed Forward Network	65
3.7.2 Training Feed Forward Network	66
3.7.3 Convolution Neural Networks	68
3.8 Conclusion	70
Chapter 4: Database of Mycetoma Tissue Microscopic images-MyData	71
4.1 Rational behind the creation of the mycetoma database	71
4.2 The distribution of Mycetoma Causative Agents and Organisms.....	72
4.3 MyData Population.....	74
4.3.1 Sample collection and Selection criteria	74
4.3.2 Sample diagnosis	76
4.4 Histopathology and Slides Preparation	77
4.4.1 Sample Preparation and Processing.....	78
4.4.2 Tissue Slides Visualization	79
4.5 Preparation of Microscopic Images in MyData	80
4.5.1 Mycetoma Tissue Images Acquisition.....	82
4.5.2 Ground-truth Segmentation of Mycetoma Grains	85
4.6 MyData: Mycetoma Histology Microscopic Images Database.....	86
4.6.1 Images conditions.....	87
4.6.1.1 Technical and human errors:	87
4.6.1.2 Adequateness of samples for publishing database:	87
4.6.2 Exclusion and inclusion criteria of samples in MyData.....	88
4.6.3 Labelling	89
4.6.4 Secondary dataset.....	89
4.7 Conclusion	90
Chapter 5: Mycetoma Causative Agent Classification Model - mAlcetoma.....	92
5.1 mAlcetoma: The Proposed Framework.....	92
5.1.1 Overview of the proposed model.	92
5.1.2 Samples and Images Acquisition.....	93
5.1.3 Pre-processing and Features Extraction.....	94
5.2 Modelling and Analysis	95
5.2.1 Quantitative evaluation.	99

5.3 Experimental Results	101
5.3.1 Causative agents' classification	101
5.3.1.1 Causative organisms' classification	104
5.3.2 Radiomics features importance.	106
5.3.3 Robustness to segmentation errors.	110
5.3.4 Model Implementation and working with GUI.....	112
5.4 Discussion.....	113
5.5 Conclusion	116
Chapter 6: Mycetoma Grain Automatic Segmentation Model - GrUnet.....	117
6.1 Image segmentation with CNN state-of-the-art	117
6.2 GrUnet: The Proposed Framework	121
6.2.1 Dataset and pre-processing.....	121
6.2.2 The Proposed Network Architecture	121
6.2.3 Training.....	123
6.3 Experimental Results	126
6.3.1 Performance evaluation of GrUnet	126
6.3.2 Comparing GrUnet with other architectures.....	127
6.3.3 Models Integration	129
6.4 Discussion.....	130
6.5 Conclusion	134
Chapter 7: Conclusion and Future Work	135
7.1 Conclusion and Limitations	135
7.2 Future perspective	138
7.2.1 Mycetoma Database.....	138
7.2.2 The Segmentation Model.....	139
7.2.3 The Classification Model.....	139
References	142

List of Figures

Figure 1.1: Mycetoma Tissue Image showing mycetoma grains rounded by a red circle. 24

Figure 2.1: Disease Progression and clinical appearance over time. 30

Figure 2.2: Mycetoma lesions showing mass, discharging sinuses and grains. (A): Eumycetoma. (B): Actinomycetoma..... 30

Figure 2.3: Prevalence of Mycetoma [2]. 31

Figure 2.4: Some of mycetoma imaging techniques. (A): X-Ray of the leg shows a massive eumycetoma cavity. (B): MRI showing massive actinomycetoma affected soft tissues and bones..... 34

Figure 2.5: Grains collection techniques [22]. (A): FNA Cytology. (B): Surgical Biopsy. 34

Figure 2.6: Culture of *M. mycetomatis* after 3 weeks of incubation. 35

Figure 2.7: Histopathological appearance of mycetoma grains in H&E stain, magnified X10. (A): *M.mycetomatis*. (B): *S.somaliensis*. (C): *A. madurae*. (D): *A. pelletieri*..... 37

Figure 2.8: FNA of some mycetoma causative agents stained with H&E. (A): *M. mycetomatis*. (B): *A. pelletieri*. (C): *S. somaliensis*. 38

Figure 2.9: Mycetoma Diagnosis Flowchart. 39

Figure 3.1: CAD System of histopathological images. Continuous line represents CAD component while dot line represents the used algorithms. 46

Figure 3.2: Binary classification model example of the different types of generalization. The figure is adapted from <https://www.geeksforgeeks.org/underfitting-and-overfitting-in-machine-learning/> 61

Figure 3.3: Signal Neuron (Perceptron) Model. 64

Figure 3.4: Multiple Neurons (MLP) Model 65

Figure 3.5: Activation Functions. 66

Figure 3.6: back-propagation vs forward--propagation. 67

Figure 3.7: Convolution operation. (A): Padding an image convolved with a 2*2 kernel. (B): From left to right: stride of size 0, 1, and 2. The figures are adapted from

https://medium.com/analytics-vidhya/convolution-padding-stride-and-pooling-in-cnn-13dc1f3ada26	69
Figure 4.1: Prevalence of eumycetoma and actinomycetoma [121].	73
Figure 4.2: Histopathology Process.....	78
Figure 4.3: Optical Light Microscope.	80
Figure 4.4: Digital Light Microscope.....	82
Figure 4.5: Mycetoma Microscopic Images. (A): Single grain. (B): Multiple grains... ..	84
Figure 4.6: Mycetoma Microscopic Images and its annotated grain. (A): Eumycetoma with fractured grain. (B): Actinomycetoma grain.	86
Figure 4.7: Example of the images included in the database. (A): Large grain. (B): Folded grain. (C): Dissociation grain.....	88
Figure 5.1: Histology diagnosis system. (A): Classical clinical setting, (B): Proposed radiomics model.	93
Figure 5.2: Sample grains of Eumycetoma (left) and Actinomycetoma (right). (A, B): tissue sections stained with H&E; (C, D): manual segmentation of the grains.....	94
Figure 5.3: Classification Error of the PLSDA model.	99
Figure 5.4: (A): 3D projection of mycetoma validation data on the first three latent variables. (B): Class predictions on a primary validation set. (C): Class predictions on the secondary dataset.	102
Figure 5.5: Receiver Operating Characteristic curves (ROC) and threshold plots... ..	103
Figure 5.6: Samples predictions and confidence intervals on the validation dataset.	104
Figure 5.7: Genus's classification on the validation dataset.	106
Figure 5.8: VIP of grains features: Variable importance scores of the PLS-DA model for discriminating mycetoma. Black bars represent texture features, blue is the first-order features, and yellow is the shape features.	108
Figure 5.9: Diameter of the grains. The first and the second rows represent the grains that have the shortest and longest diameters, respectively. (A, C): actinomycetoma, and (B, D): eumycetoma.....	109
Figure 5.10: Grains which score greatest and smallest score for selected VIPs. Actinomycetoma grains (lowest score) are depicted in the top row and eumycetoma in	

the bottom row (highest score). (A, D): Difference variance, (B, E): Small dependence low-grey-level emphasis (peak feature), and (C, F): Grey-level variance.110

Figure 5.11: An example of the generated masks using erosion and dilation.111

Figure 5.12: Effect of segmentation accuracy on classification performance.112

Figure 5.13: Mycetoma classification tool.113

Figure 6.1: SegNet Architecture118

Figure 6.2: U-Net architecture [85].119

Figure 6.3: The tissue image and grain ground-truth annotation.121

Figure 6.4: Proposed GrUnet Architecture.....123

Figure 6.5: Training curves of GrUnet on mycetoma database.125

Figure 6.6: GrUnet Prediction. Images from left to right represent the tissue image, prediction, and ground truth.....127

Figure 6.7: Classical Unet training curve with mycetoma database.....128

Figure 6.8: Prediction of gaps inside the grains. From left to the right columns represent tissue image, prediction, and ground truth.128

Figure 6.8: Prediction of gaps inside the grains. From left to the right columns represent tissue image, prediction, and ground truth.....132

Figure 6.9: Prediction of small remnants grains. From left to the right columns represent tissue image, prediction, and ground truth.132

Figure 6.9: Prediction of small remnants grains. From left to the right columns represent tissue image, prediction, and ground truth.....133

Figure 6.10: Prediction of false positive grains. From left to the right columns represent tissue image, prediction, and ground truth.133

Figure 6.10: Prediction of false positive grains. From left to the right columns represent tissue image, prediction, and ground truth.....133

Figure 6.10: Prediction of false positive grains. From left to the right columns represent tissue image, prediction, and ground truth.....133

List of Tables

Table 2.1: Comparison of eumycetoma and actinomycetoma clinical presentation..	32
Table 3.1: Brief review of related work on microscopic tissue images.	56
Table 4.1: The demographic of the studied population.	75
Table 4.2: The distribution of study samples.	76
Table 4.3: Microscopic Acquisition Conditions.....	83
Table 4.4: Summary of images in MyData considering the mycetoma organisms....	84
Table 4.5: Distribution of the Secondary dataset.	90
Table 5.1: The Split of the mycetoma database into training and validation datasets with a 70%/30% proportion.....	98
Table 5.2: Estimated metrics for the model.	102
Table 5.3: Accuracy obtained for all genes/species on the validation dataset.	105
Table 6.1: Comparing different models conducted on the test dataset.	129
Table 6.2: Integrated Models. Results on the test and secondary datasets.....	130

List of Abbreviation

PLS-DA	Partial Least Square-Discrimination Analysis
CNN	Convolution Neural Network
MRC	The Mycetoma Research Centre
WHO	World Health Organization
CAD	Computer Aided Diagnosis
ROI	Region of Interest
EM	Eumycetoma
AM	Actinomycetoma
MM	<i>Madurella mycetomatis</i>
AMM	<i>Actinomadura madurae</i>
SS	<i>Streptomyces somaliensis</i>
AMP	<i>Actinomadura pelletierii</i>
Mspp	<i>Madurella spp.</i>
Aspp	<i>Aspergillus spp.</i>
Fspp	<i>Fusarium spp.</i>

Abstract

Mycetoma is a chronic, neglected infectious disease endemic in tropical and subtropical areas that may lead to severe disability. By considering the causative agents, mycetoma is classified into eumycetoma (fungus) and actinomycetoma (bacteria). The diagnosis strategy relies on the clinical presentation and the identification of mycetoma causative agents. Accurate identification of the causative agents is a priority for mycetoma diagnosis.

The current identification tools include molecular techniques, cytology, histology and grain culturing which is the gold standard tool. Molecular techniques are the most reliable tool, but it is expensive to be used in endemic areas, while culture is time-consuming, difficult and requires expert personnel. Cytology and histology are simple, rapid, and cheap tools. However, cytology is far from being satisfactory in terms of performance because it tends to give false positive results. Although histopathology is considered to be the optimal tool to be used in endemic areas, it requires expert pathologists for conclusive identification, which are lacking in endemic rural areas.

With the advent of digital pathology, automated image analysis algorithms can be used to solve this issue. The main aim of this thesis is to develop a novel computational diagnostic method for mycetoma diagnostic using histopathological microscopic images. Firstly, we create the first database for mycetoma microscopic images. This issue arises from the need for a dataset to develop a computation model. Then, we present a novel computation method to semi-automatically discriminate the mycetoma causative agents. The method is based on the radiomics analysis of manually segmented mycetoma grains and Partial Least Square-Discrimination Analysis (PLS-DA). The presented model can play a fundamental role in the non-specialised clinical centres because it reaches an accuracy comparable to expert pathologists. Lastly, we introduce an automated segmentation method for mycetoma grains. The segmentation method is Convolution Neural Network (CNN) model based on U-net architecture. It allows the full automation of the discrimination approach. In conclusion, this thesis presents both automated diagnostic methods for mycetoma histopathological microscopic images and semi-automated differentiate methods for mycetoma grains.

Keywords: Mycetoma diagnosis, Digital Histopathology, Microscopic Images, Image Analysis, Artificial Intelligence and Radiomics.

Résumé

Le mycétome est une maladie infectieuse chronique négligée dans les régions tropicales et subtropicales qui peut entraîner une invalidité grave. En considérant les agents responsables, le mycétome est classé en eumycétome (champignon) et actinomycétome (bactérie). La stratégie diagnostique repose sur la présentation clinique et l'identification des agents responsables du mycétome. L'identification précise des agents responsables est une priorité pour le diagnostic du mycétome.

Les outils d'identification actuels comprennent les techniques moléculaires, la cytologie, l'histologie et la culture des grains qui est l'outil de référence. Les techniques moléculaires sont l'outil le plus fiable, mais il est coûteux et donc peu utilisé dans les zones endémiques, tandis que la culture est longue, difficile et nécessite un personnel expert. La cytologie et l'histologie sont des outils simples, rapides et bon marché. Cependant, la cytologie est loin d'être satisfaisante en termes de performances car elle a tendance à donner des résultats faussement positifs. Bien que l'histopathologie soit considérée comme l'outil optimal à utiliser dans les zones endémiques, elle nécessite un pathologiste expert pour une identification concluante qui fait défaut dans les zones rurales endémiques.

Avec l'avènement des approches numériques, des algorithmes automatisés d'analyse d'images peuvent être utilisés comme solution à ce problème. L'objectif principal de cette thèse est de développer une nouvelle méthode diagnostique de calcul pour le diagnostic du mycétome à l'aide d'images microscopiques histopathologiques. Premièrement, nous créons la première base de données d'images microscopiques de mycétomes. Cette contribution découle de la nécessité d'un ensemble de données pour le développement de modèles de calcul. Ensuite, nous présentons une nouvelle méthode de calcul pour discriminer semi-automatiquement les agents responsables du mycétome. La méthode est basée sur l'analyse radiomique de grains de mycétomes segmentés manuellement et l'analyse de discrimination des moindres carrés partiels (PLS-DA). Le modèle présenté peut jouer un rôle fondamental dans un

centre clinique non spécialisé car il atteint une précision comparable à celle des pathologistes experts. Enfin, nous introduisons une méthode de segmentation automatisée pour les grains de mycétome. La méthode de segmentation est un modèle de type Convolution Neural Network (CNN) basé sur l'architecture U-net. Il permet l'automatisation et la rapidité des méthodes de discrimination. En conclusion, cette thèse présente à la fois une méthode automatisée de diagnostic des images microscopiques histopathologiques du mycétome et une méthode semi-automatisée de différenciation des grains de mycétome.

Mots-clés: Diagnostic du mycétome, Histopathologie numérique, Images microscopiques, Analyse d'images, Intelligence artificielle et Radiomique.

Chapter 1: Introduction

The Mycetoma Research Centre (MRC) was established in 1991 at the University of Khartoum, Soba University Hospital, Sudan. It is recognised as a world-leading centre in various aspects of mycetoma that aims to promote research and management and provide medical care for patients. MRC is a WHO (World Health Organisation) Collaborating Centre on Mycetoma.

Mycetoma is a WHO-recognised neglected tropical disease [1]. It is a destructive and devastating infection disease of two types, either bacterial (actinomycetoma) or fungus (eumycetoma) type [1–3] . Mycetoma mostly affects the poorest of the poor young adults in rural areas. The painless nature of mycetoma, as well as diagnostic challenges often leads to late diagnosis with severe infection. Therefore, the correct diagnosis of the causative agents' level is important as the treatment varies for eumycetoma and actinomycetoma [1, 3, 4].

MRC's visions revolved around changing the life quality of mycetoma patients through the continuous development of scientific knowledge and research as well as clinical skills. One of these visions focuses on the diagnostic aspects of mycetoma. MRC is heavily involved in innovating and developing new techniques and tools for effective diagnosis and better management outcomes. In this thesis this was achieved by creating a multi-disciplinary taskforce from various domains in the field. Hence, the presented work was carried out in a collaboration between four institutions:

- The laboratory iBrain, INSERM, University of Tours, Tours, France.
- Institute Denis Poisson (IDP), University of Orleans, Orleans, France.
- Department of Mycology and Tropical Medicine, Bretonneau Hospital, Tours, France.

To achieve one of the MRC's visions, the main objective of this work is to develop an automated diagnostic model for mycetoma from histopathological microscopic images. The histopathological technique is the most used diagnostic tool, and it requires well-

trained pathologists, and that lacks in most rural areas where mycetoma is endemic. This is why this technique was the main focus of the study.

One way to tackle this issue is to consider investigating a computational diagnostic model for mycetoma. However, mycetoma has been neglected for decades by public health authorities, professionals, and the scientific community. Hence, it has not received any attention regarding computational analysis and Computer Aided Diagnosis (CAD) techniques.

In this thesis, we developed a CAD system for mycetoma histopathological diagnosis. The expertise domains of each of the partners involved in this work contributes differently towards fulfilling the main objective of the thesis. MRC leads the work on the pathology of mycetoma and sample collection, while iBrain and IDP guide the computation components. The tropical medicine department was in charge of sample preparation. The area of expertise of iBrain is in medical imaging and developing new techniques for diagnosing various diseases. IDP research is mostly dedicated to mathematics, modelling and simulations.

1.1 Context and Challenges

Mycetoma had been neglected for years before being included in the WHO Neglected Tropical Diseases List in 2016. Since then, most studies have been conducted to propose new laboratory diagnostics techniques, while few have been undertaken to improve the existing techniques. With all these studies, computerised analysis of diagnostic methods has lagged.

Therefore, there are no methods for CAD in mycetoma, and this study will be the first of its kind. Pioneering such methods faced several obstacles and challenges.

Firstly, there is no available database of mycetoma microscopic images which can be utilized to develop and train CAD models. This was the most significant challenge encountered. For this reason, we considered creating a database from scratch, starting from collecting tissue biopsies until obtaining the tissue images. Mycetoma histological microscopic image is a photograph of mycetoma-infected tissue that contain grains

(the unique characteristic of mycetoma infection). As depicted in [Figure 1.1](#), the ROIs of mycetoma histology images are the grains. The ground-truth manual segmentation of ROIs was another challenge of our work. Handling this task was rigorous and time-consuming and required expertise.



Figure 1.1: Mycetoma Tissue Image showing mycetoma grains rounded by a red circle.

Another challenge is the classification of mycetoma grains into either of actinomycetoma or eumycetoma origin because the determination of the mycetoma type is crucial for treatment and prognosis. The classification is carried out by pathologists using a set of qualitative characteristics of the visual appearance of mycetoma grains. These characteristics have many overlapping, and the discrimination relies on the knowledge of expert pathologists.

A further challenge is locating mycetoma grains in the tissue sections since the infection can not be confirmed without their presence. Addressing this issue will not only guides the conclusive diagnosis but also further the automation of the diagnosis.

In conclusion, this work aims to introduce a computational model for mycetoma diagnosis from histopathological images. The proposed model is learned and trained on a set of grains images and their ground-truth annotation (manual or automatic segmentation). This set of images is acquired specifically for this study which suggests another objective to create a database of mycetoma microscopic images.

1.2 Contributions

Our contribution to this thesis was mostly oriented toward answering the questions asked by pathologists in analysing mycetoma histology slides. We start by screening for mycetoma grains in tissue slides and then investigate the qualitative features of the grains (if any). Finally, these features are used to classify mycetoma types. We summarize our contribution as follows:

- We built a database for mycetoma histopathological microscopic images. This database was obtained from patients with various mycetoma types, duration and clinical presentations. A primary dataset was handled with a unique reproducible acquisition protocol that eliminates any source of variability resulting from technical or laboratory problems.
- We provided the ground-truth segmentation for the announced database. Single grain was considered for segmentation in each field. As a result of this, we present a database of 864 tissue images along with their ROIs.
- An image-based computation approach based on radiomics and Partial Least Squares Discrimination Analysis (PLS-DA) to semi-automatically discriminate the causative agents of mycetoma was adopted. This approach reached an accuracy rate comparable to expert pathologists at the MRC.
- A broad set of quantitative features for mycetoma grains was introduced. Three groups of features namely, shape, intensity, and texture, were computed and investigated for their contribution to the classification task. This illustrates the importance of each feature as descriptive information for mycetoma grains.
- An exploratory analysis was proposed to assess the classification model against the segmentation errors.
- A new model for the automatic segmentation of grains in tissue images using a deep learning model that is based on the U-Net architecture. It can be easily integrated with the radiomics model without increasing computation requirements as it is trained and tested without GPU.

1.3 Thesis Outlines

The rest of this thesis is organized as follows:

Chapter 2: provides a general introduction to mycetoma as a medical and public health dilemma. We discuss the knowledge gaps of mycetoma and the challenges of diagnosis. The motivation for conducting this study is also explained.

Chapter 3: reviews CAD models and the design of automated diagnostic models. Since there is no related work to mycetoma regarding the computation models, we review state-of-art studies in microscopic image analysis.

Chapter 4: creates the mycetoma microscopic images database. We first draw up a general view of histopathological technique and fundamental steps to obtain the microscopic images, the main elements to create the database. Then, we present the original data set for mycetoma microscopic images. A comprehensive detail regarding the sample collection, selection criteria, preparation, and image acquisition protocol is given.

Chapter 5: presents the proposed radiomics model to discriminate between eumycetoma and actinomycetoma. Using the created database, we explain the PLS-DA model and the training process. Also, we discuss the role of the three main groups of radiomics features in mycetoma-type discrimination. Furthermore, experimental analysis on the precision of manual segmentation and accuracy of classification is provided.

Chapter 6: introduces our proposed neural network for mycetoma grains segmentation, to develop a fully automated diagnosis tool. The chapter begins by providing a review of segmentation methods using Convolution Neural Networks (CNNs) with particular details about Unet architecture as it is the base of the proposed network. We describe the architecture of our proposed model and the network training process based on manual segmentation annotation of tissue images. Also, we compare the performance of the radiomics model on both manually and automated segmented grains.

Chapter 7: concludes the thesis with a discussion of the proposed approaches, some of their limitations and suggestions as future work to further improve research on mycetoma image analysis and mycetoma diagnosis. We also outline some of the experiments that were conducted but needed more datasets and/or further experiments.

Chapter 2: Mycetoma

Summary

This chapter introduces the historical and medical issues involved in mycetoma. [Section 2.1](#), begins with a brief description of the mycetoma journey until it was listed as a WHO NTD, followed by clinical and epidemiological background. A detailed overview of mycetoma diagnosis is given in [Section 2.2](#). Mycetoma management is discussed in [Section 2.3](#). Finally, we state our motivation for conducting this work in [Section 2.4](#) and conclude in the last section.

2.1 Introduction

2.1.1 Historical Background

In 1842, the missionary John Gill reported the first clinical case of mycetoma in an Indian city named "Madurai" [5]. Vandyke Carter first described the fungus form of mycetoma in 1860; thus, he proposed the name "mycetoma", which is driven from the Greek terms "mykes" and "oma", which means fungus and tumour, respectively [6]. Mycetoma is also known as "Madura Foot", referring to the first reported case. Chalmers and Archibald from Sudan formally classified mycetoma into two main groups, fungal and bacterial mycetoma [7], after a suggestion made in 1913 to classify mycetoma cases by considering causative organisms [8].

Mycetoma was one of the most neglected tropical diseases until 2013 when global mycetoma experts and the Drugs Neglected Diseases Initiative (DNDi) established the Mycetoma Consortium [2, 3]. They made huge efforts to address mycetoma research priorities. The Ministry of Health, Sudan, then submitted a proposal to the WHO Executive Board to include mycetoma to the list of "top 17" WHO Neglected Tropical Diseases (NTDs). On 28th May 2016, WHO included mycetoma in the NTDs list [9], [10]. This global recognition attracts media attention and raises funding opportunities. The Mycetoma Research Centre (MRC) in Khartoum, Sudan, is recognised as a world leader in mycetoma management and research. It has contributed massively to the

international recognition of mycetoma. Currently, MRC is a WHO collaborating centre on Mycetoma.

2.1.2 Overview

Mycetoma is a badly neglected tropical disease. It is a chronic subcutaneous granulomatous and disabling inflammatory disease. It is classified into actinomycetoma and eumycetoma depending on the causative organisms, either bacteria or fungus, respectively. *Madurella mycetomatis* (*M.mycetomatis*) is the most common species causing eumycetoma, while *Streptomyces somaliensis* (*S. somaliensis*), *Actinomadura madurae* (*A. madurae*), *Actinomadura pelletieri* (*A. pelletieri*), and *Nocardia brasiliensis* (*N. brasiliensis*) are the common species for actinomycetoma [2].

While mycetoma transmission mode is still unknown [10], the literature suggests that causative organisms are present in the soil, thorns, or animal dung and can enter the subcutaneous tissue through minor trauma such as stepping on a thorn, sharp objects or open wound [3]. No person-to-person transmission is reported; however, other transmission modes are not exempted [11, 12]. After trauma, mycetoma infection starts with a formation of grains within multiple cavities presented clinically as nodules. The size of these nodules increases gradually, and they spread into the skin, deep tissues, and bone. Discharge of seropurulent, purulent, blood, and grains of different sizes, colours, and textures through the sinus is frequent. The mycetoma lesions usually discharge grains, which can be black, yellow, white, or red, and they are of different sizes and consistency. It has slow progress and course and can extend to different tissue planes leading to massive deformity and disability, [Figure 2.1](#).

Mycetoma can spread through the lymphatic system and infrequently through the bloodstream. Thus, secondary satellite lesions are usually seen. This is more often linked to actinomycetoma as bacteria spread faster than fungus, and the lesion is not well encapsulated [12, 13]. More tissue will be damaged as the disease progresses, and massive mutilating surgical excisions or amputation of the affected part may be the only available treatment.



Figure 2.1: Disease Progression and clinical appearance over time.

In summary, clinically, mycetoma is characterised by a triad of painless subcutaneous mass, multiple sinuses formation, and discharge grains containing colonies of the causative organism, as shown in [Figure 2.2](#). The clinical presentation and symptoms for both types of mycetoma (fungus or bacterial) are similar [10, 14–16], although there are more than 70 microorganisms responsible for mycetoma infection [2, 13]. However, mycetoma clinical presentation and treatment outcome might vary depending on disease duration, infection site, causative organisms, and the host immune system [17].

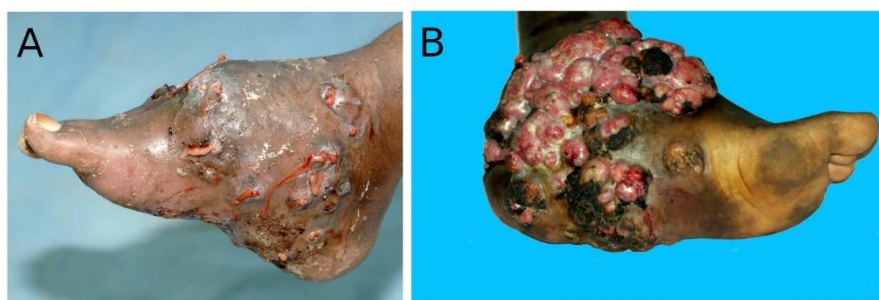


Figure 2.2: Mycetoma lesions showing mass, discharging sinuses and grains. (A): Eumycetoma. (B): Actinomycetoma.

Mycetoma has a worldwide distribution, although the global burden of the disease is still unknown. The infection is endemic in tropical and subtropical areas. These regions are characterised by a short rainy season and a long dry season [13]. The majority of mycetoma cases appear in the "Mycetoma belt" (Figure 2.3Error! Reference source not found.), stretching between the latitudes of 15° South and 30° North. The belt countries are Sudan, Somalia, Senegal, India, Yemen, Mexico, Venezuela, Colombia, Argentina and others [1, 14]. The highest prevalence was reported in Sudan, India, and Mexico. Sudan is the epicentre of mycetoma infection, with 355 new mycetoma cases/per year seen in the Mycetoma Research Centre (MRC), University of Khartoum, WHO Collaborating Centre on Mycetoma [13, 18, 19]. This number of cases is way less than the actual cases as it only counts the patients who managed to seek medical care at the MRC. Mycetoma was reported in temperate countries such as; the USA, Germany, Turkey, Philippines, Japan, Netherlands, and France [10, 12, 15, 20]. These cases are seen more often in immigrants who probably got infected in their homelands [12, 19]. This belief is guided by the fact that the actual incubation period is unknown, and it mostly takes from a few months up to 60 years for patients to seek medical consultation [12, 13, 18, 19].

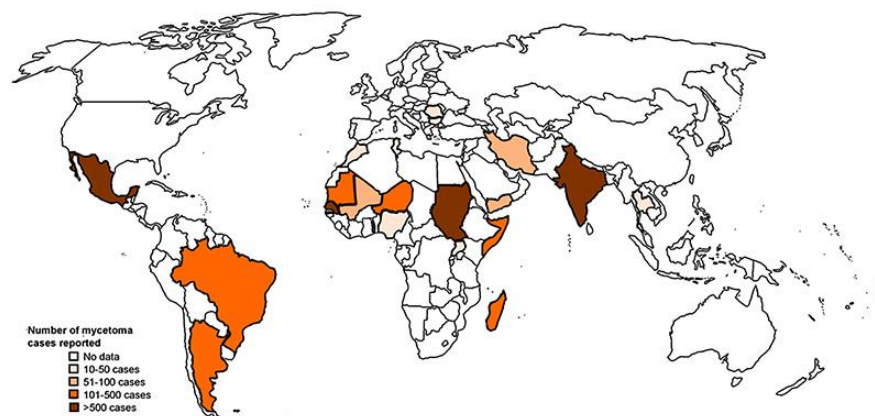


Figure 2.3: Prevalence of Mycetoma [2].

The most susceptible group to mycetoma infection is young adults, particularly males aged between 20 and 40 years in remote rural areas. Mycetoma largely affects field labourers, agriculturalists, and herdsmen [1, 8, 18]. The lower extremity and hands are the most frequently infected sites compared to the other body sites [2, 8, 14]. Women are less likely to be infected than men with a 1:3 ratio, and the explanation is not clear

[14, 18]. Genetic, immunological, and environmental factors might increase infection susceptibility [13, 15, 18]. The majority of mycetoma patients are of low-socioeconomic status with a scarcity of health education and facilities at their localities. So, they usually seek medical advice late when the disease is advanced and harder to treat. Besides the painless nature of the disease, these factors might lead to chronic deformity.

2.2 Mycetoma Diagnosis

An initial diagnosis of mycetoma in endemic areas is often made clinically through physical examinations [13, 15, 21]. Advanced cases of infection with the classical clinical triad can be easily diagnosed as mycetoma. However, an earlier disease stage with small lesions may be difficult to be distinguished from soft tissue tumours and other infectious diseases that mimic mycetoma because of the triad absence [3]. Confirmation of the infection as mycetoma alone is insufficient, and further investigations must be done to identify the causative agents and detect the spread of infection. These investigations are essential to plan the appropriate treatment strategy. Imaging and laboratory-based diagnostic tools are used to identify causative organisms and determine the extent of lesions, respectively. Usually, a combination of these tools is used to establish an accurate diagnosis.

The physicians approach the mycetoma diagnosis by examining a history of trauma located in an endemic area, the presence and number of sinuses, and the colour of grains if any. These findings hint to the clinician the infection type, whether it is fungus or bacterial. Depending on the laboratory test requested, a sample is collected from the suspected tissue for further analysis. [Table 2.1](#) summarises the major differences between eumycetoma and actinomycetoma [2, 22].

Table 2.1: Comparison of eumycetoma and actinomycetoma clinical presentation.

Feature	Eumycetoma	Actinomycetoma
Grain color	Black, pale, white, yellow	Yellow, red, pink, and white.

Grain size	Larger (0.5–2) μm	Smaller (20–100) μm
Grain texture	Coarse	Fine
Sinus (number; morphology)	Few sinuses; prominent	Many sinuses; flat
Progression	Slow	Fast
Geographic prevalence	Africa and India	South America and Asia

2.2.1 Imaging techniques

The disease extension into the different tissue planes and bones can be determined with imaging techniques. Furthermore, treatment and follow-up can be planned, and disease prognosis can be predicted [13, 15, 16, 21]. Several radiological imaging techniques are used for mycetoma diagnosis and including conventional X-ray, ultrasound, Computed Tomography (CT scan), and Magnetic Resonance Imaging (MRI) [14, 15, 21–25], [Figure 2.4](#).

Currently, the lesion ultrasound examination is the first option in the imaging diagnosis. It is accurate, non-invasive, rapid and can differentiate the two types of mycetoma and the mycetoma lesion from the non-mycetoma ones; however, it is operator dependent. CT scan can determine the bone affection accurately but not the soft tissue involvement. MRI is the technique of choice to determine the disease spread along the body planes, the treatment plans and the tissue outcome. MRI and CT are good techniques, but they are expensive and unavailable in low-resource settings.

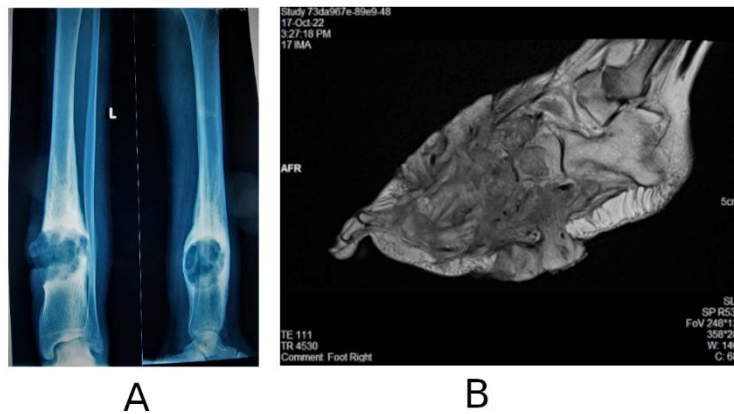


Figure 2.4: Some of mycetoma imaging techniques. (A): X-Ray of the leg shows a massive eumycetoma cavity. (B): MRI showing massive actinomycetoma affected soft tissues and bones.

2.2.2 Identification of causative organisms' techniques

Grains and tissue must be examined to determine the causative organisms. Grains are obtained either directly from the opened sinus by fine-needle aspiration technique or surgically by tru-cut needle biopsy or deep-seated biopsies (Figure 2.5). Surgical biopsies are mostly used as grains obtained from the opened sinuses are frequently contaminated and dead [13, 16, 21, 22].



Figure 2.5: Grains collection techniques [22]. (A): FNA Cytology. (B): Surgical Biopsy.

- **Grain culture and direct microscopy**

First, the grains are examined macroscopically for their size, colour, and consistency [13, 19, 22]. This can give a clue on the diagnosis but is not accurate, deceiving and indefinite [13, 14, 18, 21, 22]. Grains are crushed and mounted under a glass slide for direct microscopy examination. To provide a clear background, potassium hydroxide (10% KOH) is used; after then, grains are examined under a light microscope [21, 22]. The technique may differentiate between actinomycetes and fungi by their morphological characteristics, filament size, and pigment formation [5]. However, this method is not exclusive, and the use of an additional method is mandatory for conclusive diagnosis [16, 22].

In many centres, grains culture is a gold standard tool for identifying causative organisms. The mycetoma grains are washed several times with normal saline before plating them into the appropriate culture media in a sterilised environment. Antibiotic-free culture media are used for actinomycetes identification, while eumycetes are inoculated into media with antibiotics. The culture containers are incubated at 37°C for three weeks on average, [Figure 2.6](#). Causative agents and their species can be identified by the culture's microscopic appearance and morphology properties [22, 26, 27]. In many instances, misdiagnosis and difficulty in distinguishing the different microorganisms based on morphological features are frequent [21, 22, 27, 28]. In conclusion, grain culture is the core tool for organism identification, but it is time-consuming and requires expert microbiologists to obtain accurate results. Also, this method is vulnerable to false-positive results because of contamination.



Figure 2.6: Culture of *M. mycetomatis* after 3 weeks of incubation.

- **Molecular techniques**

The use of molecular techniques allows the accurate identification of mycetoma causative agents at the species level. DNA analysis is the key to this technique [3]. Most commonly, the amplification of genes or gene fragments followed by sequencing is used for mycetoma molecular diagnosis [29]. Molecular techniques have become increasingly attractive as they provide rapid and reliable results to improve treatment outcomes [12, 21, 22].

- **Histopathological Examination**

The histopathological examination of the surgical biopsies is useful for confirming the clinical diagnosis, but it remains ineffective for definitive species identification, particularly for eumycetoma species [12, 13, 21, 28]. Primarily Haematoxylin and Eosin (H&E) stain is used for the mycetoma diagnosis based on histology, while special stains are crucial for species differentiation and inconclusive identification of grains by H&E staining [13, 21, 22, 30]. The special staining includes Gram, Periodic acid–Schiff (PAS) stains and others.

Deep surgical or tru-cut biopsies are needed for the histopathological examination. They must contain grains to establish the diagnosis [22, 28]. Biopsies are fixed in a formalin solution and embedded in paraffin to prepare tissue blocks and histological sections. The process is described in more detail in [Chapter 4](#).

In mycetoma histopathological sections, the host tissue reactions and grains' morphological appearance are commonly seen [14, 16]. Each causative agent has a distinct histological appearance [8, 19]. The host tissue reactions against both the fungal and bacterial mycetoma are the same. These are three tissue reaction types [31]. In Type I: The neutrophils are closely attached to the surface of grains resulting in grain disintegration. In Type II: the macrophages and multi-nucleated giant cells replace dead neutrophils. The fragmented grains are mostly seen within multi-nucleated giant cells. Type III is characterised by the formation of well-organised epithelioid granulomas with Langhans's giant cells. In general, in the histological sections, the host tissue reaction types I and II are more frequently seen, while type III is the least seen.

Histological appearance of grains in H&E stain guides mycetoma differential diagnosis [21, 22, 28, 30, 32, 33], [Figure 2.7](#). *M. mycetomatis* grains are usually large (> 0.5mm) and coloured brownish. They appear rounded, oval, or trilobed with irregular outlines and grains fracture. On the other hand, most of the actinomycetoma species grains are homogeneous with round and oval shapes. *S. somaliensis* grains range from 0.5 to 2 mm. They show longitudinal cracks and transverse fracture lines. A cottony shape characterises *A. madurae* grains, and their outlier appears opaque with deep purple colour and a less dense stain in the centre. *A. pelletieri* grains are compact and dyed dark violet.

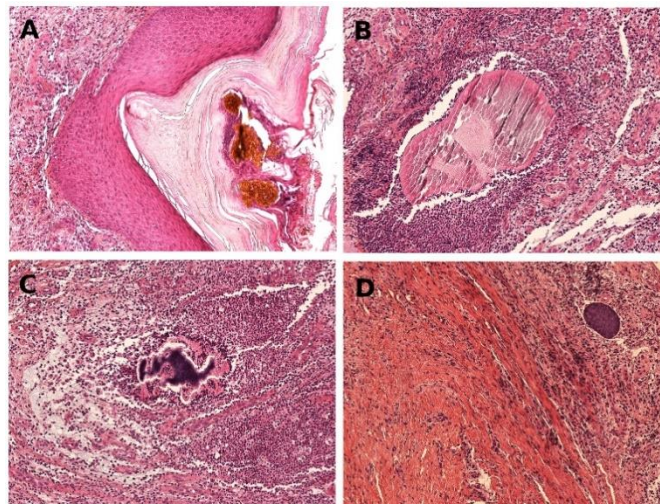


Figure 2.7: Histopathological appearance of mycetoma grains in H&E stain, magnified X10. (A): *M. mycetomatis*. (B): *S. somaliensis*. (C): *A. madurae*. (D): *A. pelletieri*.

Sometimes, grains are absent in histopathological sections; consequently, a conclusive diagnosis cannot be established. To avoid this, the surgical biopsy should always contain a good number of grains. Various cuts in the tissue block depth should be sectioned during the preparation of the histopathological sections [28]. Frequently pathologists report a background of grains taking into account inflammation and necrosis as well as grains absence which might be dropped out during the preparation of the sections. These reports are not conclusive for mycetoma diagnosis and necessitate repetition of the surgical biopsy.

- **Cytological Examination**

Fine-needle aspiration for cytology (FNAC) is a simple technique to obtain cells and grains for cytological examination. This technique is quite similar to histopathological one in many aspects. First, grains must be present in the collected aspirates to establish the diagnosis. Moreover, cell blocks instead of tissue blocks are obtained from the collected sample and stained before examining smears or sections microscopically. A fine needle attached to a syringe is used to collect cytological samples. It is inserted into the suspected mycetoma lesion and applies negative pressure while moving in at least three different directions, as illustrated in [Figure 2.5A](#). In practice, it can differentiate mycetoma from other subcutaneous lesions pathologists. In smears ([Figure 2.8](#)), we look for certain cytological properties such as; smears cellularity, inflammatory tissue reactions, and, obviously, the presence of causative organisms' grains [22, 28]. Cytology techniques do not need surgical intervention to be collected and hence, can be used in the field and epidemiological surveys [15, 21, 22, 28].

- **Serology**

Considering the long incubation time to determine causative organisms by culture and invasive surgical procedures to obtain grains in histology, efforts have been made to develop different serology assays [10, 21, 22]. Furthermore, serological methods are considered the most practical tests in developing countries because of their cost and quickness [3, 15, 21], yet there are no reliable serological tests for mycetoma diagnosis [8, 13, 15, 21]. A common challenge with proposing such tests is the lack of standardised antigens and antigens' long and tedious preparation process [3, 12, 21, 22]. Few studies have explored the use of certain serological tests to measure treatment response and early detection [8, 13, 15].

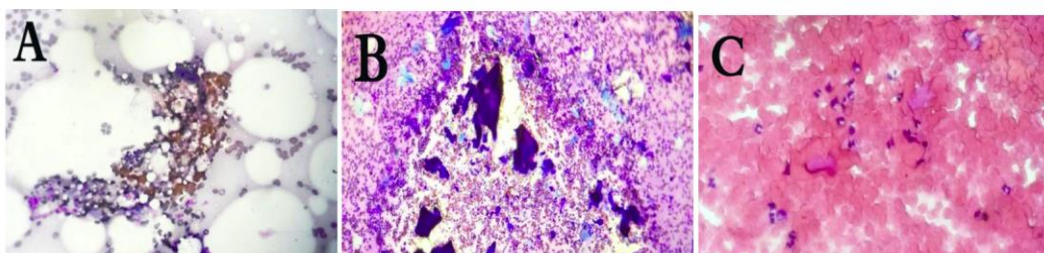


Figure 2.8: FNA of some mycetoma causative agents stained with H&E. (A): *M. mycetomatis*. (B): *A. pelletieri*. (C): *S. somaliensis*.

In conclusion, both imaging tools and organism identification techniques are complementary. Nowadays, molecular techniques are considered the test of choice in many centres. They can provide authenticated results; it is expensive and cannot be afforded by the majority of patients and centres. They require well-equipped infrastructure, which is unavailable in the endemic area [22, 29]. On the other hand, cytological and histological techniques are simple, rapid, cost-effective methods commonly used in rural areas where most affected populations are located [14, 22, 29]. However, false-negative results are common in the cytological examination as the FNA is blindly performed, and it is possible to miss grains pockets. A recent comprehensive study conducted at the MRC showed that histology is more accurate than cytology in organism identification [28]. Furthermore, ultrasound-guided aspiration cytology improved the test yield. In general, the minimum tools required to report the diagnosis are cytological and ultrasound examinations [13]. The recommended protocol for organism identification is shown in [Figure 2.9](#) [22].

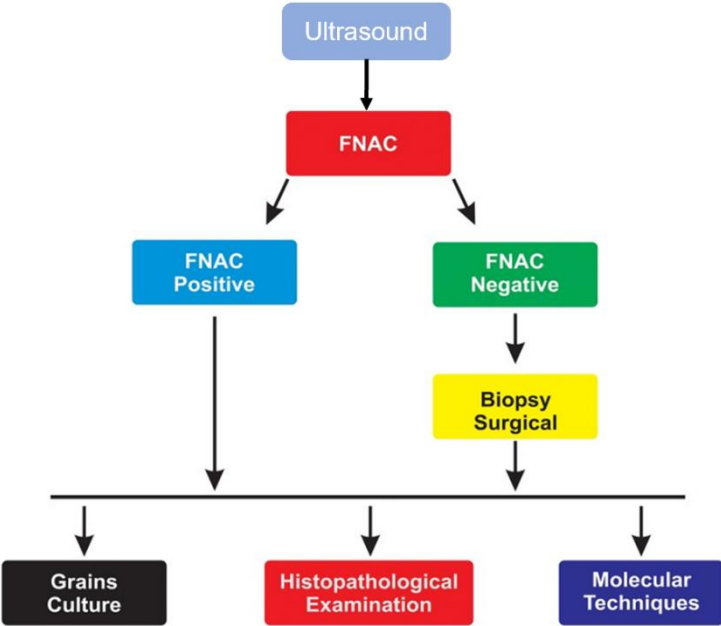


Figure 2.9: Mycetoma Diagnosis Flowchart.

2.3 Mycetoma Treatment and Management:

Although mycetoma was reported almost 200 years ago, no guidelines or protocols are approved by WHO for mycetoma treatment and management [15, 34]. Thus, any therapeutic and control programs are based on expert opinion and published case reports. The MRC developed various guidelines to assist health practitioners dealing with mycetoma based on its management experience with more than 10,000 patients.

The proper mycetoma treatment is highly dependent on the accurate identification of causative agents, as the two types are treated differently [12, 14, 22]. In general, mycetoma treatment is challenging, and the outcome is disappointing. The available medicines are not very effective, have many side effects, expensive, and are not accessible or available in many endemic mycetoma regions [15, 34]. Furthermore, it requires prolonged administration duration and thus leads to the patients' low compliance rate and high dropout rate. Many patients present late with advanced disease; the only treatment option is massive surgical excisions with enormous deformities or amputations. Early cases without deep structure involvement are curable [12, 13].

Although actinomycetoma is more aggressive than eumycetoma, with rapid progression and more rapid bone involvement, yet, it responds better to a combination of antibiotics with a cure rate of 70-90% [9, 12, 14, 15, 35]. In contrast, eumycetoma is difficult to cure; a combination of medical treatment with antifungals and surgical excisions is the recommended treatment regime [4, 19]. In some rare cases, both types of infection occur, complicating treatment.

The surgical treatment of mycetoma ranges from wide local excision, and repetitive surgical debridement for better response to medical treatment, to amputation of the affected limb [4, 32, 34]. These aggressive surgical procedures are associated with higher morbidity, deformities, and disabilities [12, 16].

Recurrence is high in eumycetoma patients. This is often due to the wide local disease spread along the tissue planes, disease biology, poor patient treatment compliance, late presentation, and poor surgical techniques [4, 12, 13].

The treatment outcome depends on the mycetoma type, site, size and tissue spread. Secondary bacterial infections are a common feature of mycetoma and frequently affect medical treatment [9].

Since treatment is prolonged, patients require long-term follow-up to monitor recovery, recurrence, and drug side effects [34]. This is often associated with a high patient dropout rate and irregular follow-up [14]. The MRC, the referral centre in Sudan, schedules regular follow-ups every six weeks until the endpoint of treatment. The cure is defined as [12, 13, 32, 33]: (i) Sinuses closure, (ii) Lesions disappearing or massively decreasing in size, (iii) Skin returns to normal, (iv) Improved disability, (v) No grains are seen on cytological or histopathological examination, and (vi) the disappearance of masses and grains on ultrasound examination.

To improve treatment response to eumycetoma, in particular, *Madurella mycetomatis* species, the most common type, DNDi and MRC launched the world's first mycetoma clinical trial for a potential new drug for eumycetoma in 2017 [9, 10].

Presently there is no control or prevention programme for mycetoma due to the knowledge gaps in its epidemiological characteristics. Hence, early detection and treatment have proved to be effective tools for reducing the disease burden [12, 15, 34]. A survey conducted in one of the endemic villages in Sudan [36] showed that barely half of the surveyed villagers used the acceptable practice in mycetoma management, and only 4% possess a good knowledge of mycetoma. Therefore, MRC practices of health education and advocacy and encouraging reporting of suspected cases will improve prognosis and lower the severity of infection [18].

2.3.1 Why is mycetoma a public health dilemma and a unique neglected tropical disease?

Mycetoma is a destructive and devastating infection that comes in either bacterial or fungus form. It mostly affects the poorest of the poor young adult in rural areas. Mycetoma is a common medical and health problem that might cause permanent deformity. The painless nature of mycetoma often leads to late diagnosis with severe infection. Consequently, the disease might develop secondary bacterial infection leading to massive disability and occasionally septicaemia [8, 9, 32].

Therefore, the correct diagnosis to the causative agents' level is important as the treatment varies for eumycetoma and actinomycetoma. However, the disease has been neglected by public health authorities, professionals, and the scientific community. Hence, early diagnosis is quite difficult, and treatment is challenging and sometimes ineffective.

The mechanism of mycetoma transmission is still ambiguous, furthermore, high-risk regions mapping is not yet accomplished, which restricts the designing of effective prevention and control programmes [3]. Presently, the active prevention mechanism considers lifting the awareness of the disease and the necessity of protecting exposed body parts in endemic areas, specifically feet and hands [15, 19, 32]. Also, promoting the importance of early reporting of suspected cases in primary care centres to be referred to specialist centres [15, 16].

Mainly, the feet are the most affected site, followed by the legs [2]. Leading to chronic morbidity and loss of function [37]. With advanced disease or when treatment fails, amputation is very likely. This has major social and economic consequences [9, 12, 14, 37]. There is a high probability of school/training dropouts for mycetoma patients, affecting their ability to secure a job, and making them economically dependent. Psychologically, patients are also affected because of inadequate health centres in endemic areas and poor treatment response and the social stigma of being physically disabled. Given this, mycetoma seriously impacts the patients, their families, and the communities [34, 37]. In general, mycetoma patients live with the disease for quite a time and are rarely cured.

The mycetoma burden is concentrated in the "mycetoma belt", but the global burden is uncertain. The number of infected people worldwide and which countries are most infected are unknown [10]. Africa seems to be the most highly endemic continent [12], where health services and education are in crisis with limited staff and resources. The number of mycetoma estimated cases is comparable to Buruli ulcer and African human trypanosomiasis (NTDs), although both data were from surveillance data [2, 3]. Hence, the approximated numbers of mycetoma cases are underestimated, but they give a general overview of prevalence and incidence. Unless surveillance data are gained for mycetoma, global burden and epidemiology would be missing [2].

Mycetoma has gone through a long journey to be globally recognised. This recognition attracts media attention and raises funding opportunities. WHO, Aljazeera, GHIT (Global Health Innovative Technology Fund), BBC, and many other governmental and non-governmental organisations produced documentaries about mycetoma [10]. Also, the PLoS Neglected Tropical Diseases journal accepted and published many papers. Despite this, numerous knowledge gaps still need to be investigated, particularly in epidemiology, transmission mode, diagnosis, and treatment [3, 9–11, 13, 15, 18].

2.4 Motivation

In 2017, the estimated number of mycetoma cases was 17607 [38]. A total of 5158 cases were seen in 2012 at the MRC alone [2]. This estimation is way less than the actual number as it only considers the published studies. Mycetoma has ranked as the third cause of amputation among individuals who presented at the Sudanese National Centre for Prosthetics and Orthotics [39].

Besides amputation, mycetoma can have other serious consequences on the patient and disease prognosis and outcome, such as; disability, depression, and recurrence [3]. Accurate identification of the mycetoma causative agent is a prerequisite for the treatment and limiting various consequences. Despite this fact, there is no simple and accurate diagnostic method available for this disease in endemic areas. Various diagnostic tools are used for mycetoma diagnosis. Histopathology is considered to be an efficient, cost-effective and time-effective tool for mycetoma diagnosis in endemic areas.

The histopathological examination method can only differentiate between mycetoma fungal and bacterial types conditionally by the availability of grains in tissue sections [22]; this is because the tissue reactions are similar in both types of mycetoma and to other non-specific chronic granuloma diseases [33]. This discrimination mainly relies on pathologists' knowledge and experience of the microscopic appearance of the organism [10, 15, 28, 30, 33]. Due to the neglect of mycetoma and its high prevalence in tropical regions, especially rural areas, it is rare to find well-trained pathologists with adequate experience in mycetoma diagnosis. To tackle this and to remove subjectivity from the diagnostic process, the presented work was conducted to provide a computerised analysis of digitised mycetoma histological images.

Digital pathology brings objectivity and enables reproducibility of the diagnostic process by using image analysis techniques. Also, it can improve diagnosis by decreasing human errors and enabling pathologists to make a diagnosis based on a larger set of diagnostic variables that might be overlooked during a visual examination.

2.5 Conclusion

Mycetoma is a WHO badly neglected tropical disease. It is caused by certain types of bacteria or fungi. The identification of the pathogen is the backbone of treatment, however, there is no simple and accurate diagnostic tool that could be used in endemic areas for this purpose. This chapter gives an overview of mycetoma and discusses the mycetoma knowledge gaps in epidemiology, diagnosis, and treatment. Also, it illustrates the motivation for conducting this work, which is proposing a computerised analysis of mycetoma histopathological images. The next chapter will review the basic processes for developing an automated diagnostic tool.

Chapter 3: Microscopic Image Analysis and Related Work

Summary

This chapter reviews the main concepts of Computer Aided Diagnosis (CAD), machine learning and Artificial Neural Networks (ANN) models. It provides the basis for understanding these concepts. In the first section, an overview of the CAD development process is given. The map of this thesis was drawn upon this strategy, starting from image acquisition and ending up with the final prediction. [Sections 3.2-3.5](#), introduced the basic components for building a CAD model and provide the state-of-the-art for each component. [Section 3.6](#) states the basic elements of machine learning models. We used this model to deal with the problem of mycetoma grains classification ([Chapter 5](#)). Then, some key details about Artificial Neural Networks (ANN) are described in [Section 3.7](#) to later develop an ANN model in [Chapter 6](#) for mycetoma grain segmentation. Finally, we ended the chapter with a conclusion.

3.1 Computer-Aided Diagnostics Models

CAD uses the computer to aid the diagnosis process by providing an interpretation of medical images. CAD of histopathological images uses approaches of artificial intelligence, image processing, and pathology to support diagnostic procedures of tissue samples. The typical CAD system, [Figure 3.1](#), involves image acquisition, enhancement, segmentation, feature extraction, feature reduction and pattern recognition [40, 41].

Depending on the application type, some CAD models might include their steps or skip others. Eventually, these models produce a new image or set of characteristics that describe the image. In the next sections, we addressed the items of the CAD

development process used to construct our automated mycetoma histopathological diagnosis.

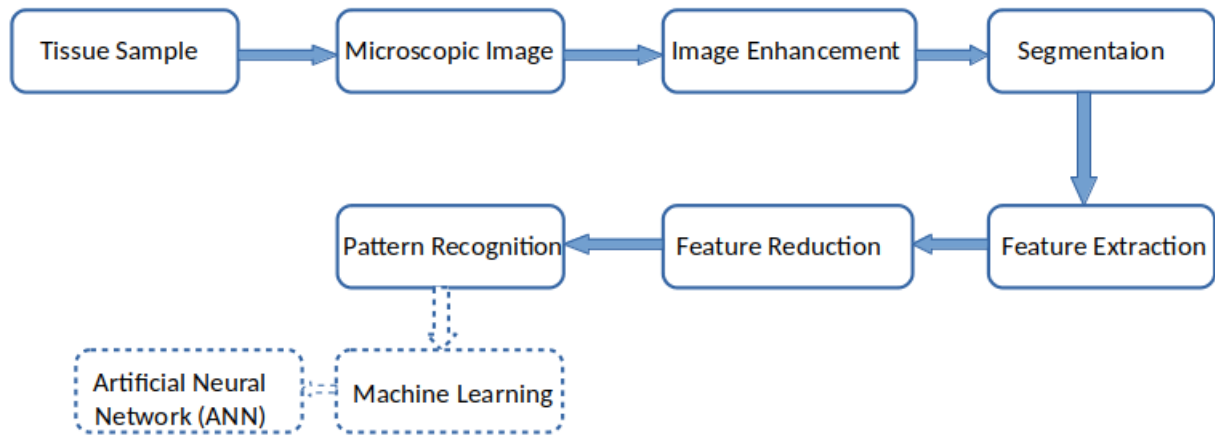


Figure 3.1: CAD System of histopathological images. Continuous line represents CAD component while dot line represents the used algorithms.

3.2 Microscopic Image enhancement

The digital microscopic image (sometimes it is called photomicrograph) is acquired from the tissue slide sample using a proper scanning machine (microscope, camera or slide scanner). Sometimes distortions might appear on the photomicrograph due to technical problems in the preparation of the histopathological slide. Carefully following the histopathological practice given in [Section 4.4.1](#) can still result in many artefacts that are traced back to the quality of tissue sections. Some of these problems are related to human skills in fixation, microtome sectioning, and the placement of the sections on the slide. Differences in the laboratory staining and cover-slipping protocols can also affect image quality by introducing changes in the staining intensity. During image enhancement, the quality of the image is improved by reducing the effect of noise and any sort of artefacts on the image. Image enhancement methods can be grouped into:

- Histogram-based techniques: image histogram shows image brightness, contrast, and quality. Therefore, these techniques are used to enhance contrast

and fix the colour variation that results from staining and illumination conditions [42–48].

- Filtering techniques: filtering aims to enhance or modify an image by removing unwanted components. While different types of filters are used in the literature [42, 49], Gaussian and median filters are the most commonly used filters utilized to smooth images and eliminate the noise of the staining process [50–53].
- Mathematical morphology techniques: these techniques process images based on shapes by considering images pixels as elements of a set. Morphological operations apply a structuring element to images. Mathematical morphology reduces the noise in the images based on the shape characteristics of the input image, which are characterized by the structuring element [54–57]. Erosion and dilation are the two basic morphological operators.
- Colour-based techniques: they are applied to the images to handle the difference in preparation, staining, lighting and imaging techniques. These techniques are divided into colour conversion [45, 54, 57–64] and colour normalisation [44, 65–69]. Normalisation modifies colour values such that the colour distribution of the source image matches a predefined reference image. On the other hand, colour conversion converts the RGB colour space of the image into a different colour space which is uniform perceptually [70]. A colour space is uniform perceptually if the change in the amount of one colour channel would be perceived by a human with the same amount of change. Conversion from RGB to grey colour space is mainly computed using the:
 1. The average method simply takes the average value of the three colour channels (R, G, and B) to obtain a grey value, [Equation 3.1](#). This method considers the contribution of three colours in image formation to be equally weighted, but this is not valid in reality. Colours have different wavelengths.

$$G = \frac{R + G + B}{3} \quad \text{Equation 3.1}$$

2. The Weighted or luminosity method considers the colours' weight in image formation, hence it provides a set of weights for three colours, as given in [Equation 3.2](#). Weighted colour conversion assigns the greatest amount of contribution with 0.59% to the green colour compared to the three colours. This is because human eyes perceive green colour the most, while it is less sensitive to red, and the least sensitive to blue colour.

$$G = 0.299R + 0.587G + 0.114B \quad \text{Equation 3.2}$$

3.3 Segmentation

Image segmentation is the partitioning of the image into distinct and non-overlapping regions of interest (ROIs). It is a primary and crucial step for the majority of CAD models. All the subsequent processes of CAD models solely depend on the quality and robustness of the segmentation.

The ROIs in histopathological images are the tissue components such as inflammatory cells and glands. Identification of these ROIs is a prerequisite for the recognition of certain diseases. In some cases, this identification is performed globally by segmenting all the tissue components or locally for specific components [71]. Generally, segmentation techniques can be divided into two classes:

1. Region-based segmentation: creates sets or regions using the properties of pixels or neighbouring pixels such as location, intensity, or texture. The threshold is the simplest method that uses a value (threshold) based on the intensity of pixels to segment the image into background and foreground [42, 44, 52, 58, 60–62, 66]. Depending on the prior knowledge of ROIs in images, such as the availability of labelled data and the number of clusters, clustering

techniques (unsupervised learning) can also be used in this class. Clustering groups the pixels in an image into clusters based on the similarity of the pixels concerning a certain property. K-means is the most commonly used method [47–50, 57, 63, 64, 72–74]. In contrast to unsupervised learning, segmentation can be carried out using a classifier that is trained on labelled images [58, 75]. The pixels of labelled classes are pre-segmented by an expert. Various supervised methods can be trained as a pixel classifier, such as a support vector machine (SVM), a k-nearest neighbour (KNN), decision trees, and boosting approaches. The Watershed technique is also considered for image segmentation [50, 55, 56, 72, 73]. It represents the images as a topological surface with its intensity values as the height and is usually applied on gradient images where the object corresponds to the catchment basins while the boundary to the watershed. Other techniques for image segmentation are region growing and region split/merge approaches [52, 75]. Region growing algorithm defines a seed and grows the seed into regions based on a similarity property and terminates the growing process when no additional pixels can be added to the regions. On the other hand, the split/merge approach splits the image into non-overlapping regions then a merging technique is utilised.

2. Boundary-based segmentation: looks for discontinuity in the image using edges or boundary techniques [61, 76]. Edge-based techniques [43, 54, 58, 77] assume that the pixels in the boundary between the background and foreground have distinct intensity values or there are discontinuities in images' pixels. These pixels are considered edges and detected by first or second-order derivative methods such as gradient or Laplacian derivative. Active contour or snake is the most popular boundary technique [43, 78]. This method defines an objective function and seeks to find the minimum value of this function by deforming continuously the contour until the image is properly segmented.

Region-based methods are more suitable when pixels of ROIs have similar values, while boundary-based methods are most appropriate when the values of neighbouring pixels of different ROIs are similar. These classes mostly consider the edge information, texture or intensity features. Hence, their performance on complex ROIs is unsatisfactory and more reasonable and highly accurate segmentation methods were proposed. Many advanced methods were developed based on learning

algorithms and deep learning techniques. Using deep learning models, especially Convolution Neural Networks (CNNs), have shown state-of-the-art performance for image segmentation [79–84]. CNN model called Unet was designed especially for biomedical image segmentation and proved to be very successful for many kinds of images [85].

3.4 Microscopic Image Features

A feature is a quantitative measurement defined for the image. Depending on the application domain, these features vary in terms of extraction method, the form of information they provide, and the methods of representing compact sets of features.

The studies in histology might be conducted on the cellular or tissue level; that is either focus on computing properties of individual cells or investigating their spatial properties across the tissue. So, feature extraction and segmentation depend on the type of study.

3.4.1 Features Extraction and Categories:

Several ways can be used to classify features and the information they offer. Different studies propose size and shape, intensity, texture, and structure as feature classes. To have a deep insight look into feature categories, the feature extraction process should be defined. First, ROI must be identified. ROI might be the whole region or part of it (and this is what is meant by segmentation). Then, applying some transformation operations (if needed) provides a single scalar value measurement.

Features can be extracted from the intensity and/or spatial relationship between pixels. Few studies benefit from spatial information, on the other hand, the intensity information is vulnerable to noise and stain artefacts [86].

The most common features classes are:

1. Morphological Features [45, 47, 49, 52, 54–58, 60, 72, 73, 76, 86–89]: It studies the size and shape of cells. These features can be generated from a variety of methods or geometrical concepts. Employing Cartesian coordinates to find size and shape is the trivial or obvious method, however, it depends on the direction and position of cells. Hence, this method is rarely used unless the goal is to study tissue architecture. Similarly, geometric moments are considered useful

shape descriptors, but they are vulnerable to the orientation of ROI. Therefore, geometric features are the ideal morphological descriptors in terms of orientation dependency. They include but are not limited to area, perimeter, inscribe circle, compactness and smoothness. Also, morphological features can be studied through the contour method by studying curvature, convex hull and convex deficiency of cells.

2. Textural Features [43–45, 47, 51, 53, 54, 56, 57, 59, 61, 62, 72, 73, 76, 86, 87, 89, 90]: It describes the variation of the spatial distribution of pixels' intensity values. Various transformations are used to extract textural features. The most common and widely transformations in used are co-occurrence and run-length matrices. Another popular transformation is the gradient transformation which measures the velocity of change in the grey-level value of pixels and produces a gradient image. Although Laplace transformation is well known used for segmentation purposes, it is also used to measure the velocity of gradient change on the transformed version of the image (gradient image). On the other hand, flat texture transformation uses a combination of the original image and median filter images to reveal holes or peels of the object. To study the topological gradient of the object (extremely small change on the surface of the object), the rice field feature was introduced. They quantify the change of grey level value in a neighbourhood defined by a particular topology. Moreover, fractal dimension studies the complexity and irregularity of shape.
3. Intensity Features [43, 45, 47, 48, 56, 66, 86, 89–91]: These features aim to study the distribution of pixels' intensity values (coloured or grey images). An image histogram is used to define the intensity features. It counts the frequency of each intensity value without including the spatial position of the pixels. Sometimes, the histogram can give a clue about the dominant intensity values. Hence, pixels' spatial connectivity could be inferred. The features could be extracted from grey or coloured histograms, the latter might utilise a single colour channel or a combination of them. From the histogram, various features can be extracted such as mean, variance, skewness, and kurtosis.
4. Structural Features [48, 54, 57, 63, 64, 66, 74, 77, 86, 88]: these features provide information about the structure of tissue and the spatial distribution of

cells. They describe the relationship between cells and provide structural information. Usually, these features are known as topological features or spatial-relation features. Commonly these types of features are used with histology images. The location of the cells is used to generate graphs, and then, analyse spatial dependency in the graph and extract features. Different types of graphs were studied in the literature, such as Voronoi diagrams and their Delaunay triangulations, the nearest neighbourhood graph, the minimum spanning tree, and the cell graph. For example, studying the Voronoi diagram constitutes convex polygons for each cell, and the area and shape of these polygons can be extracted.

3.4.1.1 Radiomics Features

Radiomics emerged in 2012 by Lambin and others [92, 93], as a new application of established techniques of CAD. A rapid increment in the number of radiomics-related applications has been noticed during the last decade [30]. Radiomics aims to extract a large number (up to thousands) of quantitative features from medical images. These features vary from trivial ones, such as first-order statistical features, to advance features involving texture and spatial characteristics of ROI. The extracted features can be used to build predictive and descriptive models for a wide range of medical applications. It is classified into three broad categories [92, 94–96]:

1. Shape features compute the geometric properties of ROI, such as perimeter, sphericity, elongation, and axis length.
2. First-ordered (global statistics) features quantify the intensity distribution of pixels within ROI through intensity histogram analysis (e.g., mean, standard deviation, energy, entropy, skewness, kurtosis).
3. Textural (second-ordered) features consider the spatial intensity distribution of pixels (i.e., the intensity pattern within the image) and describe the heterogeneity of ROI. Five main classes define the textural features:

Let δ be a neighbourhood of the pixel a , θ be an angle, i, j are intensity values.

- a) Gray Level Co-occurrence Matrix (GLCM): In δ , GLCM is the number of times a combination between i and j occurs in θ direction.

- b) Gray Level Run Length Matrix (GLRLM): in a predefined direction θ , we define run length as the number of adjacent pixels that share the same intensity.
- c) Gray Level Size Zone (GLSZM): Zone is defined as the number of connected regions with an equal intensity value. In contrast to GLRLM, the GLSZM is rotation independent.
- d) Gray Level Dependence Matrix (GLDM): a neighbouring pixel with grey level j is considered dependent on a centre pixel with grey level i if $|i - j| < \alpha$. GLDM defines the number of connected regions in δ that are dependent on a centre pixel.
- e) Neighbouring Gray Tone Difference Matrix (NGTDM): For each pixel a in δ , we define NGTDM as the absolute difference between a and the average of all the pixels in δ .

For further details, see the documentation of radiomics [97].

3.4.2 Feature Reduction:

Several classes of features could be extracted from the microscopic images, however, not all the extracted features are useful for prediction purposes. Therefore, feature reduction methods are necessary to determine the most significant, irrelevant and/or redundant features. Feature reduction is an important aspect of model building as it reduces the model complexity and allows for better generalization (Section 3.6.1) [98, 99].

Intuitively, some features can be selected, but this is unconvincing, especially with large-scale applications. Hence, two main techniques are utilized for feature reduction [78, 99–101]:

1. **Feature Selection:** this method is meant to identify of the most relevant features. This method seeks to maximize some objective function by selecting the “best” subset of features. There are three types of feature selection methods:

1. Filter: It uses the variable ranking technique, assigning a score to each feature and then selecting a subset of them. This selection is performed before the classification step and it can be done either by selecting m from n features, features that score a certain threshold or evaluating the performance of the highest-scored features based on cross-validation.
2. Wrapper: It is oriented by the learning algorithm such that it uses the performance of a particular learning algorithm to select the features. Wrapper searches for a subset of features and then measures its performance of it. Distinct searching algorithms might be used, such as; sequential searching, genetic search, and simulated annealing [102].
3. Embedded: It was introduced to overcome the computation time consumed to train the learning algorithm for every new subset in the wrapper method. Therefore, the embedded method is presented in a way such that the selection of features is integrated with the learning process. Hence, this method usually works with certain learning algorithms.

Another feature selection technique uses ensemble methods of the three methods and aggregates the selected features from several random runs as the voted features. This method yields more stable features [78, 101].

2. **Feature Transformation:** the feature selection methods are considered to be inefficient, especially with a great number of features where the whole set should be scanned without any prior knowledge about its relevance to the prediction capability. Also, some features might not be picked by the selection method because they are independent of the rest of the features in the set, hence they have a low score and this result in ignoring them by the method. Therefore, feature transformation uses the whole set to reduce dimension based on specific criteria. It transforms the actual features set into an alternative, new and more compact feature space that encapsulates many features in a single feature. Features can be transformed linearly or non-linearly depending on whether the Euclidean distance between features is assumed or not. Principal Component Analysis (PCA) and Linear Discriminant Analysis (LDA) are commonly used in literature.

3.5 Pattern Recognition

Patterns are either seen as physical entities or observed as mathematical values. Pattern recognition is the process of recognizing patterns from data, and then making predictions and decisions through these patterns by using machine learning algorithms. Hence, pattern recognition defines labels to unknown data by extracting statistical information from patterns.

In our scenario of CAD modelling, patterns are defined by the extracted features. For a given histological image, pattern recognition is essentially an image classification or clustering to show what disease it represents after extracting an appropriate set of features. Furthermore, it is possible to perform grading for the disease.

Classification methods are utilised more frequently for recognition tasks in histopathological images. Classification can be defined as a function that maps data features into a set of predefined classes to which the data belongs. It is very important to choose the appropriate classifier that deals with large and dense datasets. Many machine learning algorithms are used for image recognition, among those algorithms are logistic regression, support vector machine, linear discrimination, decision trees, and Artificial Neural Networks (ANNs). A list of the most popular algorithms is given in [Section 3.6.3](#).

Recently, Convolutional Neural Networks (CNN) have achieved state-of-the-art performance in the task of image classification and detection. It is a kind of ANN which are suited to image-processing tasks. The CNN popularity is traced back to the work presented on ImageNet classification using a network named AlexNet, which won the competition of ILSVRC-2012 [103]. In early 1995, CNN was used within the scope of medical imaging to detect nodes in lung radiological image data [104]. Since then, CNN has replaced the classical CAD methods in several medical image diagnosis contests [79–81, 105–107].

The most common CNN models include Alexnet [103], ResNet [104] which is a large variant of CNN that uses short skip connections to train CNN, VGG16 [108] which won the ImageNet localisation challenge in 2014, Inception of CNNs [109] which allow the use of different filter sizes instead of the single filter size, Densenet which use dense

connections between layers [110], and lastly the Unet architecture [85] which won the ISBI cell tracking challenge 2015 by a network that passes the low-level features to high-level during the up-sampled/downsampling process and utilizes the skip connection between corresponding layers. Generally, the CNN model has several challenges in determining the architecture, size of the network, and type and number of layers. The choice of the model affects the way how to tackle the problem under investigation.

A summary of studies conducted on tissue image analysis is shown in [Table 3.1](#). It can be noted that the majority of the work utilises Kmeans for segmentation because mostly the number of clusters is known in advance. Also, colour-based techniques are dominantly used for image enhancement.

Table 3.1: Brief review of related work on microscopic tissue images.

Organ	Enhancement	Segmentation	Features	Recognition
Cancerous tissue [47]	Threshold	Clustering (Kmeans)	morphology, intensity, and texture	KNN
Lymph [57]	colour conversion, and mathematical morphology	Clustering (Kmeans)	morphology, structural, texture	Bayesian classifier
Lymph [63]	colour conversion	Clustering (Kmeans)	structural	SVM, Bayesian, and KNN
Brain [74]	-	Clustering (Kmeans)	structural	ANN
Brain [64]	colour conversion	Clustering (Kmeans)	structural	Bayesian and ANN
Breast [48]	threshold	Clustering (Kmeans)	Intensity and structural	SVM
Bone [77]	-	Edges technique	structural	SVM

Lung [87]	-	Clustering	morphology and texture	ANNs, SVM, and an ensemble of them
Skin [90]		manually	intensity, and texture	Linear discriminant
Breast [88]	colour conversion	Region growing	morphology and structural	SVM
Urine bladder [89]	colour conversion	Active contour	morphology, intensity, and texture	Bayesian classifier
Prostate [72]	-	Clustering (Kmeans) and watershed	Texture and morphology	SVM
Prostate [76]	-	boundary (Graph cut)	Texture and morphology	boosted decision trees (Modest AdaBoost)
Breast and prostate [111]	filter		Apply filter on image to get shape features	CNN trained on shape and original
Breast [58]	colour conversion	Edge and threshold	morphology	- mainly applied for segmentation
Brain biopsy [59]	colour conversion	morphological gradient	texture	Bayesian classifier
Colon gland [75]		Region growing		SVM
Breast tissue [73]	Colour normalization	Kmeans and watershed	morphology and texture	Naïve Bayes, SVM, Adaptive Boosting, Random Forest, and ANN
Neuroblastoma verve [42]	Histogram and filter	threshold		

Lymph [43]	histogram	Boundary and edge	Intensity and Texture	KNN
Prostate [45]	Colour conversion and threshold	-	Intensity, morphology and Texture	Gaussian, KNN, and SVM
Cervical [44]	Colour normalization	threshold	Texture	SVM
Kidney [50]	Gaussian filter	Kmeans and watershed	texture	Bayesian
Kidney [51]	Gaussian filter	threshold	texture	-
Oral cavity [52]	median filter	Threshold and Region Growing	morphology	-
Skin [53]	median filter	manual	intensity	Fuzzy C-means
Prostate [49]	filter	Kmeans	morphology	unsupervised manifold
Breast [54]	colour conversion and mathematical morphology	edge-based	textural, structural, and morphology	SVM
Liver [55]	mathematical morphology	watershed	morphology	KNN and SVM
Liver [56]	mathematical morphology	watershed	morphology, intensity, and textural	SVM
Cancerous tissue [91]	Colour normalization	manually	intensity	linear discriminant classifier (LDA)
Cancerous tissue [66]	colour normalization	threshold	intensity and structural	KNN

Rectal [67]	colour normalization	NA	-	CNN
Breast [68]	colour normalization	-	-	-
Cancerous tissue [69]	colour normalization	-	-	-
Prostate [60]	colour conversion	threshold	morphology	KNN
Breast [61]	colour conversion	threshold and morphology	textural	discrimination and decision tree
Lymphoma [62]	colour conversion	threshold	textural	quadratic discriminant

The traditional procedures for CAD development require a manual extraction and identification of “handcrafted” features. On the other hand, ANNs provide an unsupervised method for extracting features by making use of data and multi-layered architecture. Therefore, they address the development of the CAD model by combining both feature extraction and pattern recognition [67, 73, 111].

3.6 Machine Learning

Machine learning is a subfield of artificial intelligence that aims at training computer systems to perform some specific tasks. It mimics human behaviours and gives computers the ability to learn, therefore it gained its name. Formally, machine learning can be defined as learning computer from experience E in the form of data items to solve a given task T with respect to the performance measure P . Hence, it said that the computer is learning the task T if its performance P improves and produces the correct prediction for the given data items [112].

The basic concepts presented in this section and the next one are reviewed from [112–115].

3.6.1 Learning Strategies

The data items of a given experiment E can be defined as a finite data set $D = \{x_i\}$ or $D = \{x_i, y_i = f(x_i)\}$, where x represents input data, and y is the label of data. According to the type of data items, machine learning models can be grouped into three main broad categories:

- **Supervised Learning:** For this type of learning, the model deals with the labelled data and estimates the function f that maps the input x to the output label y based on the rule that defines each pair (x_i, y_i) in the dataset. An example of this learning is classifying of images into a set of predefined classes.
- **Unsupervised Learning:** This type of learning draws inferences from unlabelled data and discovers hidden patterns. The clustering of data into non-overlapping clusters with similar patterns is the most common illustration of unsupervised learning.
- **Reinforcement Learning:** It interacts with dynamic data and reacts accordingly by performing certain actions. Reinforcement learning provides feedback in terms of rewards by trying these rewards and without learning which action to take.

In practice, the data D is divided into three groups: training, validation, and testing. During the learning process, the training data set is used to train the model, while the validation data set is responsible for tuning the parameters and examining generalization to provide the correct prediction of unseen data. Finally, the model's performance is evaluated through the test data set.

The generalization of the machine learning model is a major challenge in model training. Generalisation means that the model would perform well on the learning data but fail on other data sets. To monitor the model generalization, training errors and the difference between training and validation errors are explored. For a good

generalization, both values of errors should be small. In general, there are three cases of generalization (Figure 3.2):

- Under-fitting: It occurs when the model is simple and does not capture the pattern of the data. Also, the limited data points that are relevant to the given task and the model performance does not improve even with increasing the data points and retraining the model. Under-fitting is explained by not small training error.
- Over-fitting: It is caused by a complex model that fit the data point in the training dataset perfectly and shows very poor fitting on the unseen dataset. Hence, the difference between the training and validation errors would be quite large.
- Correct-fitting: this fitting provides adequate performance on both data sets of training and validation with an acceptable complexity model and sufficient data points related to the training process.

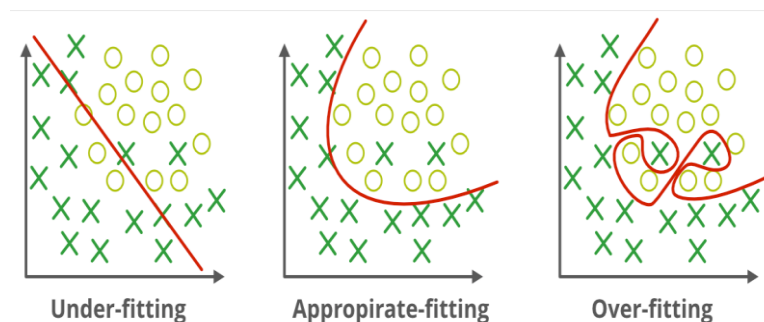


Figure 3.2: Binary classification model example of the different types of generalization. The figure is adapted from <https://www.geeksforgeeks.org/underfitting-and-overfitting-in-machine-learning/>

3.6.2 Hyperparameters tuning

During the training process, some parameters cannot be learnt directly, and they are called hyper-parameters. These parameters are fixed before the beginning of the learning process and define the properties of the model, such as the complexity and speed of the model. Hyperparameter tuning is the process of choosing the ideal set of

hyperparameters for learning the model. It is a crucial step to train a model as it controls the overall performance of the model.

Looking for the optimal set of hyperparameters can be treated as a searching algorithm which can be tedious and computationally expensive. Grid search and random search are commonly used for tuning the model. The grid search algorithm chooses a grid of hyper-parameter values and searches for the best set of values in the grid by evaluating all of them. This algorithm is computationally expensive as it scans all the combinations for evaluation. This limitation is addressed by the random search algorithm because it goes through random values within the grid to define the best hyper-parameters.

3.6.3 Popular machine-learning models

We attempted to list the most popular machine learning algorithms. However, there are dozens of these algorithms, therefore it was more convenient to categorize them by considering their similarities in the learning strategies. Here is a list of some of these groups is given:

- **Clustering Algorithms:** they are concerned with organising the data into groups or categories while minimising the similarity between these groups. Clustering algorithms use the patterns of the data for this organisation. The most popular clustering algorithms are Kmeans and Hierarchical Clustering.
- **Decision Tree Algorithms:** they are tree-like models built from the values of data features. The prediction is made by traversing the tree based on the conditions given in the tree nodes until reaching the leaf which represents the decisions. Decision tree algorithms work for both classification and regression tasks. The most popular decision tree algorithms are Classification and Regression Trees (CART) and Conditional Decision Trees.
- **Bayesian Algorithms:** these models employ Bayes theorem for the prediction of regression and classification tasks. The most popular Bayesian algorithms are Naive Bayes, and Gaussian Naive Bayes.

- **Regression Algorithms:** these algorithms use a performance measure iteratively to refine the modelling of the relationship between data features. Regression algorithms are suitable for learning unlabelled data. Some examples of popular regression algorithms are Ordinary Least Squares Regression (OLSR), linear regression and logistic regression. We will use an algorithm from this group in Chapter 5.
- **Artificial Neural Networks (ANNs) Algorithms:** they are inspired by the structure of human biological neural networks. The more classical methods are Perceptron and Multilayer Perceptron (MLP). We will discuss these algorithms in detail in the next section as they will be used later in Chapter 6.
- **Dimensional Reduction Algorithms:** these types of algorithms are similar to clustering algorithms; the main difference is that dimensional reduction algorithms use unsupervised methods to find hidden data patterns and summarize them with less information. The main goal of these algorithms is to visualize high-dimensional data or compact the dimension of data to be used in the supervised learning method. Some of the most relevant methods are Principal Component Analysis (PCA) and Principal Component Regression (PCR).
- **Ensemble Algorithms:** this group of algorithms are very powerful and popular because it combines the predictions of multiple weaker models that are independently trained. The final prediction is concluded by merging those predictions in some way. Some examples of ensemble methods are Boosting, Bootstrapped Aggregation (Bagging), AdaBoost, Gradient Boosting and Random Forest.

3.7 Artificial Neural Network

Artificial Neural Networks (ANNs), often called Neural Networks, is a machine learning model inspired by the biological neural network and mimics the human brain to perform tasks based on external information and then decides which action to take based on specific rules. ANNs hierarchically process the input through a set of layers. Each layer

extracts more abstract features compared to the previous layer, these features are utilized to decide the ANN outcomes.

In 1958, Frank Rosenblatt introduced the artificial neuron model called perceptron [116], [Figure 3.3](#). This model receives the inputs X . Then, it calculates the weighted sum Σ by considering the input with their associated weights W and an extra input called bias b . The activation function σ performs a non-linear transformation on the weighted sum to obtain the final output $z = \sigma(X \cdot W + b)$. The neuron model is believed to be the base of ANNs since the latter can be defined by a set of connected neurons that are arranged in layers.

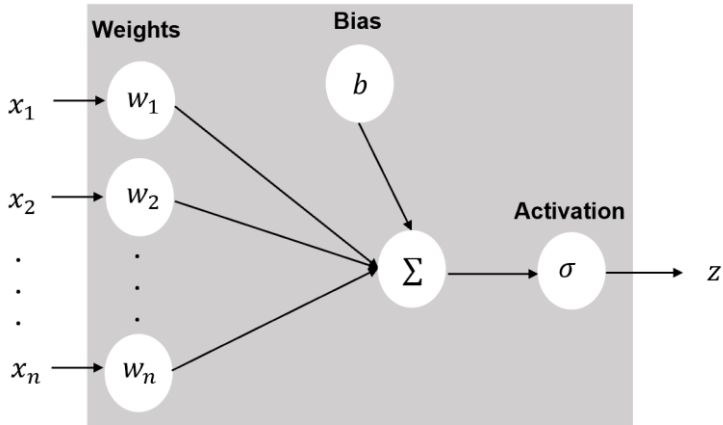


Figure 3.3: Signal Neuron (Perceptron) Model.

ANNs, often called Deep Neural Networks (DNN), refer to the case where the network has at least three layers. [Figure 3.4](#) illustrates the first DNNs proposed in 1969, called Multilayer Perceptron (MLP). There is the input layer, one or more layers of feature extraction called hidden layers, and the output layer where the outcome is generated.

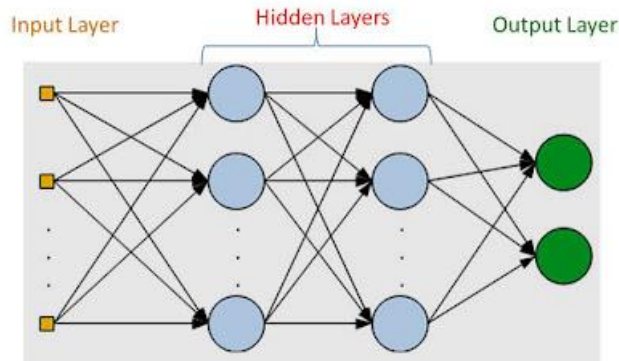


Figure 3.4: Multiple Neurons (MLP) Model

Next, we will explain the process of how a combination of neurons is activated for different outcomes and final decisions. That is, training the ANN to strengthen the weights of the inputs that carry meaningful information and correct prediction.

3.7.1 Feed Forward Network

Feed-forward network (FNN) $f(x; \theta)$ is a mathematical function that is parametrized by θ which represents the model parameters (W, b) . FNN applies a series of transformations to an input x to produce an output $y = f(x, \theta)$. The function f can be defined as:

$$f(x) = (f_n \circ \dots \circ f_1)(x)$$

The f_i 's are of the form $f_i(x_i; \theta_i) = \sigma_i(W_i f_{(i-1)} + b_i)$ which is a non-linear function (σ) of the weighted sum of all the outputs from the neurons of the previous layer. The output of this non-linear operation is called the activation layer.

Activation Function:

Throughout the network, each activation layer is passed to the next layer and calculated using the activation function until the network reaches the final output layer. The activation functions are used to get the final output of each layer and map the resulting value into a specific range depending on the function used. They allow the learning of complex structures and features by adding a non-linearity property to the network. The most common activation functions are:

- The sigmoid $\sigma(x) = 1 / (\exp(-x) + 1)$

- The hyperbolic tangent $\tanh(x) = (exp(2x) - 1)/(exp(2x) + 1)$
- The Rectified Linear Unit $ReLU(x) = max(0, x)$.

Both sigmoid and tanh transform values are between $[0,1]$ and $[-1,1]$, respectively. On the other hand, ReLU sets negative values to zero, which allow the deactivation of neuron with a linear combination less than zero. This is why it converges faster compared to the sigmoid and tanh functions. Therefore, ReLU is the most commonly used function [117]. [Figure 3.5](#), shows the plot of these activation functions.

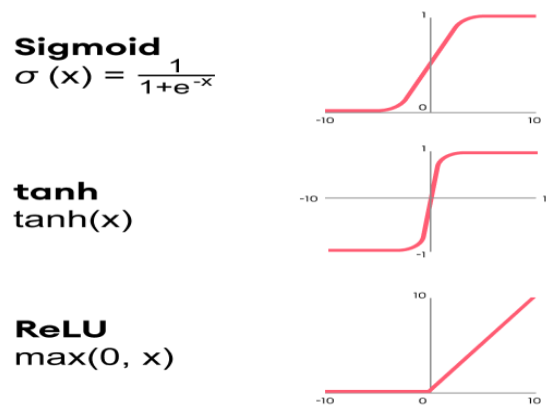


Figure 3.5: Activation Functions.

3.7.2 Training Feed Forward Network

In the previous section, we review the basic structure for building the ANN and the definition of FNN. Now, we will describe how to learn FNN from the data to obtain the value of θ .

Gradient Descent

Mathematically, gradient descent (steepest descent) is an optimisation algorithm for finding the local minimum point for a differential function. The optimisation algorithm investigates the problem of minimizing or maximizing a function $y = f(x)$. The derivative f' , $\partial y / \partial x$, or ∇f defines the direction of the change in the value of x that decreases the value of y . This help in the problem of minimizing the function. Therefore, gradient descent explores the value of change in the negative direction, that is $-f'$.

Let γ be a real small value representing the distance in the negative direction of function change and x_0 a starting point, then $x_1 = x_0 - \gamma \nabla f(x_0)$ for x_1 is the improved local minimum point. More generally, gradient descent starts with an initial point x_0 and keeps improving until it obtains a local minimum point using the iteration:

$$x_{(n+1)} = x_n - \gamma \nabla f(x_n)$$

In terms of ANNs, a function $y = l(\theta)$ is defined to measure the difference between estimated and actual values for a data point. This function is called the loss function or error function. Using γ which is called the learning rate, gradient descent aims to find the global minimum point of the loss function, but this is not always possible [113]. This is one of the limitations of the gradient descent, and there is no way to distinguish a local from a global minimum point. Another factor that affects finding the minimum point is the size of the learning rate, that is because the value of γ will affect the convergence to the point and if it is too large the point might be overshoot.

Back-propagation

Backpropagation sometimes called "backward propagation of errors", aims to improve the weights of neurons by calculating the gradient of the error function considering the weight of the neurons. Thus, it is used to train FNN. Figure 3.6 illustrates the backpropagation compared to the forward-propagation. The weights of each layer are updated with respect to the gradient of the previous layer. This is why we reduce errors by updating the weights of all layers.

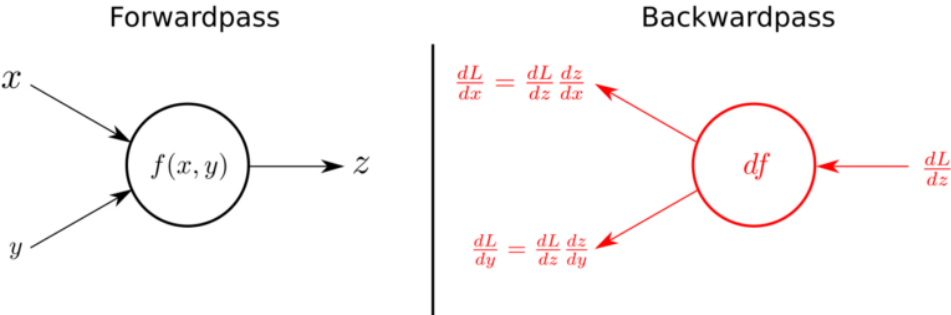


Figure 3.6: back-propagation vs forward--propagation.

Typically, the whole training dataset is fed to the FNN to compute the gradient. This technique is called Batch Gradient Descent. It is time-consuming and computationally expensive. Another way to handle this is to use Stochastic Gradient Descent (SDG) which updates the weights after every single sample in the training dataset. However, SDG is considered to have a weak estimation of the gradient, and it can easily escape shallow local minima points. An alternative is mini-batch Stochastic Gradient Descent (mini-SDG) which uses randomly selected batches of the training dataset. The experiment showed that using mini SDG is more efficient compared to batch gradient descent and SDG [118].

3.7.3 Convolution Neural Networks

Convolution Neural Network (CNN) is a class of FNN that considers the structure of inputs in the training process. It can study high-dimensional inputs such as 2D and 3D images. CNN was introduced in 1989 [119]. It has many applications in natural language processing and computer vision.

CNN architecture is defined from three main layers:

- Convolution layer: It is the basic building block used in CNN that performs a mathematical operation called convolution. Convolution is defined as a linear operation between two matrices. In this domain, convolution involves the multiplication of input I and a set of weights W . The matrix W represents the convolution matrix which is a set of learnable kernels (filters) that captures the spatial features from an image. Spatial features refer to the arrangement of pixels and the relationship between them in an image. They help us to identify the object accurately, the location of an object, as well as its relationship with other objects in an image. Given a 2D input image $I \in \mathbb{R}^{r,c}$, the size of the convolved output $O \in \mathbb{R}^{r',c'}$ is governed by the padding and stride sizes. Padding (p) is the number of pixels added around the input matrix to preserve the size of the input image. This is because, after multiple convolution operations, the size of the input decreases as it is processed by the kernel $W \in \mathbb{R}^{k,k}$. Stride (s) is defined by the number of pixels that shifts over the input matrix. Hence, the size of the output is $r' \times c'$ where $r' = \frac{r+2p-k}{s} + 1$ and $c' =$

$\frac{c+2p-k}{2} + 1$. The convolution operation with an illustration of padding and stride is given in Figure 3.7.

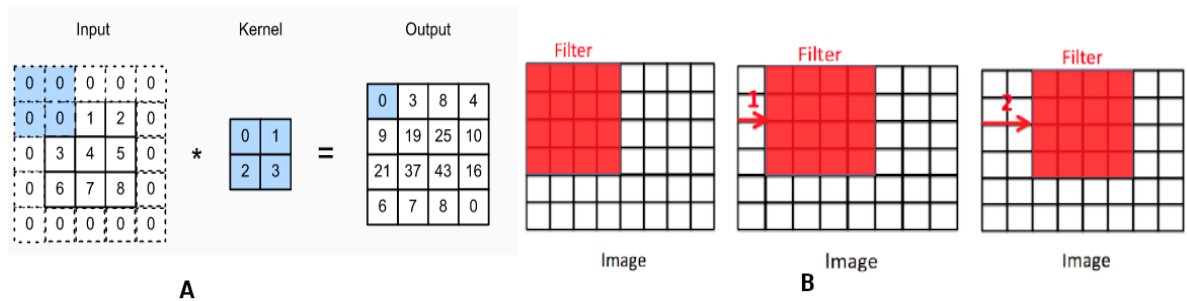


Figure 3.7: Convolution operation. (A): Padding an image convolved with a 2*2 kernel. (B): From left to right: stride of size 0, 1, and 2. The figures are adapted from <https://medium.com/analytics-vidhya/convolution-padding-stride-and-pooling-in-cnn-13dc1f3ada26>.

- Activation layer: It consists of a nonlinear activation function that is applied on the feature maps which results from the convolution operation and generates the activation map as an output. The activation layer allows the network to learn more complex functions.
- Pooling layer: this layer has no learnable parameters and operates on each feature map independently. It aims to merge similar semantic features into one by reducing the spatial size of the feature map progressively, hence sometimes, it is called a down-sampling layer. Since semantically similar features can be in different locations in the previous feature map, it is necessary to reduce the image size successively to obtain a global vision of the previous feature maps. Down-sampling can be performed by computing the maximum or average value of the nearby units, which is called max pooling or average pooling, respectively. Another way of performing the down-sampling is to use a stridden convolution with a size bigger than 1. The pooling layer reduces the number of features and the network computation.

3.8 Conclusion

Over the years, mycetoma does not receive any attention in terms of computation diagnostic methods. Developing such methods requires the essential knowledge of CAD and machine learning models. For this reason, this chapter reviews the fundamental concepts of these models. We described the main components of the CAD model and the quantitative features used for computation diagnostic computation models. Also, we provided an insight into machine learning algorithms learning strategies and their most common types.

After reviewing the available literature, three key issues are identified and guide the work presented in this thesis. Firstly, colour-based techniques are dominantly used for the enhancement of histopathological images. While clustering techniques especially, Kmeans are used for the segmentation task, these techniques might not apply to mycetoma tissue images because, with the variability in mycetoma grains, it is difficult to determine the number of clusters or to correctly segment without supervision. Secondly, the extraction of the handcrafted features is influenced by the type of study and the features that describe the ROIs. Thirdly, there is no standard method for choosing of the pattern recognition model classifier. Also, CNN is becoming the most popular tool for most medical imaging-related tasks.

The next chapter will introduce the first mycetoma database of histopathological microscopic images. This database constitutes the first step towards proposing automated diagnostic methods that make use of some of the methods and techniques reviewed in this chapter.

Chapter 4: Database of Mycetoma Tissue

Microscopic images - MyData

Summary

This chapter describes the creation of the first database of microscopic images of mycetoma tissue. It details the pipeline of its construction from the mycetoma species distribution and the patient sampling to the acquisition protocol through the histological procedures. The first section of the chapter states the motive for the need for the creation of this database. [Section 4.2](#) presents the epidemiological distribution of mycetoma causative agents which reflect the sample presented in the database. Then, a detailed description of the study population is given in [Section 4.3](#) including sample selection and diagnosis. [Section 4.4](#) review the pipeline of the histopathology process. This is followed by the preparation of the microscopic images. Finally, a comprehensive elaboration of proposing the mycetoma database is introduced along with the summary of the data and labels. The last section provides the conclusion of the chapter.

4.1 Rational behind the creation of the mycetoma database

Image analysis models have emerged in the last three decades as a key approach in the medical domain, even more recently with numerous developments in deep learning models. These models aim to provide methods for improving patient care. Some of the tasks for medical image models are the exploration of images, segmentation, and classification. For example, these models could be used to predict and treat diseases, discover new drugs, and develop diagnostic approaches.

However, no approach was ever developed to address the diagnosis of mycetoma. This can probably be related to the neglect of mycetoma, not only concerning the health aspects but also the computation aspects. To allow the development of a mycetoma image analysis model, a mycetoma database is required. For this reason,

we got the motive to create the first database for mycetoma histopathological microscopic images, called MyData, with specific and homogeneous standards. This database could be used by the scientific communities for the modelling and analysis of mycetoma histology analysis. Also, it can give more insights into producing to produce more effective diagnostic parameters and strategies using histopathology.

Data is the most important aspect of medical image analysis models, and without it, any model cannot be trained to perform its intended purposes. In practice, there is an abundance of places where datasets for machine learning models can be found. These datasets can be well-suited for the development of CAD approach for various diseases. With the gathered clinical data, the database created in this thesis will be released as the first specialized database for mycetoma grains in tissue images. This database will enable researchers to combine image analysis models and biology to make mycetoma diagnostics more efficient and cost-effective.

As was discussed in [Chapter 2](#), mycetoma is a unique neglected tropical disease in terms of health, economic and social impacts on patients and communities. Furthermore, many knowledge gaps remain challenging to resolve because they are closely related to each other. Initially, the reason for creating the mycetoma database was driven by the need for a microscopic image dataset to develop and train the diagnostic machine-learning models. The availability of such accurate and affordable models in rural areas could also assist in the confinement of more mycetoma cases within their environments and entourage which can indirectly contribute to the epidemiology of mycetoma. Therefore, we believe the benefits of this database might extend the intended purpose of advancing the diagnostic knowledge gaps.

4.2 The distribution of Mycetoma Causative Agents and Organisms

To introduce the mycetoma database, it is essential to define the epidemiological distribution of mycetoma causative agents. This is because the database must be representative of mycetoma cases worldwide.

Globally, almost 40% of mycetoma cases are caused by eumycetoma [2, 120]. However, eumycetoma is more dominant in some regions, such as central African

countries, whereas actinomycetoma is common in the Americas and the Middle and Far East [121]. Furthermore, within the same region and between the neighbouring countries, there is an uneven or mixed distribution of eumycetoma and actinomycetoma [2, 121], [Figure 4.1](#). This epidemiological distribution of mycetoma causative agents shows that the majority of countries report mixed cases of eumycetoma and actinomycetoma, while few countries have a high proportion for either of them. For example, eumycetoma is more frequently seen in Sudan with 73% and this percentage decrease to 42% in India, in contrast, Mexico reports only 3% of eumycetoma cases [121].

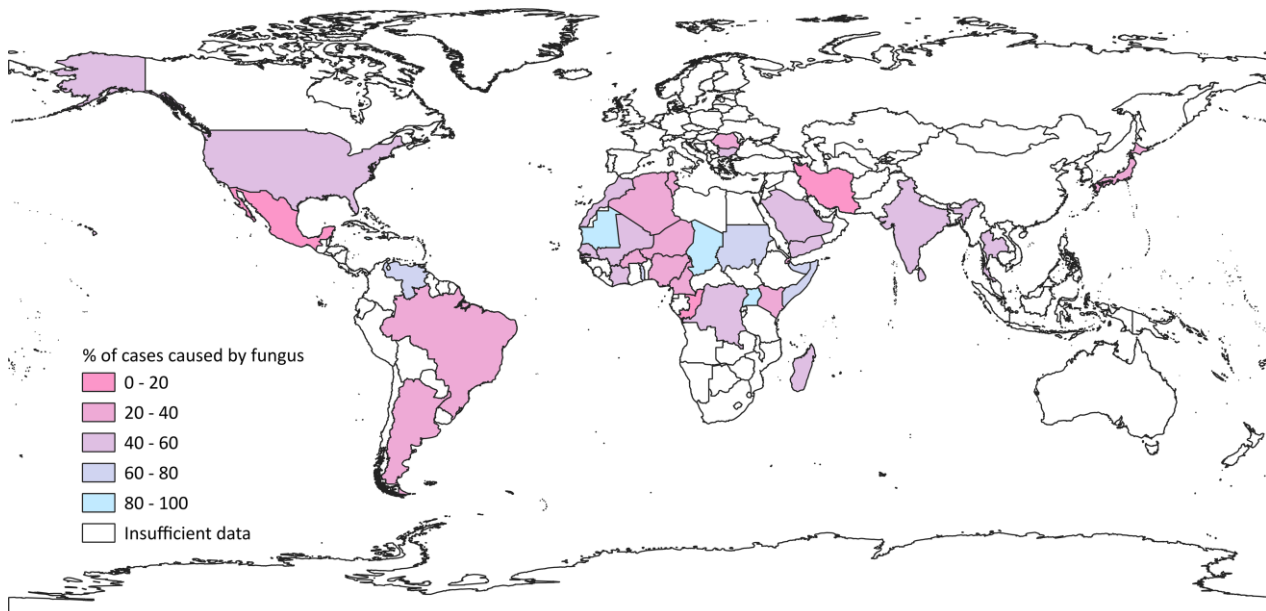


Figure 4.1: Prevalence of eumycetoma and actinomycetoma [121].

While the pathogens causing mycetoma are either fungal or bacterial, overall mycetoma can be caused by up to 70 different causative organisms [1]. Worldwide, the prevalence of mycetoma agents has been reported in [2] and recently in [121]. Considering the geographical regions, the authors of [121] found predomination for two species namely *Madurella mycetomatis* (*MM*) and *Nocardia spp.* This could be explained by the fact that their study focused on qualitative data rather than quantitative. As a result of this and the fact that even within the country, there are unbalanced mycetoma types, the mapping performed in [2] stands out for the

distribution of mycetoma causative organisms. Consequently, the most common causative organisms are *Madurella mycetomatis* (MM), *Actinomadura madurae* (AMM), *Streptomyces somaliensis* (SS), *Actinomadura pelletierii* (AMP), *Nocardia brasiliensis* and *Nocardia asteroides*. However, *Nocardia* prevalence is dominant in South America and Asia, and less frequent in Europe and Africa.

The sample of MyData database was collected at the MRC. Hence, the representation of the mycetoma types reflects the geographical distribution of mycetoma in Sudan where eumycetoma is more dominant. In addition, the organism MM, AMM, SS, and AMP are included in the database because *Nocardia* spp are commonly unseen in Sudan.

We considered the inclusion of the mycetoma organism in our database, although specifying them does not affect the treatment choices but the prognosis of the disease. Knowing this information could be suitable in cases where the created database is investigated for different purposes besides developing machine learning models for causative agent identification.

4.3 MyData Population

4.3.1 Sample collection and Selection criteria

Initially, MyData database included 180 patients with confirmed mycetoma infection who were seen at the MRC or from the field surveys in Sudan. Surgical biopsies were obtained from patients with various mycetoma types, duration and clinical presentations. Thirty-eight patients who had biopsies devoid of any grains and were excluded from the study. This is attributed to the fact that grains are the basis of diagnosis, and the conclusive diagnosis is not possible without their presence, even if the clinical symptoms are consistent with mycetoma infection.

Therefore, MyData database included samples from 142 patients with mycetoma infection. The patients were randomly selected among patients seen during the last five years to ensure homogeneity and accuracy of the diagnosis, regardless of age, sex, or race.

The ethical committee of Soba University Hospital, Sudan approved the study after collecting written informed consent from patients. A summary of MyData database population is given in [Table 4.1](#).

Table 4.1: The demographic of the studied population.

Age in years	10 -70	
Sex	Male	89
	Female	53
Type	Eumycetoma	80
	Actinomycetoma	62
Site of infection	Hands	40
	Feet	68
	Others	34
Duration in years	<1	18
	>1-5	69
	>5-10	46
	>10	9
Lesion size	Small (< 5 cm in diameter)	35
	Moderate (5–10 cm)	59
	Massive (> 10 cm in diameter)	48

The samples collected in this study originate mainly from Sudan, which impacts the distribution of mycetoma causative agents in our data. While we selected the samples

to balance the eumycetoma and actinomycetoma classes, we did not consider the genus and species for the selection step.

4.3.2 Sample diagnosis

Culture diagnosis of mycetoma cases has been performed by specialized microbiologists from the MRC to identify the causative agents. We review all the histology tissue blocks with the corresponding culture diagnosis and checked for misdiagnosis and/or incorrect identification of causative agents. In case of any conflict, the sample is excluded from the database.

In the second step, we explored all our data on the genus and species that caused the mycetoma. The identification of fungus species using culture is usually misidentified [2]. Therefore, in this study culture technique was used to identify actinomycetoma at the species level and eumycetoma at the genus level. For some of the eumycetoma samples, a molecular technique was used to assess them at the species level.

All the actinomycetoma samples in our database were identified as either *AMM*, *SS* or *AMP*, assessed using both grain culture and histopathology. Regarding our eumycetoma data, for 32 patients, we used both grain culture and histopathology to assess them as *Madurella spp. (Mspp)*, *Aspergillus spp. (Aspp)* or *Fusarium spp. (Fspp)*, and for 48 patients, we used a molecular technique to assess them as *MM* (*MM+*) or not *MM* (*MM-*). This data is summarized in [Table 4.2](#).

Table 4.2: The distribution of study samples.

Causative agent	Species	No. Patients
Eumycetoma	<i>Madurella spp. (Mspp)</i>	22
	<i>MM+</i>	29
	<i>MM-</i>	19
	<i>Aspergillus spp. (Aspp)</i>	8

	<i>Fusarium spp. (Fspp)</i>	2
Actinomycetoma	<i>Actinomadura pelletieril (AMP)</i>	9
	<i>Actinomadura madurae (AMM)</i>	9
	<i>Streptomyces somaliensis (SS)</i>	44

4.4 Histopathology and Slides Preparation

This section describes the fundamental steps of the histology process to prepare the tissue slides. These slides are imaged using an appropriate device to obtain the microscopic tissue images.

Histopathology studies the microscopic anatomy of biological tissue and examines any irregularity in manifestations in tissue to decide whether it is healthy or not [122, 123]. The name Histopathology is proposed by combining the Greek terms "Histos" which means tissue, "Pathos" which means disease, and "Logos" for study [124]. Generally, histology involves many processes from sample fixation to diagnosis. [Figure 4.2](#) yields a comprehensive view of this process.

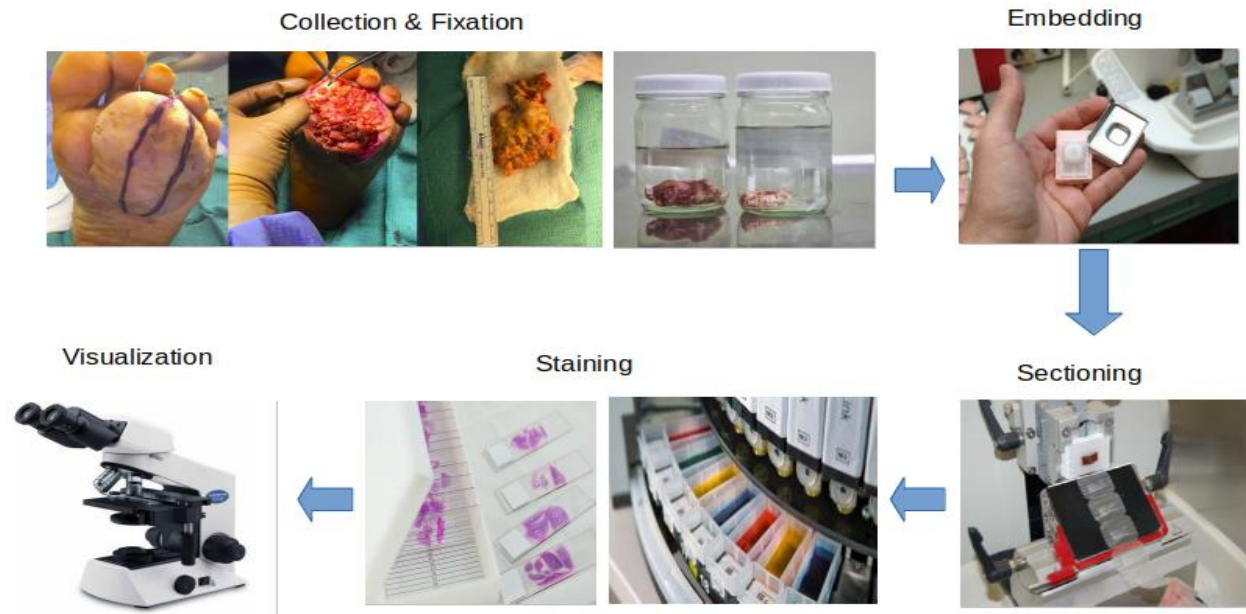


Figure 4.2: Histopathology Process.

4.4.1 Sample Preparation and Processing

Tissue collected from sight is under investigation for further examination through surgery or biopsies. Starting from collection until the yield of final remarks or diagnosis, three main steps are described and used in the standard histological practice. These fundamental steps and processes of histology slide preparation are reported extensively [123, 124]. These include:

- **Collection and fixation:**

The histology process starts when a physician obtains good-quality tissue for examination. Tissue can be collected through fine needle aspiration, tru-cut needle biopsy, or surgical biopsy. Larger biopsies allow for several slides and hence further examination and investigation. The collected biopsies are dipped into a fixative solution to prevent tissue from breaking down and microorganism growth. The fixation should be done immediately after collecting tissue from patients. Most commonly, Formaldehyde (formalin) is used for fixation. This process slightly reduces the size of the tissue before embedding.

- **Embedding and Sectioning:**

Embedding is performed to solidify the tissue to allow the production of thin tissue sections. The fixative tissue is embedded in supporting material, mostly paraffin wax, and produces tissue blocks. A microtome is used to cut tissue sections from tissue blocks. Usually, sections are cut with (3-5) μm thickness. After cutting, the sections are exposed to a heated water bath to melt paraffin and get rid of any wrinkles. Eventually, these sections are mounted on microscope glass slides to preserve them from damage and enhance visual quality for further analysis.

- **Staining:**

At this point, the glass slides are barely visible under the light microscope. So, the tissue sections need to be stained to add contrast that assists in identifying or distinguishing ROIs. Different stain types can be used, although Haematoxylin and Eosin (H&E) stain is the most commonly used stain in histopathology. Furthermore, many pathologists argued that H&E would continue leading for the next 50 years [125]. The staining process can be performed manually, semi-automated, or automated. The outcome, a stained histology slide, would be ready for screening and examination by the pathologist. For certain applications, this step is not applicable, and the result of sectioning is visualized for diagnosis.

The same process mentioned above is applied for mycetoma tissue slide preparation. H&E stain is the main focus of this work. It is considered a primary tissue stain as it is an easy, quick, well-established method, and allows visualization of all the tissue components and grains. All the slides' sections were stained with H&E according to standard routine laboratory procedures at Bretonneau Hospital, Tours, France. H&E is usually performed to distinguish between different tissue components. It stains nuclei with blue colour and gives the connective tissue a pink colour. Stained sections show mycetoma grains morphology as well as the tissue reaction and components.

4.4.2 Tissue Slides Visualization

The tissue slides cannot be seen with the naked eye, rather they have to be visualized under microscopy for appropriate diagnosis. The microscope is a device used to enlarge small objects without changing their actual physical size [126]. This

enlargement is known as magnification, and it is expressed in the form ($n \times$) to denote the number of times the object is being enlarged. Depending on the type of sample and investigation to be conducted, various types of microscopes can be employed such as optical or light, electron, and fluorescence microscopes. The optical light microscope, [Figure 4.3](#), is the oldest design of the microscope and yet the most popular one. It uses a system of lenses and visible light for object magnification. For mycetoma histopathological slide visualization, an optical light microscope is utilised.



Figure 4.3: Optical Light Microscope.

4.5 Preparation of Microscopic Images in MyData

This section describes the need for digital pathology and its advantages. Also, it provides the main steps of the acquisition of microscopic images from tissue slides to introduce the database.

Generally, in the diagnostic process, pathologists investigate for particular features within tissue slides, such as cell morphology and tissue structure and components. This investigation is mostly influenced by pathologists' experiences. The manual analysis of histology slides is very challenging since each section can contain many structures with uneven distribution of cells across the tissue, which might be surrounded by different tissue types. Furthermore, the reliability of the analysis is

closely related to the pathologist's experience. This is why working with histology slides manually is time-consuming and requires an experienced and skilled pathologist.

Digital pathology emerged as a sub-field of pathology that focuses on the acquisition, management, and interpretation of information from digital images [126, 127]. These images are often called photomicrographs. Digital pathology uses a computer algorithm to analyse images of tissue slides and report some clinical outcomes. With the growing trend of digital pathology, slide digitalization has been appended to the standard histopathological processes. This has several advantages, such as: i) It enables comparative analysis and links the screening process with different diagnostic tools. ii) Digital images can be shared with diverse physical locations, which could be useful for diagnostic consultation with specialized centres or pathologists and enhance teaching experiences. iii) Storing digital slides is more practical than glass slides which can be damaged, faded, or lost. Also, glass slides need more space to be kept.

Until the early 90s, the digital microscope, [Figure 4.4](#), was the most dominant method for slide digitalization [126]. It was invented as a modification to the optical microscope by mounting a digital camera on the optical microscope. Besides direct viewing of slides under the microscope, the camera can capture slide images or display them on a computer monitor if it is available. The computer software allows displaying different variants of the object and its magnified copies, filming the slide, and image archive. A new era of digital pathology began with the novel invention of the Whole slide imaging technique (WSI) often referred to it as "virtual microscopic". WSI employs whole slide scanners to capture the whole slide in a single shoot so-called digital slide. It is known to produce faster and more high-quality microscopic images. However, when adopting WSI for slide digitisation, the setup and maintenance cost is a major limitation [127].



Figure 4.4: Digital Light Microscope.

4.5.1 Mycetoma Tissue Images Acquisition

As mentioned in [Section 4.3.1](#), the database included tissue blocks of 142 patients. The tissue slides of these patients were handled with a unique reproducible acquisition protocol to ensure a uniform database.

Microscopic images were captured in RGB colour space with Nikon Eclipse 80i digital microscope ([Figure 4.4](#)) under the conditions given in [Table 4.3](#). We used the digital microscope instead of WSI because it is commonly available in endemic areas laboratories, especially rural areas. Furthermore, the digital microscope is easy to use and set up.

Table 4.3: Microscopic Acquisition Conditions.

Parameter	Value
Brightness control	Knob 5/10 ND8 On ND32 On
Field diaphragm	Highest level
Highest level	10×
Dimension and Quality	800 × 600
Colour	Enhance and white auto
Field diaphragm knob	Highest level
Filter	6
NCB11 Filter	Off

The database contained a total of 864 microscopic tissue images from 142 patients. It is composed of 471 eumycetoma and 393 actinomycetoma images. For each patient, different grains were considered, with an average of six grains per patient. [Table 4.4](#) gives the summary of database images. Although the screening of tissue slides focuses on capturing a single grain in each field ([Figure 4.5A](#)) some slides have contiguous grains, which led to the appearance of many grains in one image ([Figure](#)

4.5B). In the latter case, we consider one grain per image to be included in the database.

Table 4.4: Summary of images in MyData considering the mycetoma organisms.

Causative agent	No. Images	Species	No. Images
Eumycetoma	471	<i>Madurella spp. (M spp)</i>	149
		<i>MM+</i>	167
		<i>MM-</i>	110
		<i>Aspergillus spp. (Aspp)</i>	36
		<i>Fusarium spp. (Fspp)</i>	9
Actinomycetoma	393	<i>Actinomadura pelletieril (AMP)</i>	57
		<i>Actinomadura madurae (AMM)</i>	62
		<i>Streptomyces somaliensis (SS)</i>	274

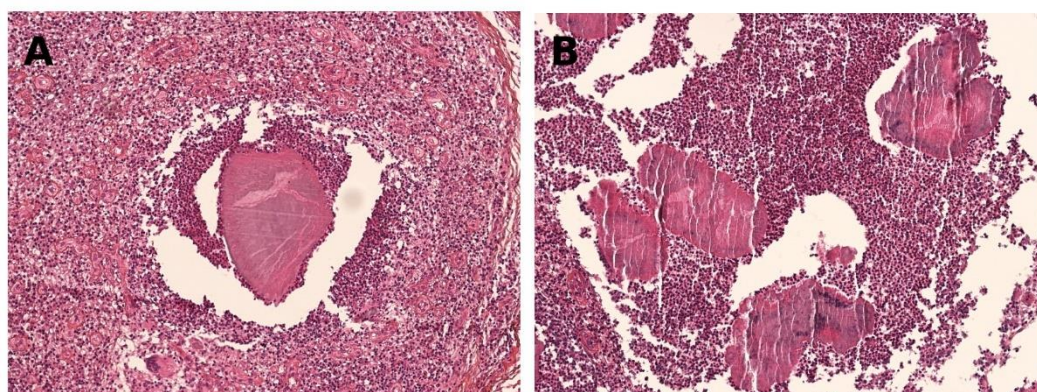


Figure 4.5: Mycetoma Microscopic Images. (A): Single grain. (B): Multiple grains.

4.5.2 Ground-truth Segmentation of Mycetoma Grains

To establish the histology diagnosis, in the beginning, the grain(s) must be located within the tissue to determine the causative agents for the appropriate treatment. Hence, mycetoma grains are the ROIs of the tissue image. Consequently, performing manual grain segmentation was necessary to produce a complete and proper database of mycetoma tissue grains and their associated grains annotation. In this way, this database could be used for any computational tasks related to histology tissue diagnosis.

From microscopic images of mycetoma-infected tissues, grains were manually segmented using ImageJ software. We generate an annotation of each image in the data set by assigning a label for each pixel in the image as ROI or background. These labels are set as 1 for ROI and 0 for background. Then, the original images and their annotations can be used for machine learning model training and validation.

The accuracy of any machine learning model will depend on the accuracy of our manual segmentation. Therefore, this segmentation is carried out in a way that constricts the border of the grain and avoids the inclusion of any other tissue components or inflammatory cells unless they are inside the grain itself. Also, the annotated grains should contain all the grain's area even if there is a slide background within the grain and/or fracture in the grain appearance. [Figure 4.6](#) shows illustrative microscopic images along with the ground-truth grains.

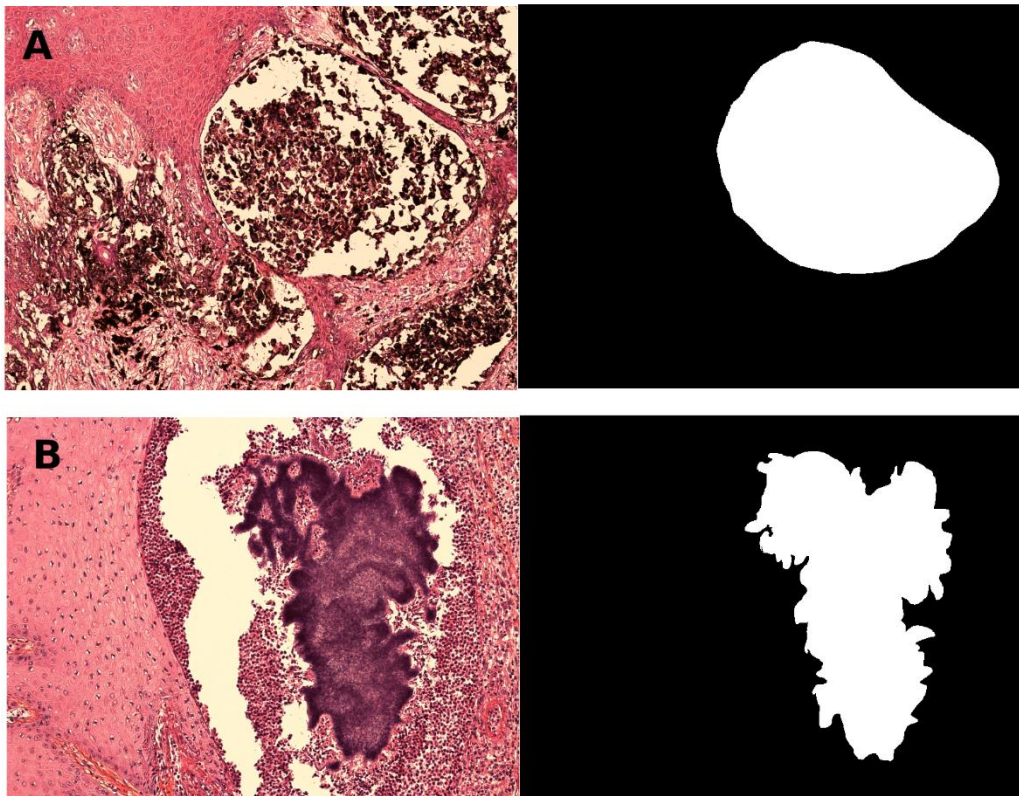


Figure 4.6: Mycetoma Microscopic Images and its annotated grain. (A): Eumycetoma with fractured grain. (B): Actinomycetoma grain.

4.6 MyData: Mycetoma Histology Microscopic Images Database

During the last decades and with the increment of computational power and high-quality digital microscopes, many histopathological image databases have been introduced. However, mycetoma has not gained any benefit in this revolution. Hence in this section, we construct the first database of mycetoma histopathological microscopic images. This database will be used throughout this thesis to build two computational models which turn into an automated diagnostic model based on microscopic tissue images of mycetoma.

4.6.1 Images conditions

4.6.1.1 Technical and human errors:

The tissue samples used for preparing the MyData database were collected, labelled, prepared and diagnosed by a group of laboratory technicians and pathologists. After collection, the labelled samples are sent for processing and diagnosis using histopathological and culture techniques. Once the results of both investigations are available, we compare them to ensure they are identical, otherwise, the sample is removed from the database. Also, double-check the labels of the samples and the result is made. Hereby, we eliminate any source of errors in the diagnosis process.

One of mycetoma histology diagnostic obstacles is the complete or partial vanishing of grains in tissue slides though they exist in the tissue blocks. Mostly, this is caused by the sectioning or mounting of the section on the slides. Mycetoma grains sometimes have a solid or rigid texture which results in improper sectioning because of the fine thickness of slides. We prepared two slides for each patient sample to ensure that the tissue slides of all the samples contained grains.

The folding of sections in the slides and their dissociation is a common issue in classical histology tissue processing. Therefore, we considered this issue to be a normal condition in mycetoma tissue processing. Slides with folds are handled as regular slides and maintained within the database. In addition, among the two prepared slides, we utilised the slide that contains the grain and, at the same time, has a better appearance in terms of folding and tissue separation.

4.6.1.2 Adequateness of samples for publishing database:

MyData database was initially collected and prepared for the purpose of developing a diagnostic model for mycetoma. Later, the possibility of publishing this database to the scientific communities was considered. The collected samples reflect the epidemiological distribution of mycetoma in Sudan, the epicentre of mycetoma. In Sudan, 73% of the recorded case are eumycetoma while *MM*, *SS*, *AMM*, and *AMP* are reported as the common mycetoma organism.

Consequently, we believe MyData database is adequate for publishing because mycetoma is a neglected disease hence the size of the database is acceptable and comparable to the total infected population. Also, the causative organism contained in this database covers the most common organisms reported in Europe and Africa and is less frequent in South America and Asia. In light of this, the MyData database is a good start for the first mycetoma histopathological microscopic database and could be expanded in the future.

4.6.2 Exclusion and inclusion criteria of samples in MyData

Considering the aforementioned conditions, we defined the following criteria for the inclusion and exclusion of images from the presented database:

- For each patient, all the grains in the tissue slide are included regardless of their size and shape.
- Sometimes the grain could be bigger than the image size, although it fits the field size, in this case, the part of the grain which is visible within the image size is included in the database, [Figure 4.7A](#).
- Sections which show partially folded grains ([Figure 4.7B](#)) are included, while completely folded grains are removed from the database.
- Two reasons caused the dissociation of mycetoma tissue sections either tissue reaction or tissue processing, [Figure 4.7C](#). Both cases of dissociation are included.

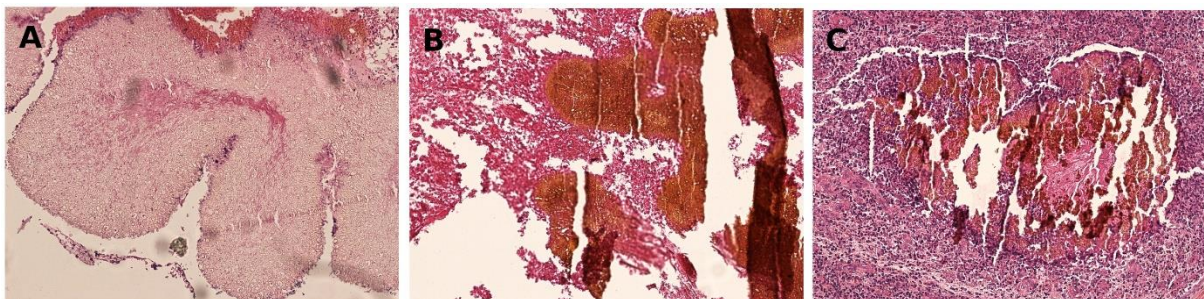


Figure 4.7: Example of the images included in the database. (A): Large grain. (B): Folded grain. (C): Dissociation grain.

4.6.3 Labelling

Image labelling identifies the image's content by assigning informative tags to the images in the database. Labels provide a context to the images such that the machine learning model could learn from them and make the correct task.

Labelled was defined with consideration for the patient ID to avoid statistical bias. We use the notation FM and BM for eumycetoma (fungus) and actinomycetoma (bacterial), respectively. The naming format is main-type_subclass-number_patient-ID_grain-number. For example, *BMC1_3_4* means it is the first subclass of actinomycetoma sample from patient 3 for grain 4. A suffix is appended to the name of the image to indicate whether it is the original image or the ground-truth segmented grain of the same image.

In some cases, the collected tissue is quite big for embedding in one block therefore, it is possible to have a duplication of tissue blocks for the same patient. One label is given for these blocks, just different numbers of grains.

4.6.4 Secondary dataset

In the secondary dataset, the H&E staining process was performed manually with the local procedure, and no specific instructions were given for image acquisition. An Olympus 1.3MP integrated digital microscope was used for image capturing with 10× magnification, while lighting and tuning conditions were not unified. Therefore, this dataset covered several sources of technical variability that can limit the performance of predictive models [128].

The secondary dataset consisted of 12 actinomycetoma and 14 eumycetoma tissue images. It was collected from 26 mycetoma patients, with one tissue image per patient.

[Table 4.5](#) gives the distribution of the secondary data set.

Table 4.5: Distribution of the Secondary dataset.

Causative agent	Patients	Samples	Genus	Patients	Samples
EM	14	14	Madurella spp.	11	11
			Aspergillus spp.	3	3
AM	12	12	AMP	2	2
			SS	8	8
			AMM	2	2

4.7 Conclusion

This chapter presented the creation of the first database of mycetoma histopathological microscopic images, called MyData. It also provided detailed information on the samples used to create this database. This database is appropriately collected, prepared, analysed, and labelled. MyData database contains 864 microscopic tissue images along with the segmented ground-truth grains images from 142 patients. It includes 80 eumycetoma and 62 actinomycetoma samples and covers four of the five most common mycetoma species reported globally. Because of this, we believe this database is the first step towards creating a broader and larger database with various species from all over the globe, especially since a specific preparation and acquisition protocol is provided. MyData opens the space for recruiting more laboratories around the globe for the collection of new samples. It also encourages creating databases for different types of mycetoma images such as X-rays and ultrasound images.

In addition, we provided a guideline and optimized protocol for the preparation and acquisition of the image. Using this guideline for image production has many benefits such as: maintaining consistency and improving quality assurance, reducing errors and enhancing productivity, and avoiding the loss of the information presented in the data.

Because the MyData database will be used to develop machine learning models for mycetoma based on histopathological images, we intended to cover the factors that impact the success of such models. One of these factors is the quality and variability of the histopathological image acquisition. In the domain of histopathological image analysis, the quality is defined by the preparation of tissue slides and image acquisition protocol. Heterogeneous dataset from different laboratories is a concern making it difficult to deploy machine learning model to all the datasets at once. Yet this heterogeneity is necessary for the model to operate efficiently at different sites with different inputs. We incorporated a relatively small dataset with heterogeneous preparation and acquisition with MyData, which has a homogeneous standard.

The next chapter will propose a machine-learning model that differentiates between mycetoma types using the MyData database.

Chapter 5: Mycetoma Causative Agent Classification Model - mAlcetoma

Summary

In the previous chapter, we detailed the creation of the first database of mycetoma histopathological microscopic images to be used for the development of machine-learning models for diagnostics purposes. In this chapter, this database was used to develop a model that addresses the problem of identifying mycetoma type in a tissue image. Identifying mycetoma type is an essential step in mycetoma management since it greatly affects treatment choices. Incorrect differential diagnosis of mycetoma can have serious consequences on the patient and the disease prognosis and outcome. Throughout this work, the classification of mycetoma refers to differentiating between eumycetoma and actinomycetoma from grains features in histopathological microscopic images. Hence, this chapter describes our proposed model for mycetoma classification. We introduced a computational method based on radiomics and Partial Least Squares Discrimination Analysis (PLS-DA). The chapter is organized as follows; [Section 5.1](#) presents the methods used in our experiments. [Section 5.2](#) elaborates on the proposed classification model and presents the experimental results in [Section 5.3](#). We summarize the chapter with the main findings and discussion in [Section 5.4](#). A conclusion of the work is finally given.

5.1 mAlcetoma: The Proposed Framework

5.1.1 Overview of the proposed model.

The traditional mycetoma histopathological differential diagnosis used by pathologists is illustrated in [Figure 5.1A](#). The pathologist examines the H&E tissue slide to determine the causative agents and hence the mycetoma type. Optical light microscopes are used to visualize these slides. Commonly, a digital camera is

mounted on these microscopes to capture the microscopic images. Another alternative for this system is the digital microscope. Both systems can capture the images of the H&E stained tissue slide and transform them into a coloured image for agent identification.

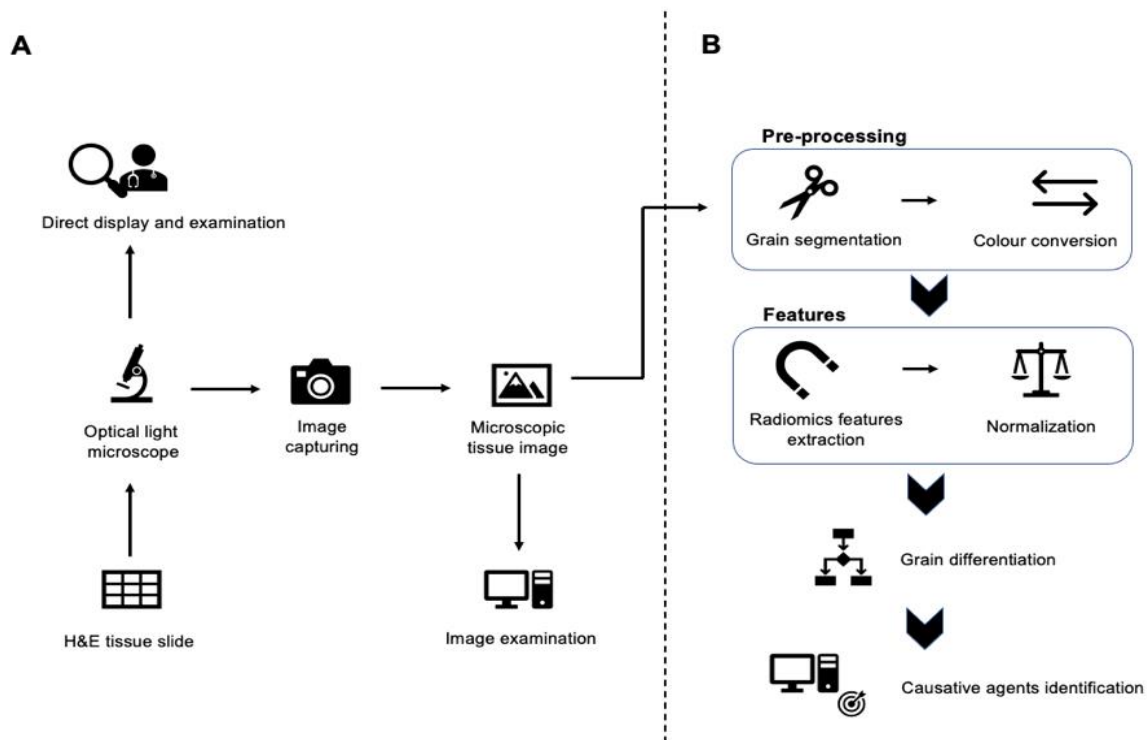


Figure 5.1: Histology diagnosis system. (A): Classical clinical setting, (B): Proposed radiomics model.

The presented mAlcetoma model is based on the analysis of H&E histopathological microscopic images from tissue biopsies obtained from mycetoma patients. Therefore, the model aims to identify the causative agents of a given mycetoma biopsy. Our proposed model is introduced as a complementary assistant tool to the routine histopathological pipeline, as depicted in Figure 5.1B. It is comprising of three main components: pre-processing, feature extractions, and classification.

5.1.2 Samples and Images Acquisition.

Two sets of data were utilised for this part of the study, namely the primary dataset and the secondary dataset which are described in Chapter 4.

The primary set was acquired following a unique protocol and used to train and validate the model. While the secondary dataset was used to evaluate the robustness of the model for the technical variability.

5.1.3 Pre-processing and Features Extraction.

Pre-processing should be performed before applying any classification method to improve the quality of the input images. When dealing with microscopic images, pre-processing step aims mainly at normalizing different colour variations. These variations include staining conditions, tissue section thickness, and microscopes models. Various methods have been proposed to address problems that are related to staining ([Section 3.2](#)). The weighted grey version of the original RGB images is considered throughout our experiment.

[Figure 5.2](#) shows illustrative eumycetoma and actinomycetoma microscopic images in the first and second columns, respectively, along with the segmented grains.

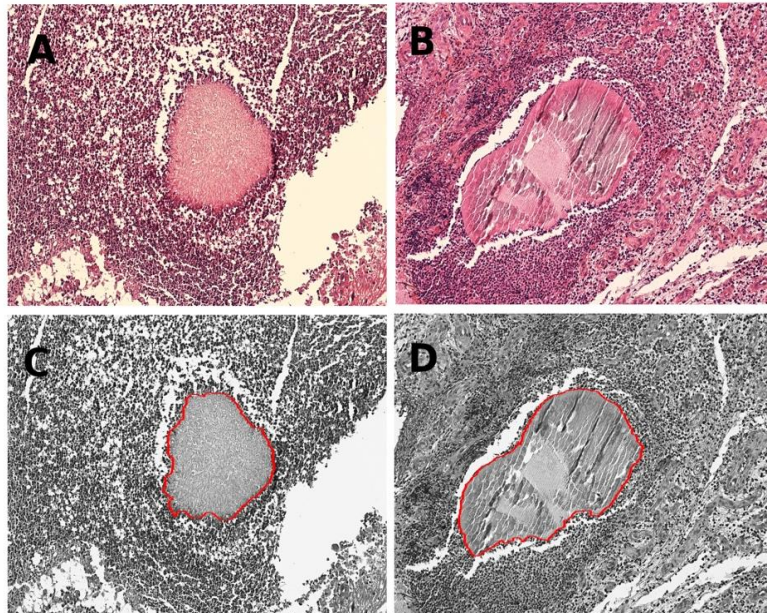


Figure 5.2: Sample grains of Eumycetoma (left) and Actinomycetoma (right). (A, B): tissue sections stained with H&E; (C, D): manual segmentation of the grains.

Grains in microscopic images are characterized through Radiomics features ([Section 3.4.1](#)). These features were composed of 102 variables divided into nine shape descriptors, 18 first-order statistics, and 75 texture features. Shape features were extracted from the grains labelled masks, while all other features were based on grey intensity values at the pixel level in microscopic image classes. Labelled masks are ground-truth grain images where background and grains pixels are set to zero and one, respectively. PyRadiomics package version 2.2.0 was used for feature extractions [97].

The extracted features might have a different scale and range of real-valued variables, which can put more weight on a variable with a large range. Therefore, a fundamental step of feature pre-processing is applied to ensure that features are on the same scale and equally important. Standardization (z-transformation) is a feature scaling technique which results in a zero mean and unit variance of features, that is, each feature (X) is re-scaled to ensure the mean (μ) of 0 and the standard deviation (σ) 1.

Radiomics features are standardized by auto-scaling and used as an input to build the predictive model using [Equation 5.1](#), where x_i is a real value of the sample i for a feature z and where m is the number of samples. Auto-scaling uses standard deviation as a scaling factor and converts features into differences that are relative to their standard deviation, hence the features are analysed based on correlation [129].

$$x_{i-scaled} = \frac{x_i - \mu_{x_i}}{\sigma_{x_i}}$$

$$\mu_x = \sum_{j=1}^m \frac{x_j}{m}$$

Equation 5.1

$$\sigma_x = \sqrt{\sum_{j=1}^m \frac{(x_j - \mu_x)^2}{m - 1}}$$

5.2 Modelling and Analysis

A Partial Least Square-Discrimination Analysis (PLS-DA) model was adopted for mycetoma grains classification. PLS-DA is a supervised classification method that

combines the properties of the Partial Least Square (PLS) regression model with a classification technique. For PLS-DA modelling, the features set X of the image is analysed. X is a $m \times n$ matrix, and each row represents the different extracted features of one individual sample, where m indicates the number of samples and n is the number of features. The class membership is translated into a dummy column vector Y by values of "1" and "-1" that indicate if a sample is a eumycetoma (EM) and actinomycetoma (AM).

The procedure of the PLS-DA model is given in [Pseudocode 5.1](#) [130–132]. The source of variability was modelled by Latent Variables (LVs), which are linear combinations of the extracted features in X . The maximum variation of X is determined by the weight vector $W \in \mathbb{R}^{m,1}$. The whole set of features X was used for grains classification due to the ability of the PLS-DA model to reduce the impact of the irrelevant features. Hence, the loading vectors ($P \in \mathbb{R}^{n,1}$) and ($Q \in \mathbb{R}^{1,1}$) are the coefficients assigned to features in their linear combination with various magnitudes based on the importance of features, so loading vectors indicate the influence of each feature on each LV. Similarly, X-Score ($T \in \mathbb{R}^{m,1}$) represents the coordinates of samples in the LVs projection. Each LV generates a variation which sums up the total variation contributed by the other LVs. The residual variation not estimated by the current LV is updated as a new feature set. In practice, the number of LVs is chosen to achieve the lowest error, and it is important to note that a sufficient number of LVs could produce perfect performance.

Pseudocode 5.1: PLS-DA Model Construction.

Input: Features Set ($X \in \mathbb{R}^{m,n}$), dummy variable ($Y \in \mathbb{R}^{m,1}$), and the number of LVs (A)

Output: Regression Matrix (B)

for i in A do

Weight Vector: $w = XY$

X-Score: $t = \frac{Xw}{\sqrt{\sum w^2}}$

$$\text{X-Loading: } p = \frac{t'X}{\sqrt{\sum t^2}}$$

$$\text{Y-Loading: } q = \frac{Y't}{\sqrt{\sum t^2}}$$

$$\text{Regression Coefficient : } b_i = w(pw)^{-1}q.$$

$$\text{Residual of X: } res_x = X - tp$$

$$\text{Residual of Y: } res_y = Y - tq$$

$$X = res_x$$

$$Y = res_y$$

end for

$$\text{Regression Matrix: } B = \{b_1, b_2, \dots, b_A\}.$$

Eventually, matrix B provides the regression coefficients which describe the relationship between mycetoma grains features X and mycetoma classes Y .

For the prediction purpose, the model uses the regression coefficients B and features set X of unknown samples to predict whether they are FM or BM as follows:

$$Y_{pred} = XB$$

Since the PLS-DA model is inherited from the PLS model, the estimated Y_{pred} is never an integer with an exact membership (i.e 1 or -1). Several decision rules can be used to convert the predicted values into their essential classes [130]. In this study, rather than using the default zero value as a classification threshold. We proposed to estimate it based on Bayes's theory to optimise the class membership. The Bayesian threshold calculation assumes the predicted values of both classes fit into a Gaussian distribution. This gives the probability of any sample belonging to class EM/AM from its predicted value Y_{pred} . The estimated threshold value is selected at the point where the number of false positives and false negatives is minimised on the training data set [133–136].

The images of the different patients from the primary dataset were randomly split into training/validation with 70%/30% proportions. A summary of the data set is presented

in Table 5.1. Each patient's data were forced to be either in training or validation set and not spread between both to avoid statistical bias.

Table 5.1: The Split of the mycetoma database into training and validation datasets with a 70%/30% proportion.

Causative agent	Species	Training	Validation
EM	<i>Madurella spp. (Mspp)</i>	99	50
	<i>MM+</i>	120	47
	<i>MM-</i>	71	39
	<i>Aspergillus spp. (Aspp)</i>	26	10
	<i>Fusarium spp. (Fspp)</i>	6	3
AM	<i>AMP</i>	41	16
	<i>AMM</i>	50	12
	<i>SS</i>	192	82
	Total:	605	259

All the PLS-DA analysis was performed using MATLAB software version R2017b, libPLS library [137] and homemade MATLAB routines.

5.2.1 Quantitative evaluation.

According to recommended practices discussed in [130, 138], the PLS-DA model can be validated by three different strategies; internal, external, and optional methods. Generally, optional methods such as bootstrapping and permutation tests are rarely used, and the data size governs the choice of using internal and external strategies. Internal methods such as cross-validation are used with a small dataset ($N < 1000$). The proposed model was assessed using two different ways, internal validation and bootstrap as an optional validation method.

First, we performed Cross-Validation (CV) as an internal validation method to assess the complexity of the model by determining the optimum number of LVs. This allows us to evaluate the complexity of the model considering the predictive ability of the model itself [130, 134]. The proposed model was trained with Venetian blinds 10 folds-Cross-Validation (10 CV), and the minimum CV classification error was considered to select the LVs number [134, 139–141]. In our experiments, the smallest error was associated with 16 LVs, [Figure 5.3](#). However, using a high number of latent variables can often be associated with overfitting. This means that the model would perform well on the learning dataset but fail on other data sets. To prevent overfitting and have a stronger generalisation capacity, we opted for fewer variables and considered seven latent variables. The difference in CV error between using 16 LVs (0.0656) and 7 LVs (0.07281) was small in the training data, and the model behaved better on testing data.

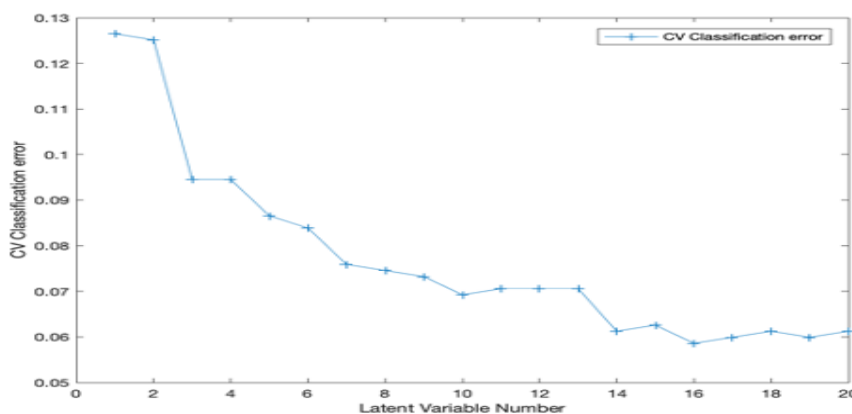


Figure 5.3: Classification Error of the PLSDA model.

Secondly, we employed a bootstrap test for further assessment of the model's robustness and estimates of the uncertainty of the prediction. In the bootstrap technique, new datasets were generated by applying sampling with replacement techniques of the original dataset [141]. In the beginning, we compute the residue of our model $F \approx y_{real} - y_{pred}$. Then, bootstrap the newly generated samples and estimate the residuals bootstrap \hat{F} . Finally, the confidence interval for each sample in the model is evaluated using the quantiles. We define upper and lower limits of intervals such that they are asymmetric and specific through the percentile method setting the number of bootstraps β and α is the degree of confidence:

$$\hat{F}\beta\left(\frac{\alpha}{2}\right) \leq y \leq \hat{F}\beta\left(1 - \frac{\alpha}{2}\right)$$

Furthermore, the Variable Importance in Projection (VIP) score was analysed to understand the importance of each feature in the PLS-DA model and how strongly they contribute to the classification. For the features set X , VIP measures the weight of each feature in X using the explained variance of each LV (Equation 5.2) and accumulates the weights that were produced from each LV to reflect the importance of the feature [142]. Usually, it is considered that VIP scores have a threshold value of 1, meaning that the features which score greater than 1 in the model are significant for the prediction ability [143].

$$VIP = \sqrt{\frac{A \sum QT \frac{W}{norm(W)^2}}{\sum QT}} \quad \text{Equation 5.2}$$

where Q , T , and W represent Y loading, X -score, and weight matrices, respectively.

Finally, the performance of the model was evaluated through diagnosis accuracy, Matthew's Correlation Coefficient (MCC) [144], F1 score [145], sensitivity and specificity. Equation 5.3 gives the formulas for these measurements where TP and TN are the numbers of true positive and negative cases, and FP and FN are the numbers of false positive and negative cases. To evaluate the robustness of the model, the area under the curve (AUC) was also computed by aggregating the model's performance across different thresholds.

$$Acc = \frac{TP + TN}{TP + TN + FP + FN}$$

$$Spec = \frac{TN}{TN + FP}$$

$$Senc = \frac{TP}{TP + FN}$$

Equation 5.3

$$MCC = \frac{TP * TN - FP * FN}{\sqrt{(TP + FP)(TP + FN)(TN + FP)(TN + FN)}}$$

$$F1 = \frac{TP}{TP + \frac{1}{2}(FN + FP)}$$

5.3 Experimental Results

5.3.1 Causative agents' classification

The projection of the primary validation data set is shown in [Figure 5.4A](#). It depicts the scores plot and projection of samples concerning the first three LVs generated by our prediction model. LVs represent the combinations of the grain features that best discriminate between eumycetoma and actinomycetoma. The plot demonstrates a separation for the discriminated classes in the estimated feature space, where two loose clusters can be identified for the mycetoma classes.

The class prediction for the validation dataset is given in [Figure 5.4B](#). The threshold of 0.0635, obtained from Bayes' theorem, is shown as the horizontal red dashed line and applies to sample classification. A sample is labelled as AM if it scores a value greater than 0.0635 and EM otherwise. With this prediction, many EM samples were misclassified compared to AM. It might indicate that while most eumycetoma samples were correctly classified, a few samples presented similar actinomycetoma radiomics features.

To assess the model on external data set, the secondary dataset was used to evaluate the robustness of the model with images from new patients with distinct acquisition

parameters and slide preparation techniques. [Figure 5.4C](#) shows the classification of the secondary dataset. The proposed model achieves 96.15% accuracy confirming the robustness of our approach compared to the results obtained in the validation dataset.

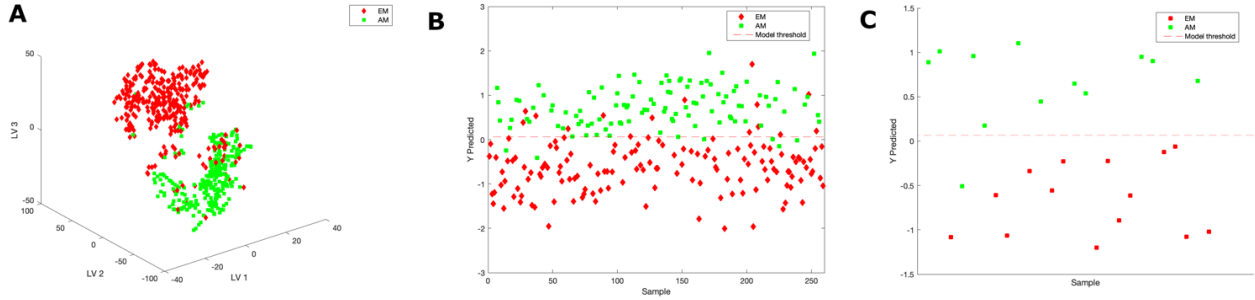


Figure 5.4: (A): 3D projection of mycetoma validation data on the first three latent variables. (B): Class predictions on a primary validation set. (C): Class predictions on the secondary dataset.

On the primary dataset, our model reached an accuracy of 92.2% on the training set and 91.89% on the validation set, with respective sensitivity of 93.5% and 94.5% and specificity of 90.9% and 90.3%. Matthew’s correlation was 0.844 and 0.838 for respectively the training and validation sets. On the secondary dataset, the model reached an accuracy of 96.15%, with a sensitivity of 100% and a specificity of 91.67%, with Matthew’s correlation of 0.925. The AUC was respectively 0.9531 and 0.8958 for the primary and secondary validation datasets. These results are summarized in [Table 5.2](#). Based on our experiments, the model is reliable and robust with similar results obtained between training and validation. The value of sensitivity and specificity are good estimates of the model, and they are compatible with the prediction in [Figure 5.4B](#).

Table 5.2: Estimated metrics for the model.

	Primary dataset		Secondary dataset
	Training	Validation	Validation
Accuracy	92.2%	91.89%	96.15%

Matthew's correlation	0.844	0.838	0.9250
F1-score	0.9578	0.9273	0.9655
Precision	0.9578	0.9571	0.9333
Sensitivity	0.935	0.945	1.0
Specificity	0.909	0.903	0.9167
AUC	0.9741	0.9531	0.8958

The Bayesian threshold estimation for class discrimination is illustrated in [Figure 5.5](#) where the ROC curve ([Figure 5.5A](#)) and Sensitivity/Specificity for each threshold ([Figure 5.5B](#)) are presented. An AUC of 0.9531 was achieved on our data.

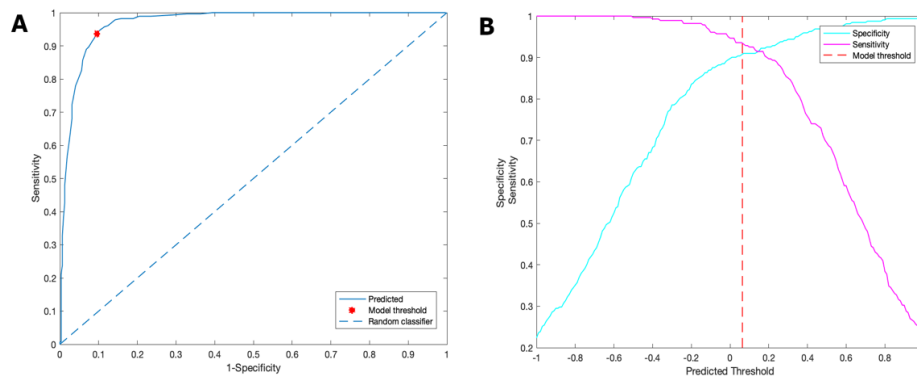


Figure 5.5: Receiver Operating Characteristic curves (ROC) and threshold plots.

Recognizing the uncertainty of mycetoma prediction can provide better insight into the classification. To do this, we employ the residual bootstrap. Due to the random nature that results from replacement, the bootstrap method can result in different outcomes when applied to the same dataset. To overcome this and maintain the reliability of the bootstrap, the number of bootstraps was optimized to obtain the lowest standard

deviations. Thus, we repeat the calculations 100 times for a different number of generated datasets (1000, 2000, and 3000 samples) and observe the standard deviation of the residuals. Consequently, we obtain the lowest standard deviation with 2000 resampling. We computed the confidence intervals at 95% and registered the lower and upper limits ranging from -0.4 to 0.5 for our prediction. These values produce the error bars of our dataset and provide a better understanding of the prediction uncertainty, [Figure 5.6](#). This plot brings our attention to the fact that some samples score values near the threshold value, which suggest the features of these samples class have a great amount of similarity to other class. This cannot be observed using the metric in [Table 5.3](#), hence the confidence intervals show the importance of analysing the uncertainty of the prediction.

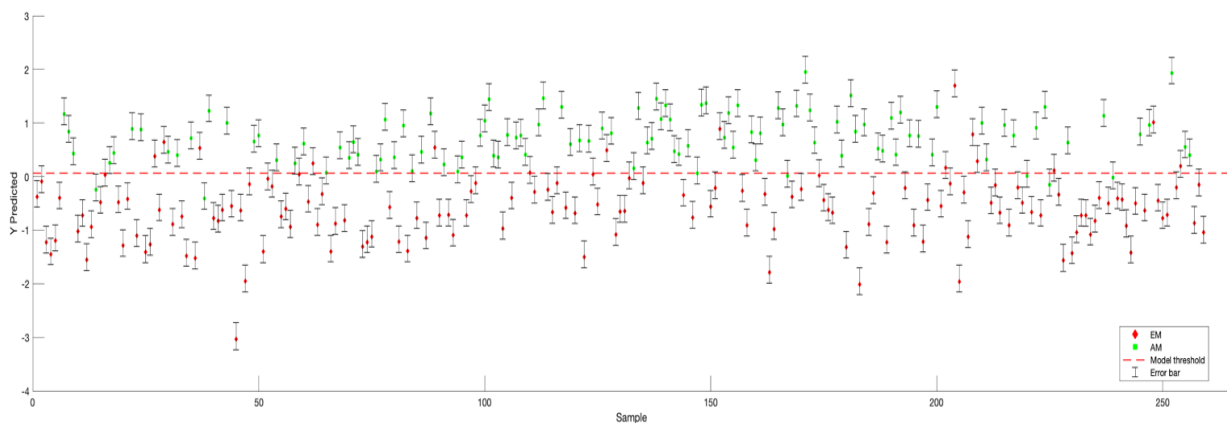


Figure 5.6: Samples predictions and confidence intervals on the validation dataset.

5.3.1.1 Causative organisms' classification

Although mycetoma management is mainly guided by the correct identification of the causative agents, there is a correlation between prognosis and species identification. Therefore, it was interesting to inspect the ability of our proposed model on the classification of genus/species besides causative agents. As given in [Table 5.1](#), the training and validation data set is composed of the same proportion of each species to ensure the balance distribution of species.

[Table 5.3](#) shows the performance of our model across different species. We computed the model's accuracy for mycetoma species during the training and validation process

to assess whether the obtained accuracy demonstrate overfitting. Clearly, two species of eumycetoma (*Aspergillus* and *Fusarium*) show poor performance compared to the other species because there are few samples for the model to train. The species classification for the validation dataset is given in [Figure 5.7](#).

Table 5.3: Accuracy obtained for all genes/species on the validation dataset.

Species	No. Images	Training accuracy	No. Images	Validation accuracy
AM - SS	192	94.79%	82	93.9%
AM - AMM	50	93.18%	12	91.6%
AM - AMP	41	100%	16	100%
EM - Madurella spp.	99	97.98%	50	94.0%
EM - Aspergillus spp.	26	88.89%	10	60.0%
EM -Fusarium spp.	6	100%	3	0%
EM - MM+	120	90.02%	47	91.4%
EM - MM-	71	95.83%	39	92.3%

We should emphasise that the same model of eumycetoma and actinomycetoma classification was used to measure the performance of the species classification. Our proposed model is trained for a binary classification task and therefore it is not suitable for predicting the species.

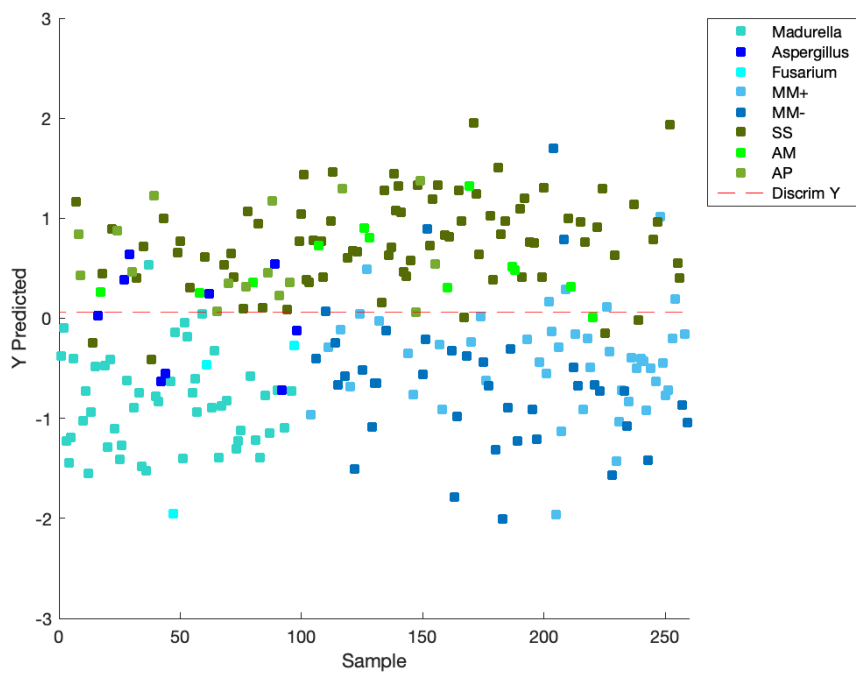


Figure 5.7: Genus's classification on the validation dataset.

5.3.2 Radiomics features importance.

The VIP scores obtained on the primary dataset for the radiomics features of the grains are presented in

Figure 5.8. Analysing VIPs score of grain features with a threshold value equal to 1 qualified more than 40% of the features to be significant for differential diagnosis. Therefore, a threshold of 1.2 was considered to highlight the most important features.

In our experiments, we found that the role of shape features was trivial, while texture features were dominant for classification. We observed that most of the significant features were related to grains' variance, entropy or complexity. The top VIP score was reached by the joint distribution of low grey values and spatial connectivity between a pixel and its neighbours. This feature is an indicator of the homogeneity of textures and the tendency for closer blocks to have similar spatial variation. The data shown in [Figure 5.9](#) illustrates the great heterogeneity in shapes that can be found in histopathological data. These shape features, which obtained a very low VIP, were not important to achieve a good classification. On the contrary, [Figure 5.10](#) represents samples of grains that score the lowest and highest VIPs for some of the top classification features. Among them Grey Level Variance which measures the variance in grey-level intensity of the consecutive and adjacent blocks within the grains. In contrast, difference variance indicates the heterogeneity of texture inside the grains.

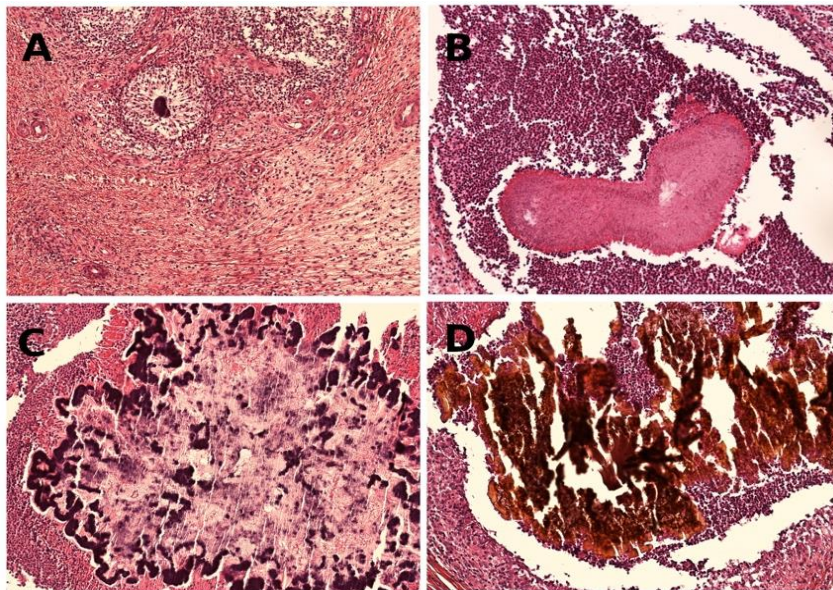


Figure 5.9: Diameter of the grains. The first and the second rows represent the grains that have the shortest and longest diameters, respectively. (A, C): actinomycetoma, and (B, D): eumycetoma.

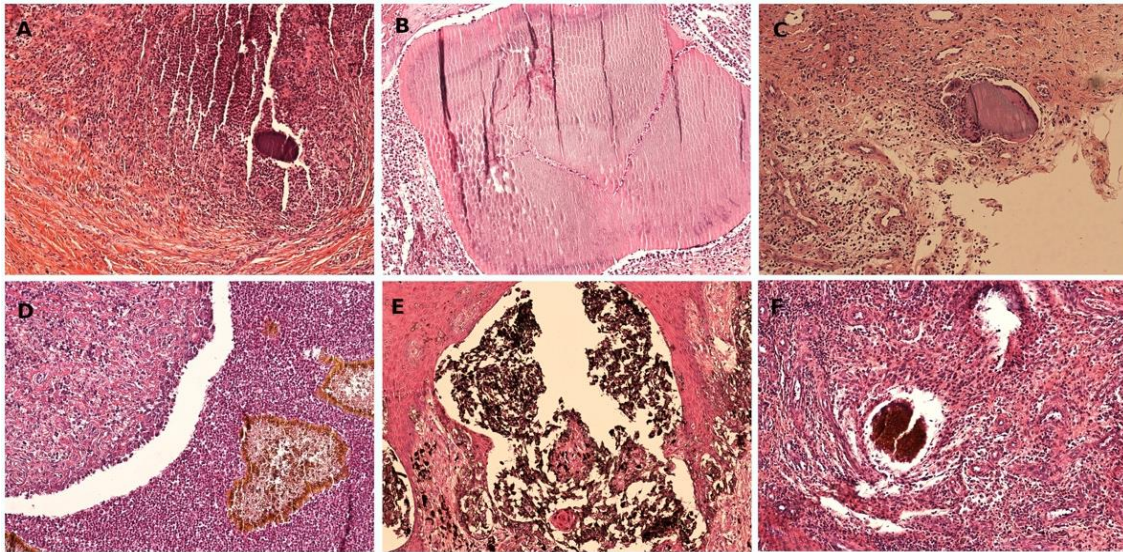


Figure 5.10: Grains which score greatest and smallest score for selected VIPs. Actinomycetoma grains (lowest score) are depicted in the top row and eumycetoma in the bottom row (highest score). (A, D): Difference variance, (B, E): Small dependence low-grey-level emphasis (peak feature), and (C, F): Grey-level variance.

5.3.3 Robustness to segmentation errors.

Since that not all users of our approach will be experts in mycetoma grains segmentation (they probably will not master selecting only the grain without any other tissue components or background), we assessed and optimized the proposed approach against segmentation errors. To do so, we automatically created a set of 26 different segmentation of the grains. They were obtained by eroding and dilating the ground truth (GT) of each grain with different sizes of the morphological structuring element.

Dilation is defined as the process of expanding the actual boundaries of an image, while erosion shrinks these boundaries [86]. Both processes are generated by calculating some binary operator of the image and a structuring element (SE). SE is a small binary image constitutes of zeros or ones pixels, and its size specifies the size

of SE. The arrangements of the pixels define the shape of the SE, for example, it can be a line, ring, square, etc.

Since mycetoma grains tend to be oval-shaped, disks were used as structuring elements with a radius range [1,10] for erosion (E) and [1,15] for dilation (D). [Figure 5.11](#) shows an example of a GT mask and four generated masks with 5 and 10 erosion and dilation, which is expanding and shrinking the GT by 5 and 10. We separately trained the model 26 times, using each segmentation set, and for each trained model we predicted the causative agents using the 26 segmentation sets to assess the performance of the model considering all the training and validation possibilities amongst these segmentations. We also considered the training using the union of the 26 segmentation sets (U). The accuracies obtained for all the configurations are presented in [Figure 5.12](#). We observed the relative robustness of the method to segmentation errors both in training and validation. As expected, it appeared that the tendency to segment inside or outside the actual contour of the grain should be coherent between the training and usage of the proposed method. Based on these results, we decided to train the model with the GT segmentation set and we recommend for the users that manual segmentation should be preferably slightly inward rather than outward of the actual border of the grain.

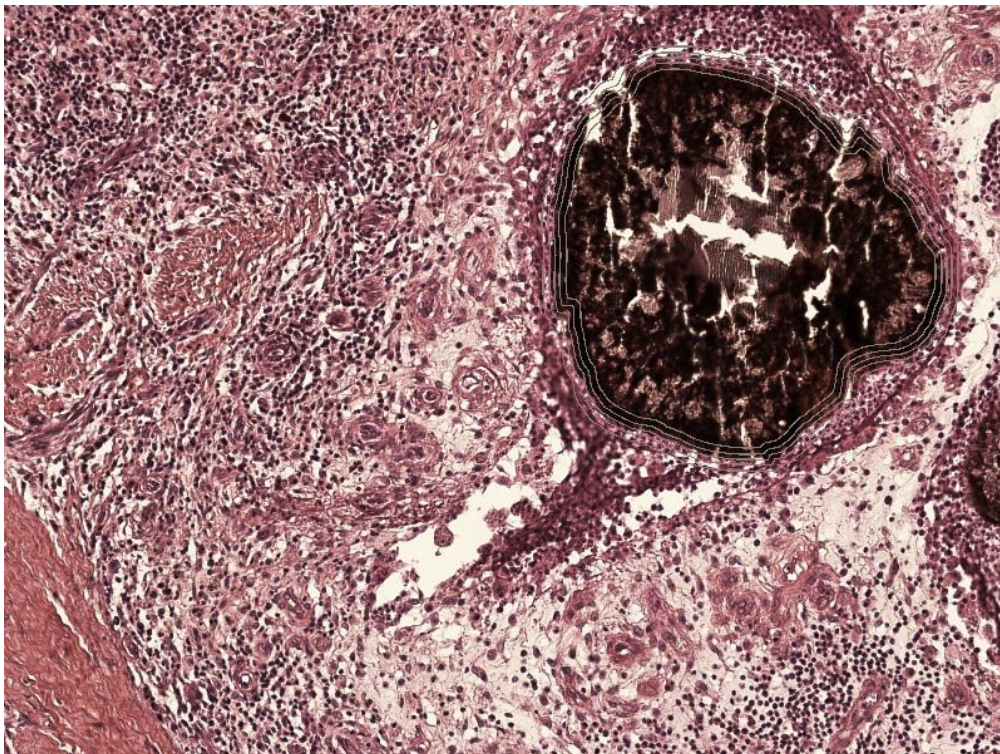


Figure 5.11: An example of the generated masks using erosion and dilation.

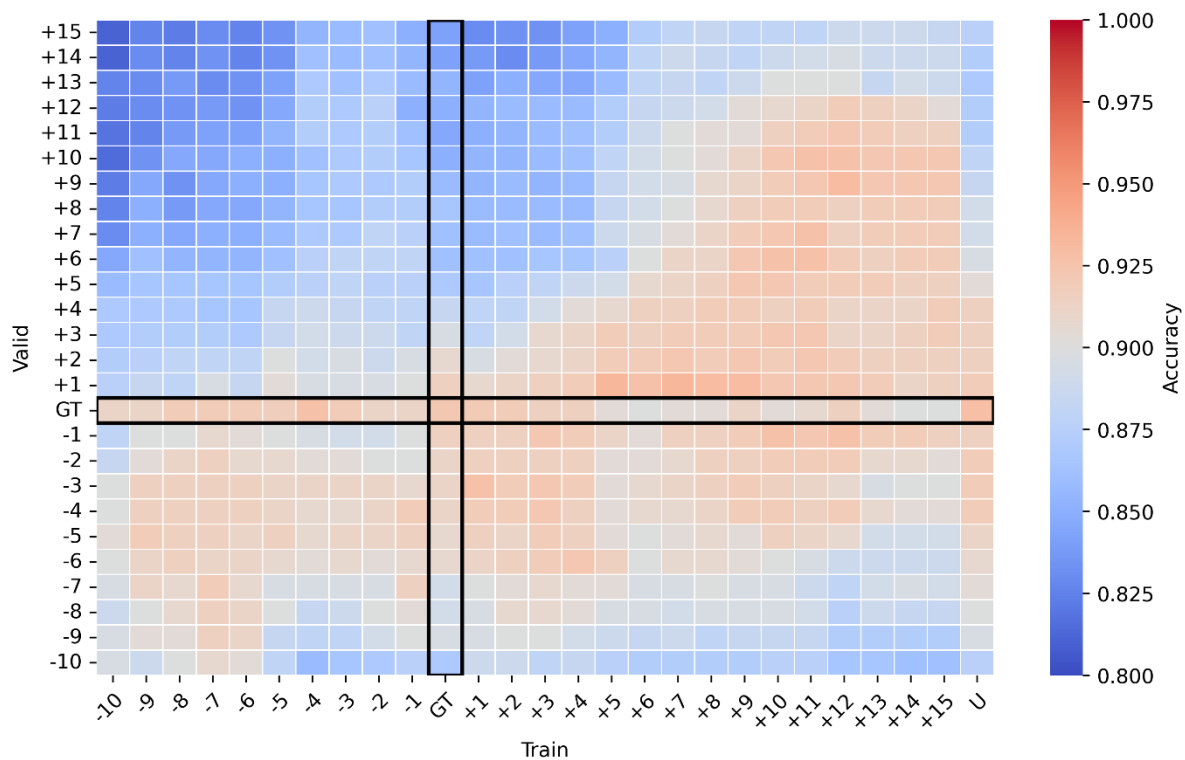


Figure 5.12: Effect of segmentation accuracy on classification performance.

5.3.4 Model Implementation and working with GUI

Aiming to facilitate the use of our model, we developed a graphical user interface (GUI) using MATLAB app designer in MATLAB 2021b. The GUI implementation can be used for both manual segmentation and classification. To illustrate the use of GUI, we will use a eumycetoma image. After launching the tool, the main window appears with two panels for images and results and a button for the analysis. Firstly, the user should upload a tissue image and then either upload ROI or draw it. Loading the images correctly activates the analysis button allowing the tool to analyse images by calculating the radiomics features and the prediction of mycetoma type. Lastly, the prediction results are given with an option of saving the computed radiomics features. [Figure 5.13](#) depicts the main window and predication steps.

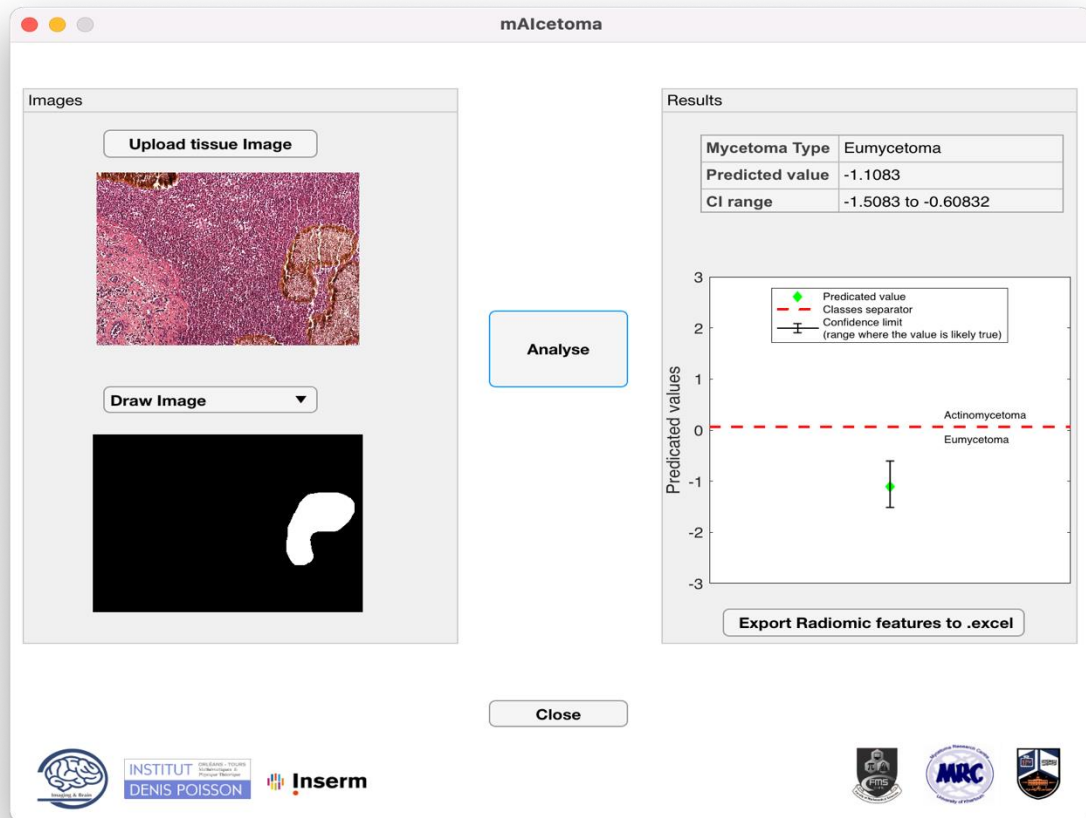


Figure 5.13: Mycetoma classification tool.

5.4 Discussion

Proper mycetoma management and treatment require accurate identification of mycetoma causative agents [3, 30]. Currently, histopathological technique seem to be the optimal method for the identification of mycetoma causative agents in terms of performance, cost and time [22, 28, 33]. However, the ability of pathologists to discriminate between eumycetoma and actinomycetoma is restricted by their knowledge of the microscopic appearance of the causative agents. Furthermore, some agents look very similar to each other [10, 30, 33]. Hence, the judgment is vulnerable to false results. Therefore, in this chapter, we pioneered a computational method to differentiate between eumycetoma and actinomycetoma from grains' quantitative features in histopathological microscopic images.

The performance of our method was evaluated in terms of sensitivity, specificity, accuracy, AUC, MCC and F1 score. On our data, the proposed model achieved an accuracy of 91.89%, a sensitivity of 0.945, and a specificity of 0.903. The obtained results were in line with the reported results from trained expert pathologists from the MRC [28]. The 92% accuracy of expert pathologists indicates that our proposed model has the potential to be as efficient as an expert. The model scored an MCC metric of 0.838, which indicates solid statistical accuracy taking into account the different sizes of classes. An AUC of 0.9531 on the primary validation set indicated that the proposed model has discrimination ability. AUC and MCC values were homogeneous, which again supported the model's power to separate the classes. This was further assessed and supported by the bootstrap evaluation, which expresses the range where the prediction is more likely to be true. Based on the results of our dataset, the proposed approach had discriminative, objective and reproducible qualities that are promising to reduce the need for highly specialised pathologists for diagnosis in endemic areas.

In this study, we mainly considered H& E staining for causative agents' identification, whereas special stains such as gram, Zeilh Neelsen, and Periodic acid-Schiff (PAS) stains are known to be effective for identifying organisms [22, 30]. Our rationale is to propose a method that can be used in the most rural clinical centre where H& E histology is used in routine examination of mycetoma cases. It aims to improve mycetoma diagnosis while maintaining simplicity and cost to the minimum level. The same logic was applied to the acquisition protocol of histopathology microscopic images. The employed image acquisition and sample preparation methods are feasible in many clinical centres with histopathology departments.

The results of this work were drawn from both a primary set of images using uniform image acquisition parameters and a secondary data set with distinct acquisition parameters and slide preparation techniques to evaluate the robustness of the model. We observed a good classification on both datasets, with a slightly increased one on the secondary dataset. Considering the small size of the secondary dataset, the variability can affect the performance of the model, and the results should be considered more cautiously in the secondary dataset. Nevertheless, the results on this secondary dataset were very good, which is a positive sign for the robustness of the model to the variability in acquisition parameters.

Regarding the most important features used for the classification, it is interesting to note that the ones promoted by our model differ from some usually found in the literature where several studies proposed size, mostly diameter, and the border of the grains as characteristic features of the mycetoma grains [8, 22, 33, 146]. Eumycetoma is supposed to have the largest grains, while actinomycetoma grains are supposed to vary from small to medium. Based on our results, textural features are the most dominant and powerful features for differential diagnosis. The top textural features were difference variance, small dependence low-grey-level emphasis, grey-level variance, and complexity. These features illustrate that eumycetoma tends to have a non-uniform and complex pattern within grains, and it is usually composed of connected blocks that are less homogeneous. On the other hand, actinomycetoma grains are compact with a simple or regular pattern. These results are of particular interest due to the reported fact, that eumycetoma grains are known to be harder with a coarse texture and tend to be fractured [15, 22, 30, 33]. Hence, we believe that our proposed model provides quantitative features that are quite similar to the qualitative features used by expert pathologists. In light of the aforementioned results, we can conclude that the discriminating features of mycetoma types depend on the variation in texture for the adjacent regions within grains. In other words, the homogeneity of textures and the tendency for closer blocks to have similar spatial variation.

An inherent limitation of this first study on a lightly supervised image analysis approach for diagnosis of mycetoma causative agent is consecutive to the local recruitment in Sudan. Our datasets naturally reflect the local distribution of mycetoma causative agents and organisms. As described in [Chapter 4](#), our datasets include three genera of AM (*AMP*, *AMM*, *SS*) with a higher prevalence of *SS* and five different subclassifications of EM (*Msp*, *MM+*, *MM-*, *Aspp*, *Fsp*) with a higher prevalence of *MM+*. This is coherent with the worldwide distribution of mycetoma [2], where *MM+* and *SS* are reported as the most prevalent forms of mycetoma in Sudan. We had a few cases of *Aspp* and *Fsp*, which is reflected in our results as the accuracy obtained for these classes was not as good as for the most frequent ones in [Table 5.3](#). It is also known that *Nocardia* is rarely observed in Sudan and indeed none of our patients was affected by this type of mycetoma. Consequently, our model was not trained equally on all types of mycetoma grains and not trained at all for some. Therefore, the proposed approach should currently only be considered for patients from regions of

the world where the distribution of the most common causative agents is similar to Sudan. Further studies are needed for regions that present *Nocardia* or another genus of mycetoma that were not observed in our dataset. Currently, we believe that our model would perform best in Africa except for Uganda, where *Nocardia* is prevalent. The results we obtained on our dataset are encouraging to appeal for larger studies that would include patients worldwide, to develop a method that could be used in all endemic areas.

5.5 Conclusion

We proposed the mycetoma classification model from manually segmented grains in this chapter. The proposed method uses radiomics in conjunction with PLS-DA to effectively discriminate between actinomycetoma and eumycetoma with 91.8% accuracy and robustness to sample preparation techniques. Our model has a performance comparable to expert mycetoma pathologists [28]. The model takes into account the uncertainty of classification, hence providing a range of prediction confidence. Furthermore, the manual segmentation precision was investigated to assess its accuracy in model performance. This shows that including other tissue components reduces model accuracy. The obtained results show model's potential and suggest it might reduce the need for expert pathologists in non-specialized clinical centres to perform histological-based diagnosis of mycetoma causative agents. Therefore, the proposed model could be integrated into routine histopathological mycetoma diagnosis procedures. Although a larger and more diverse dataset is needed to introduce an application that can be used on all continents, we deploy an application that could be carefully used in regions with a causative agent distribution similar to Sudan. In the next chapter, we will introduce a CNN model for grain segmentation to further automate of the proposed radiomics model.

Chapter 6: Mycetoma Grain Automatic Segmentation Model - GrUnet

Summary

In the previous chapter, we presented a classification model for mycetoma types from manually segmented grains. While we showed that the proposed classification model was robust to the segmentation errors, we expect that many users of the model will have limited grain segmentation experience. To increase the automation and reproducibility of our model, we intended to propose an automated segmentation method. This chapter aims at proposing a segmentation model and integrating it with our classification model to make a fully automated approach. The proposed model is a CNN network that segments mycetoma grains from tissue images. It is a modified version of Unet architecture with a small number of weights in each layer. The chapter is divided into four sections. Firstly, CNN architectures for image segmentation are described. In [Section 6.2](#), we start with a brief description of the data set and pre-processing, and the proposed architecture and the training procedures are described. Then the experimental results are given in [Section 6.3](#) followed by a discussion in [Section 6.4](#). We conclude the contribution of this chapter in the last section.

6.1 Image segmentation with CNN state-of-the-art

In this section, we review some of the most used CNN architecture in image segmentation with Unet. Image segmentation can be considered a classification task where the aim is to label each pixel of the image. Recall CNN definition ([Section 3.7.3](#)), it is applying sequences of operators on input to obtain abstract features which are fed into a predictor (classifier). Hence, CNN has been heavily used for image segmentation problems.

One of the first CNN models to segment images considered the image as a set of patches, which is a small window inside the image, as an input and predicts the label of its centre pixel. This model is time-consuming and does not look at the structural relation between the neighbouring pixels. Long and others [147] proposed a new architecture that segments an entire image in only one forward pass through the network. They proposed a novel concept named “skip connection” to overcome the problem of ignoring the global structural relation between pixels. Skip connection combines structural and local information by gathering feature maps channel-wise for a given layer with previous layers. In their network, skip-connection was performed between intermediate up-sampled layers and lower layers and summing both feature maps. Also, the features are up-sampled in the last convolution layer to reach the spatial size of the input image.

Rather than performing the up-sampling in the last convolution layer, another network called SegNet was proposed [148] and gradually execute the up-sampling, [Figure 6.1](#). The network consists of two symmetrical parts, an encoder and a decoder. The encoder is similar to the classical CNN structure, while the decoder uses convolutional layers, and a newly introduced layer called the up-sampling layer. Up-sampling layer increases feature maps' size as a reverse layer to the pooling layer in the classical CNN structure. Therefore, the decoder increases the feature map size until the original image size is reached.

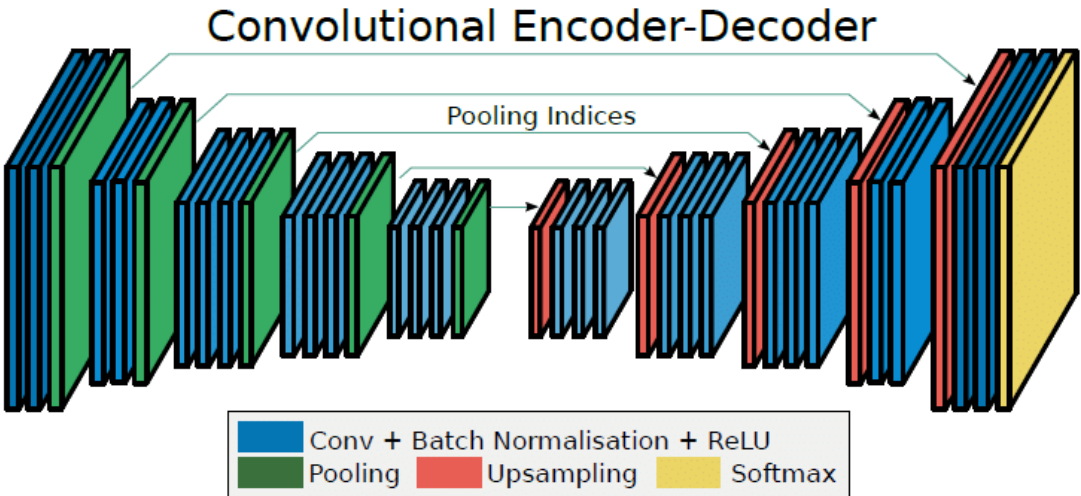


Figure 6.1: SegNet Architecture

Some studies suggested using CNN models fused with other techniques or models for segmenting cells (nuclei). The work presented in [82] merged the information of the cell bounding boxes extracted using a Fully Convolutional Neural network (FCN) with the CNN model to segment the cell in each bounding box. Song and others [83] presented a CNN model with shape-prior information for segmenting the cervical cells. The model incorporated high-level prior information to reconstruct the border of the overlapped cell and integrate it with the information from multi-scale CNN that increase the contrast among the cell components and remove image noise. Another work [84] utilized the probability map generated with CNN to initialize the shape, and then the final segmentation would be completed by a deformable model and a sparse shape model.

In 2015, Ronneberger and colleagues [85] proposed Unet architecture which is the state-of-the-art network for image segmentation. It is a U-shaped segmentation network with two symmetrical paths, namely contracting and expansive, [Figure 6.2](#). The network down-sample image by max pooling and up-sample it through transposed convolutions. Each down-sample step doubles the number of feature channels while the up-sample reduces it to half. Also, it uses a skip connection between down-

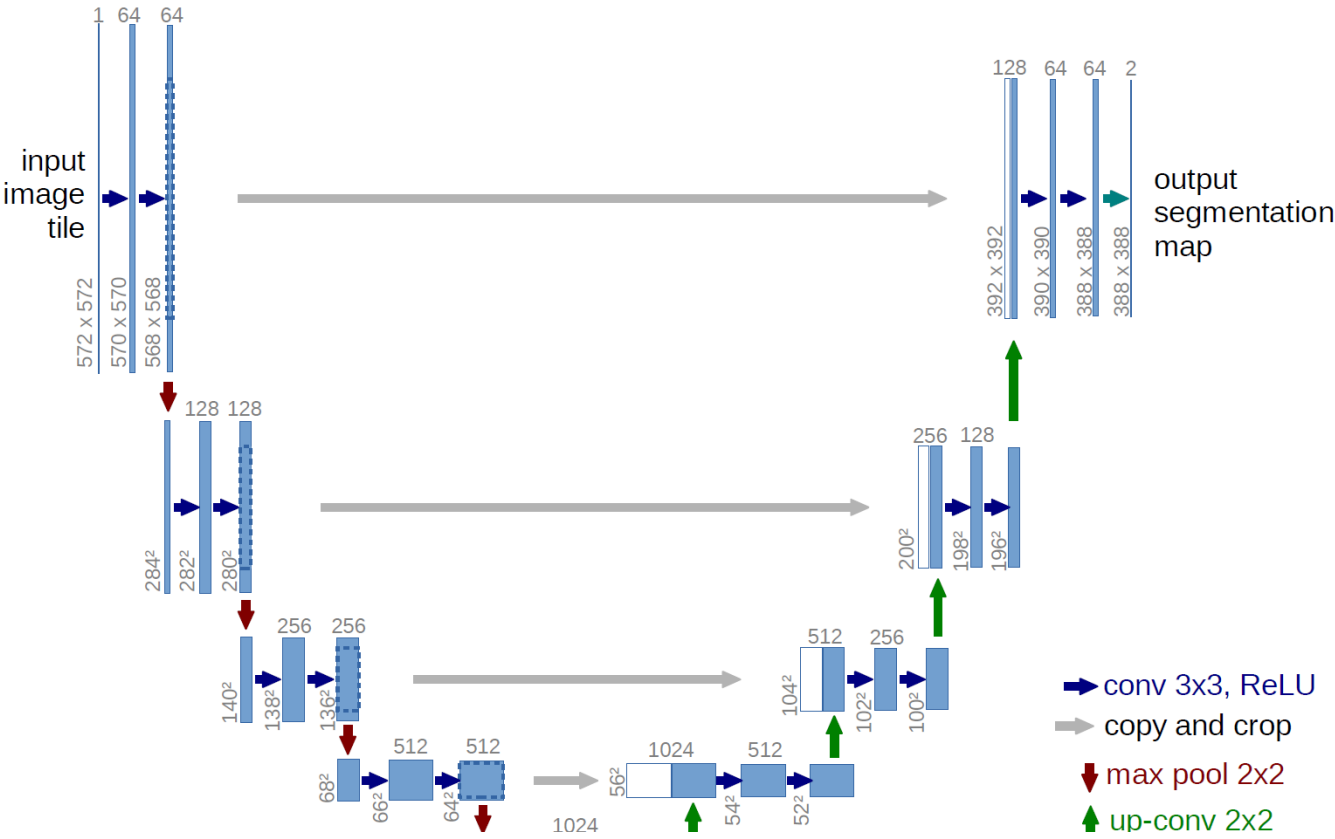


Figure 6.2: U-Net architecture [85].

sampling and up-sampling. Unet architecture is the most popular and successful network for medical image segmentation. Hence, our proposed network (presented in the next section) is a modified version of Unet specially targeted for grain segmentation in histopathological tissue images.

U-net has adapted in many of the recent works in histopathology image segmentation. It was used for the multi-organ nuclei segmentation model [149] using adversarial learning. Another U-net model was proposed for the segmentation of the skin biopsies, and it proved to be robust against the variations in staining and tissue thickness [150]. Attention-Guided deep Atrous-Residual U-Net [151] was introduced as a modified version of Unet for gland segmentation. It is comprised of Atrous-Residual units for encoder-decoder modules, which allow for the extraction of more gland-specific detailed features, this results in competitive results over existing state-of-art methods. Other Unet versions were proposed by modifying the encoder and decoder blocks for prostate image segmentation, residual and multi-resolution Inception-based blocks were used in [152], while residual blocks only were used in [153]. SU-net is a CNN model that fused two variants of Unet architecture (Shallow U-net (SU-net) and Deep U-net (Dunet)) for automatic cancer detection and segmentation in whole-slide histopathology images [154]. This setting of multiple networks fusion exhibits the capability of the model in capturing the various morphological features. The work presented in [155] firstly trains Unet on the perineural invasion dataset to define the boundary of the ROI, then improve the segmentation performance by using a boundary dilation method and a loss combination technique. The U-net like model has been adapted for prostate segmentation [156].

Furthermore, Unet has also been extended to histopathological image analysis. It was used to normalise the stain colour of the microscopic images using an adversarial training approach [157]. Also, different topologies of Unet were used to remove noise from the images [158]. Unet architecture also demonstrated its effectiveness in non-medical imaging and unsupervised segmentation. W-net [159] uses the encoder-decoder structure where both the encoder and decoder were a separate U-net model. It achieves significant results as a powerful feature extractor even without the use of labels.

6.2 GrUnet: The Proposed Framework

6.2.1 Dataset and pre-processing

The Mycetoma data set is composed of 864 tissue microscopic images from 142 patients. The images were captured in RGB colour space with size 600 X 800 and 10X magnification. A comprehensive data description was given in [Section 4.5.1](#).

Ground-truth annotations were performed manually. [Figure 6.3](#) shows an example of a grain image with its corresponding ground truth. It should be noted that the ground-truth segmentation is defined for one grain, even if the image has more than a grain.

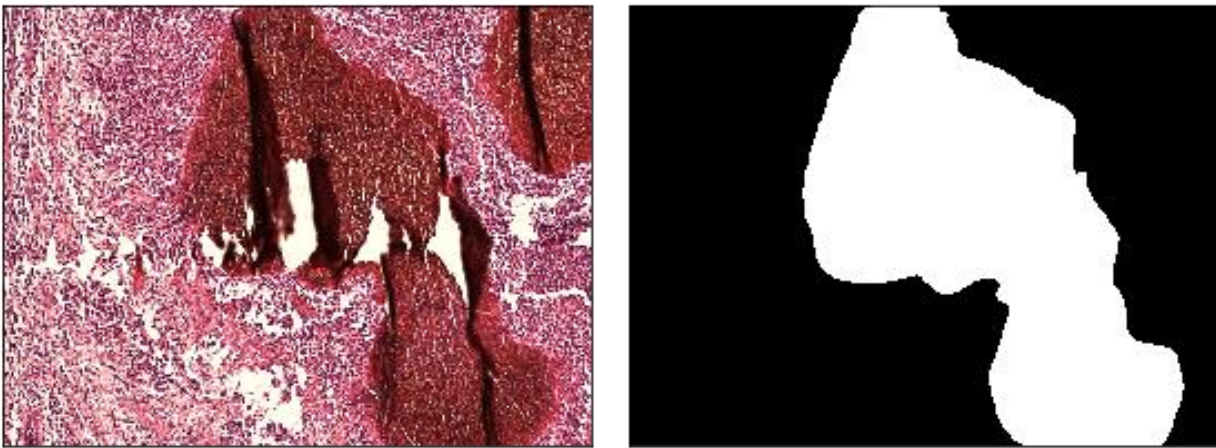


Figure 6.3: The tissue image and grain ground-truth annotation.

All the images were converted into greyscale images and resized to 800×800 . The colour conversion was computed using weighted conversion ([Section 3.2](#)).

6.2.2 The Proposed Network Architecture

Our proposed network architecture, called GrUnet is illustrated in [Figure 6.4](#). It is a modified variant of the Unet architecture described in the previous section.

As mentioned in [Chapter 3: Chapter 3](#), in the case of the implementation of the CNN model, several parameters must be optimized and considered to perform a specific task correctly. One of these parameters is the size of the database to train and validate the model. It is well known that developing a CNN model requires quite a big database

depending on the complexity of the model and the problem. However, we assumed the size of our database could be insufficient for the training of the classical Unet architecture. For this reason, we decided to start our experiments by exploring a modified variant of the Unet architecture.

To build GrUnet, we introduced some changes to the classical U-net architecture. We kept the filter size to be small with 64 maxima. Also, we replaced pooling layers with strided convolution layers. This is based on the studies that show this strategy simplifies the network architecture without reducing the performance [160]. GrUnet is constructed with encoder blocks, decoder blocks, a bridge that connects the encoder with the decoder, and a skip connection to provide the decoder block with additional features for better segmentation.

Each encoder block is composed of (3 X 3) convolution layers followed by the RELU activation layer. We used convolutions with a stride equal to 2 for down-sampling while maintaining the same number of filters and features in the two levels. The bridge is built of four convolution layers and closed by (3 X 3) deconvolution layer with stride 2.

The decoder path consists in two blocks, both of which begin with concatenation (skip connection) of convolution and deconvolution layers and sum up the features channels. This allows the combination of local and spatial information. The first block is composed of three convolution layers followed by the RELU activation layer and deconvolution with stride 2, while the deconvolution layer is replaced by convolution with a sigmoid activation layer for the second block. Contrary to the classical Unet, our network does not change the number of feature channels through down-sampling or up-sampling, it is rather changed by controlling the stride size of the last convolution layer in each encoder block or first convolution layer in each decoder block.

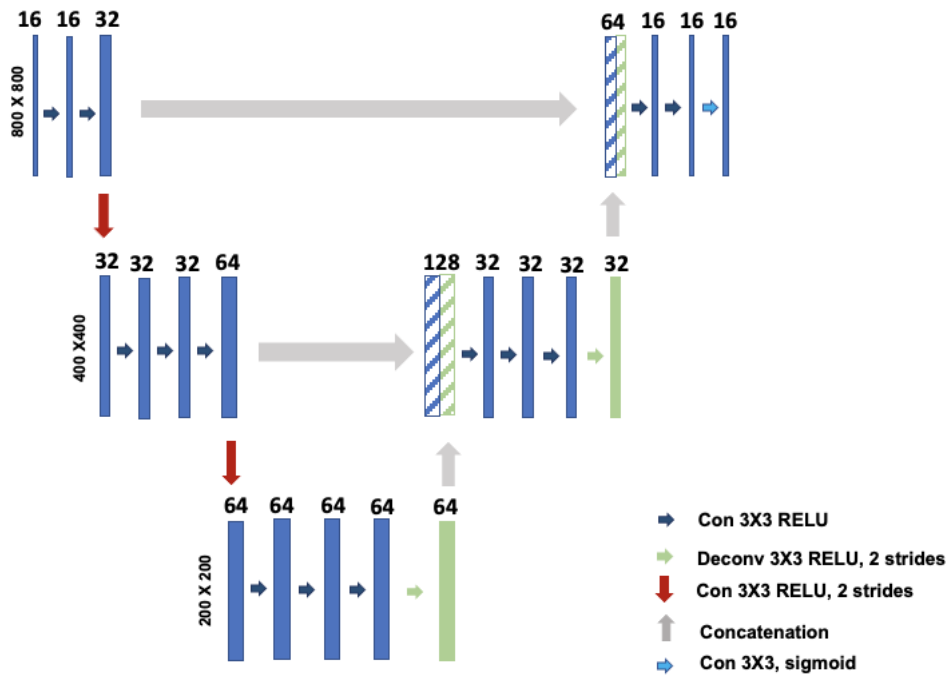


Figure 6.4: Proposed GrUNet Architecture.

6.2.3 Training

The GrUet was trained and evaluated on the mycetoma dataset. The dataset is divided into training, validation and testing sets with a proportion of 65%, 20% and 15% respectively. Division of the dataset is a common practice to avoid overfitting. There is no overlapping between the three sets to control the training and monitor the model's performance. The training set is employed to adjust the network parameters and evaluate the network using the validation dataset. The final evaluation of the network to check for the generalization of the result is carried out through a test set.

The network was trained with a 0.1 learning rate (LR) and Stochastic Gradient Descent, meaning that the network weights are updated after every single sample in the training dataset (batch size 1). The training occurs for 100 epochs which is the number of times the network passes through the entire training data set. It starts at the defined LR and reduces it with a factor of 0.5 for every ten epochs in case no improvement is obtained for the loss score of the validation dataset.

For the training, we used the AdaDelta optimizer [161] and binary cross-entropy loss function [113]. AdaDelta is an extension of the gradient descent that speeds up the training process in many ways such as scaling the learning rate based on the accumulated gradient over a time window. Binary cross-entropy (BE) is used in binary classification tasks by comparing the predicted values (P) and actual values (Y), which can be either 0 or 1, [Equation 6.1](#).

$$BE(Y, P) = -Y \log(P) - (1 - Y) \log(1 - P) \quad \text{Equation 6.1}$$

To avoid overfitting, we used a stopping criterion for the training process called Early stopping [113]. Early stopping stops the learning earlier by examining the validation performance when it starts either decreasing while the training performance is improving or at convergence. Investigating these criteria improves the generalization of the model. In our implementation, the training stops, and the evaluation metrics are reported after 10 epochs if no improvement is recorded for the loss score of the validation dataset.

In addition, data augmentation was considered to increase the data set and avoid overfitting. It boosts and enlarges the training data set by creating new data by manipulating the original dataset. We added rotated, shifted, and flipped variants of the images to the training dataset.

[Figure 6.5](#) illustrates the training curves of our proposed network. The earlier stopping criterion takes place after 56 epochs; hence the training stopped and reached the best performance in the validation dataset.

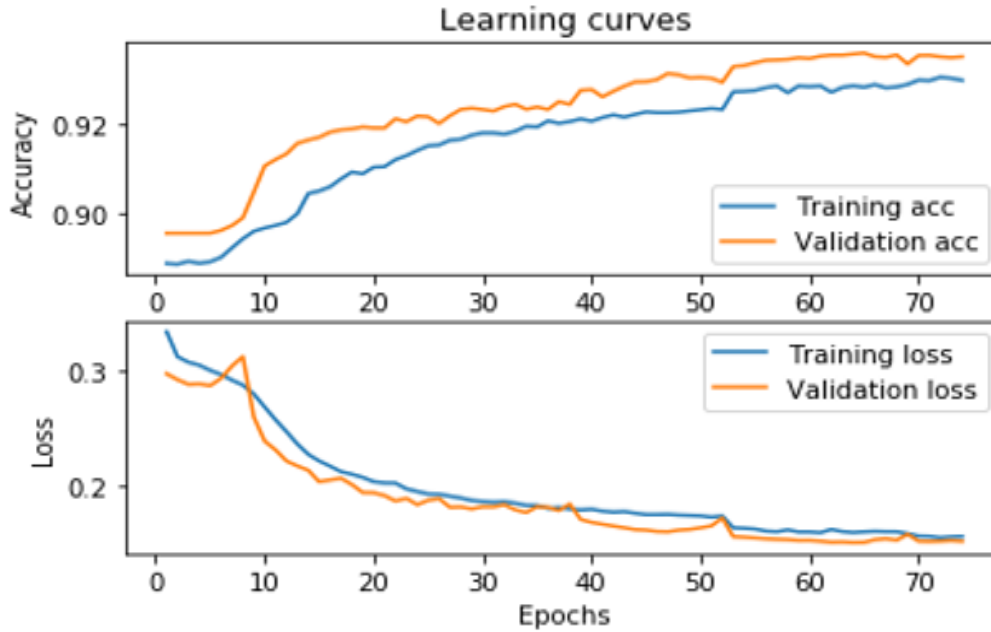


Figure 6.5: Training curves of GrUnet on mycetoma database.

The experiment was computed on iMac Retina 4,2 GHz Quad-Core Intel Core i7, 16GB RAM and Radeon 4 GB graphic. The network was built with Keras [162] and TensorFlow [163] python packages.

Evaluation metrics:

We assess the performance of GrUnet using the most common segmentation metrics namely: Accuracy, Area Under Curve (AUC), Sensitivity, Specificity, Dice coefficient, and Jaccard coefficient after applying a 0.37 threshold on predication. In addition, Dice and Jaccard coefficients [81] measure the similarity between the predication (P) and the ground-truth (Y), Equation 6.2. These coefficients range in the interval $[0, 1]$ with higher values denoting more precise segmentation results. A score of 1 indicates a perfect similarity between the prediction and ground truth.

$$Dice(Y, P) = \frac{2|P \cap Y|}{|P| + |Y|}$$

$$Jac(Y, P) = \frac{|P \cap Y|}{|P \cup Y|} \quad \text{Equation 6.2}$$

Also, we measure the proportion of the true prediction (true positive TP and true negative TN) to the total prediction, whether they are positive or negative by computing the accuracy using Equation 6.3. Although accuracy is considered a poor measurement for imbalanced classes, still it is broadly used in segmentation tasks as it is easily calculated and interpreted. Specificity and sensitivity calculate the accuracy of segmenting the background and grains (Equation 6.3), respectively. Furthermore, AUC provides a measurement for the performance across different thresholds.

$$Acc = \frac{TP + TN}{TP + TN + FP + FN}$$

$$Spec = \frac{TN}{TN + FP}$$

Equation 6.3

$$Senc = \frac{TP}{TP + FN}$$

6.3 Experimental Results

6.3.1 Performance evaluation of GrUnet

The prediction of the grains segmentation for some examples using GrUnet is given in Figure 6.6. Evaluation of the model on the test dataset, we obtained dice, accuracy, specificity and sensitivity of 0.5707, 92.03%, 0.9688 and 0.5293 respectively. These metrics are inconsistent with the qualitative results obtained in comparing the actual grains in the tissue images and predicted grains (Figure 6.6A). We believe this outcome occurred because many grains were not labelled as ground truth although they are part of it and the model predicted them successfully. Besides this, the training curves in Figure 6.5 has a reasonably stable fitting and it does not demonstrate any overfitting.

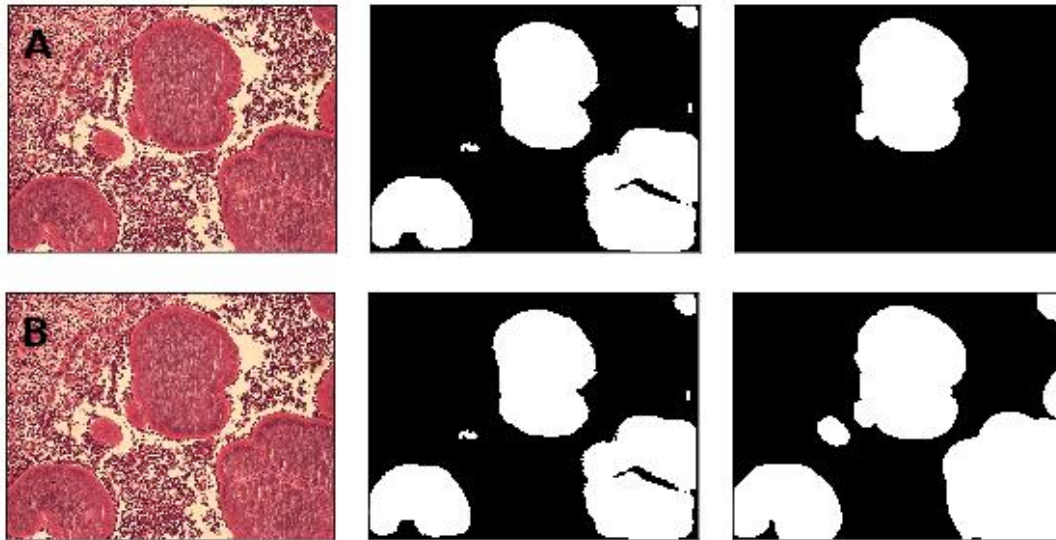


Figure 6.6: GrUnet Prediction. Images from left to right represent the tissue image, prediction, and ground truth.

For this reason and to explore how ground-truth inclusion can affect metrics, we updated the ground-truth segmentation of the test dataset only to include all the grains in the image rather than a single grain. After this, the metrics on the updated test dataset were computed. They achieve dice, accuracy, specificity and sensitivity of 0.7843, 93.8%, 0.9706 and 0.5803, respectively. An example from the test dataset is given in [Figure 6.6B](#).

6.3.2 Comparing GrUnet with other architectures

Even though we made a hypothesis that the small size of the database might limit the performance of the classical Unet, an experiment was conducted to segment the grains using Unet architecture. The model was trained using data augmentation with 563 images and validated with 171 images. The Unet architecture achieved relatively good performance in terms of fitting and similarity between ground truth and prediction, as given in [Table 6.1](#) and [Figure 6.7](#): Classical Unet training curve with mycetoma database.

Figure 6.8: Prediction of gaps inside the grains. From left to the right columns represent tissue image, prediction, and ground truth. Figure 6.9. Hence and because of the popularity of Unet in

medical image segmentation, we attempted many Unet versions with various blocks, filters and kernel size, optimizers, and loss functions, still the performance improved slightly.

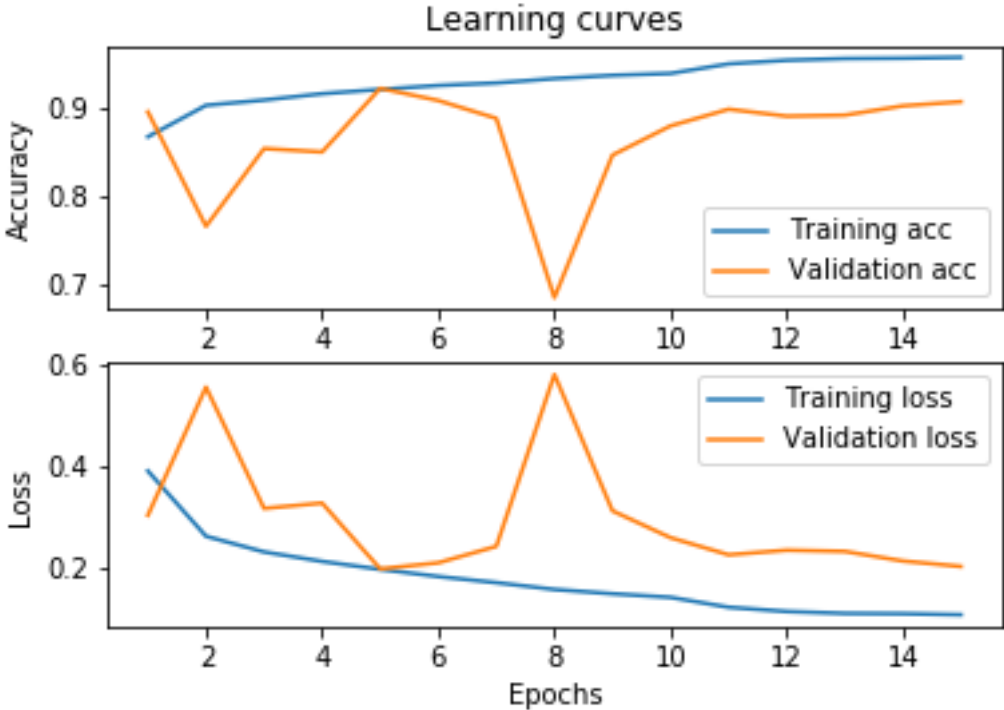


Figure 6.7: Classical Unet training curve with mycetoma database.

Figure 6.8: Prediction of gaps inside the grains. From left to the right columns represent tissue image, prediction, and ground truth. Figure 6.9: Classical Unet training curve with mycetoma database.

We consider another model with a different architecture to segment mycetoma grains. The choice of architecture was based on the idea of finding a model that shows a good performance on segmenting tissue components with a visual appearance similar to mycetoma grains. This is because mycetoma grains have a unique structure and morphology, and their segmentation from tissue images has not been investigated before. An assumption of similarity between mycetoma grains and glands was made. Consequently, we explored the recent models used for histopathological tissue gland segmentation presented in [81]. CUMedVision [164] was retained as it achieved the best performance for segmenting the glands by incorporating multi-level feature representations with fully convolutional networks (FCN) with Deep Contour-Aware

Network (DCAN). The result obtained with CUMedVision for grain segmentation is presented in [Table 6.1](#).

Table 6.1: Comparing different models conducted on the test dataset.

Experiment	AUC	Spec	Sens	Accuracy	Dice	JAC
<i>GrUnet</i>	0.9383	0.9688	0.5293	92.03%	0.5707	0.4503
<i>Unet</i>	0.9331	0.9426	0.5935	90.63%	0.5364	0.4320
<i>CUMedVision</i>	0.7502	0.5233	0.2710	75.38%	0.3068	0.2871

The three models were compared considering their performance in segmenting mycetoma grains. The result of Unet indicates that the network might be simple for the grains' segmentation task as it shows under-fitting. Furthermore, CUMedVision demonstrates weak performance in comparison to the Unet model. This encourages us to present GrUnet for mycetoma grains segmentation as it proves to have significant achievements.

6.3.3 Models Integration

The GrUnet segmentation model was proposed to automate the diagnostic process; hence it is necessary to merge GrUnet with the classification model introduced in the previous chapter.

The GrUnet model was utilised to predict the mycetoma grains in the tissue images of the test dataset and the secondary dataset (described in [Section 4.6.4](#)). These predicted grains were examined for their performance as inputs to the classification model. It should be noted that the test dataset is different from the dataset used for the evaluation in [Chapter 5](#).

First, radiomics features were calculated for the predicted grains images in both of the datasets. Then, these features are provided as input to our PLS-DA model for classification. In [Table 6.2](#), we compare the accuracy of mAlcetoma with the manually segmented grains and the combination of mAlcetoma and GrUnet.

Table 6.2: Integrated Models. Results on the test and secondary datasets.

Dataset	Dice coefficient	Accuracy of integrated models	Accuracy of mAlcetoma
Test	0.5707	88%	90.8%
Secondary	0.3750	50%	96.15%

6.4 Discussion

Mycetoma treatment depends on correctly identifying causative agents, whether fungus or bacterial, as they are treated differently. This identification can be carried out using different laboratory tools. Histopathology is the most commonly used tool. For establishing the histopathological diagnosis, in the beginning, we must locate the grain(s) within the tissue and then determine the causative agents of the grains.

Initially, a classification model was proposed to determine the causative agents from the grains assuming that the stakeholder can locate the grains, perform a manual segmentation and feed it to the classification model. While this strategy demonstrates a significant performance, it lacked automation. For this reason, it was important to present an automated segmentation method.

This chapter introduced a CNN model for grain segmentation from tissue images. The model is a modified version of Unet architecture with a small number of weights in each layer. As an opposite of classical Unet architecture, it consists of only two layers of encoder and decoder blocks linked with the bridge. Also, a maximum of 128 features

map is computed, and only a couple of down-sampling is performed using stride rather than pooling which reduces the complexity of network architecture while maintaining the efficiency of the network. This qualifies our proposed network to be a lightweight version of Unet architecture. The training was performed without a GPU, and it takes 8 hours on a Quad-Core Intel Core i7 CPU. In the same way, the prediction of mycetoma grains for a single tissue image usually takes less than two seconds.

The network was trained, evaluated and tested on the mycetoma dataset. As mentioned in [Chapter 4](#), a tissue image could have more than a grain, but we considered only one grain per tissue image. Consequently, we should emphasize the fact that only one grain for each image is used during the training process, although it is possible for an image to contain multiple grains. The qualitative outcomes of the testing data set show that our network outperforms the grains used as ground truth by predicting all the grains in the image. For this reason and the purpose of inspection of the obtained quantitative metrics, the ground-truth grains for the testing data set were renewed and all the grains were labelled accordingly. And the evaluation metrics were computed for both versions of the test data set.

Our results demonstrated that there is a 78% similarity between the network predictions and ground-truth annotations (renewed dataset). When analysing the quantitative metrics obtained in comparison to the visual appearance, we recognized that the network does not label any existing holes or gaps inside the grain to be part of it while these parts are considered as grains in the ground truth ([Figure 6.10](#): Prediction of gaps inside the grains. From left to the right columns represent tissue image, prediction, and ground truth).

[Figure 6.11](#): Prediction of small remnants grains. From left to the right columns represent tissue image, prediction, and ground truth.[Figure 6.12](#)). These gaps occur either as a result of slide preparation or the nature of the grains. From this observation, it is clear that the dice metric is affected by this condition as it is presented in many images within the test dataset.



Figure 6.10: Prediction of gaps inside the grains. From left to the right columns represent tissue image, prediction, and ground truth.

Figure 6.11: Prediction of small remnants grains. From left to the right columns represent tissue image, prediction, and ground truth. Figure 6.12: Prediction of gaps inside the grains. From left to the right columns represent tissue image, prediction, and ground truth.

Analysing the true positive and true negative prediction carried out through accuracy, sensitivity and specificity of the network. The network score accuracy of 93.8% displays the percentage of correctly classified pixels regardless of whether they are grains or backgrounds. But this metric is inappropriate for imbalanced classes because it does not consider the proportion of grains and background pixels in the image. Therefore, it is worth examining the sensitivity and specificity, which provides a measure of correctly classified pixels for grains and background classes, respectively. A low specificity corresponds to a small number of correctly classified background pixels, while low sensitivity corresponds to a low accuracy of correctly classified grain pixels. We obtained a specificity of 0.9701 and a sensitivity of 0.7659. Meaning that the model has a tendency of classifying the pixels as background and this is consistent with the fact that the proportion of background to grains is higher in tissue images. In addition, the sensitivity metric is in line with the dice metric indicating the consistency of the results concerning the overlapping between actual and predicted grains.

It is interesting to note that the presented model outperforms the ground truth that was used to train the network. The model can predict all the grains in the images, even the smallest remnants, [Figure 6.13](#): Prediction of small remnants grains. From left to the right columns represent tissue image, prediction, and ground truth.

Figure 6.14: Prediction of false positive grains. From left to the right columns represent tissue image, prediction, and ground truth. Figure 6.15: Even though, sometimes the network predicts false positive grains, as given in Figure 6.16: Prediction of false positive grains. From left to the right columns represent tissue image, prediction, and ground truth.

Figure 6.17, which limits the performance of the proposed study towards making a conclusive diagnosis.



Figure 6.13: Prediction of small remnants grains. From left to the right columns represent tissue image, prediction, and ground truth.

Figure 6.14: Prediction of false positive grains. From left to the right columns represent tissue image, prediction, and ground truth. Figure 6.15: Prediction of small remnants grains. From left to the right columns represent tissue image, prediction, and ground truth.



Figure 6.16: Prediction of false positive grains. From left to the right columns represent tissue image, prediction, and ground truth.

Figure 6.17: Prediction of false positive grains. From left to the right columns represent tissue image, prediction, and ground truth.

Furthermore, we assessed the quality of segmentation on its ability to correctly classify the mycetoma causative agents by using our radiomic model. The model was developed to classify eumycetoma and actinomycetoma from a manually segmented grain. The test datasets of both actual ground truth and predicated grains are examined with the classification model. The accuracy was 88% and 90.8% for predicated and actual grains, respectively. These metrics are consistent with the segmentation errors

of eroding the ground-truth grains described in the previous chapter. Therefore, the performance of our predicated grains on the radiomics model is comparable to the manual segmentation. The mAlcetoma model was investigated for its efficacy against manual segmentation errors. The difference in accuracy between actual and predicated grains is similar to the accuracy obtained when the manual segmentation is conducted inside the actual borders of the grains. On the other hand, examining the secondary dataset shows a big difference in the accuracy of the two frameworks. One way to interpret this result is that GrUnet could have a modest performance when it is exposed to a dataset with a specification different from the training dataset. Hence, this could directly affect the classification accuracy in the combined models. This drawback could be addressed by retraining the GrUnet model with several datasets that do not have the same acquisition protocol.

6.5 Conclusion

The presence of mycetoma grains in the tissue sections is crucial for establishing the diagnosis, hence detecting the grains constitutes a core step. This chapter introduces a method to segment the grains from tissue images and integrates it with our classification model, which uses the manually segmented grains. The manual segmentation of mycetoma grains required time and experience. Also, the automated grain segmentation furthers the introduction of the fully automated diagnostic method. The proposed approach is based on CNN segmentation models in medical images, particularly because it is a modified variant of Unet architecture. According to our experiments, the proposed framework demonstrates significant performance on mycetoma histopathology microscopic images that leads to 93.8% segmentation accuracy and 0.7843 dice coefficient. Furthermore, this study showed that our presented segmentation model coupled with the previously proposed classification method reached comparable results with those obtained using manual segmentation. In the following chapter, we will draw the conclusions and perspectives of our work in this thesis.

Chapter 7: Conclusion and Future Work

7.1 Conclusion and Limitations

Mycetoma is a WHO-recognised neglected tropical disease. It is a major public health problem that frequently affects young adults and children in remote rural areas, causing deformities, disabilities and sometimes death. Mycetoma research has mostly focused on the disease's clinical and laboratory aspects. Although molecular identification of mycetoma causative agent is the most accurate, culture methods are still the gold standard techniques in mycetoma laboratory diagnosis. Most of the diagnostic studies were conducted to propose new techniques, while few were conducted to improve the existing techniques. With all the studies, computerised analysis of used diagnostic methods has lagged behind. This could be explained by the fact that mycetoma is a neglected disease, its prevalence is concentrated in poorly developed regions and among people with low socioeconomic status. Also, the painless, slow progression and non-contagious nature of this disease might be an extra cause that mycetoma does not receive much attention in terms of Computer Aided Diagnosis (CAD) research.

To keep up with the modern era of CAD and, at the same time, facilitate the diagnostic process while maintaining the simplest technique that could be used in endemic rural areas, we investigated the possibility of proposing an automated diagnostic model for mycetoma. Since the imaging techniques come at the second stage of diagnosis, we explore the laboratory techniques with their pros and cons and to which extent they are valuable and useful or accurate in the diagnosis.

This thesis focused on the analysis of histopathological microscopic images. Although histology is not the gold standard or the most accurate, it is still an optimal tool within limited resource environments and/or rural areas. Automating mycetoma histopathological analysis could significantly affect time, cost and quality of diagnosis.

Until 2013, mycetoma had been neglected for years before being included in the WHO neglected tropical diseases list. Although this draws the attention of media and scientific communities, this recognition is mostly limited to endemic areas and personnel interested in tropical medicine. This was the reason for outlining [Chapter 2](#)

to provide a handbook for general and essential information regarding mycetoma, its diagnosis and management. Also, it draws the state-of-art for mycetoma research and knowledge gaps and the motivation for proposing the computational method for mycetoma diagnosis.

Since we are pioneering an automated method for mycetoma diagnosis, in [Chapter 3](#), we reviewed the CAD studies of histopathological images. The reviewed studies focus on the main steps involved in developing mycetoma histology methods, namely image enhancement, segmentation, features, and pattern recognition. The most challenging part was investigating the choice of an appropriate features category that could be descriptive for mycetoma tissue images. Radiomics features sound promising as they combine several categories in three broad feature classes. We also extensively explore machine learning and artificial neural network methods.

Creating the mycetoma database was the main focus of [Chapter 4](#). The tissue samples were collected from mycetoma-confirmed patients seen and managed at the MRC. The paraffin blocks were prepared and sent to the Bretonneau Hospital in France. Following a uniform sectioning and H&E staining procedure, we prepared the histopathological slides for 142 patients. Several histopathological slides containing different grains were prepared for each patient, with an average of six grains per patient. Because grains are the unique characteristic of mycetoma infection, it was necessary to manually segment grains (ROIs) for each histopathological slide. The database consisted of 864 mycetoma grain microscopic images with their ground-truth segmented grain. It is acquired with a homogeneous and unique reproducible acquisition protocol. The work done in this chapter resulted in the first database of mycetoma microscopic images. This database could be of great benefit to many researchers who are interested to study this neglected disease and improving healthcare.

Although the database included 142 patients from the MRC with the two types of mycetoma, it does not comprise all the mycetoma species. Currently, there are more than 80 different causative species with uneven geographical distribution. The MRC's patients are either Sudanese or from neighbouring countries where *Madurella mycetomatis*, *Actinomadura madurae*, *Streptomyces somaliensis*, and *Actinomadura pelletierii* are the most common species. Therefore, our database focused on these

species for actinomycetoma as well as the *Madurella* genus in general and especially *Madurella mycetomatis* for eumycetoma.

Depending on the mycetoma causative agents, regardless of species, the treatment requires prolonged administration of antifungal or antibiotics drugs. This identification remains challenging, difficult and disappointing. Hence, identifying mycetoma causative agents plays a significant role in the treatment process. The incorrect identification can seriously affect the patients and the disease prognosis and outcome. As a result, [Chapter 5](#) mainly concentrated on proposing a model to classify eumycetoma and actinomycetoma correctly. We aimed to decrease or eliminate all the sources that could affect the accuracy. As we were unaware of how the auto-segmentation or the variation in the preparation of samples might impact the model, we introduced a model that was trained and validated using the mycetoma database with the manually segmented grains. The trained model achieved promising results with an accuracy of 91.89%, which is comparable to the result of expert pathologists (92.8%) while using manual analysis.

Even though the classification model showed significant performance, this performance is likely limited by the mycetoma species that were represented in the database and used for the training of the model. Because of this, our model will likely misidentify any other species. And it is expected to perform better in Europe and Africa compared to South America and Asia. So, this limitation should be investigated carefully in future studies considering the geographical distribution of the other species.

One of the aims of this work was to provide a set of quantitative features that describe the two mycetoma types and try to correlate them with qualitative features in use by pathologists. We explore the three main groups of features used by pathologists to diagnose mycetoma: the grains' shape, colour, and texture. Hence, 102 radiomics features were investigated and examined for their discrimination ability in mycetoma-type classification. This showed that the shape features were not relevant to any discrimination tasks, while texture features were important.

The promising results of the classification model as well as the fact that the manual segmentation of mycetoma grains required time and experience, encouraged us to propose a method to segment the grains from tissue sections and combine it with our classification model. [Chapter 6](#) introduced a CNN network that was inspired by Unet

architecture to automate grains' segmentation. According to our experiments and results, the proposed framework demonstrates significant performance on mycetoma histopathology microscopic images, leading to 93.8% accuracy on the segmentation task and 0.7843 dice coefficient.

We integrated both the classification and segmentation models to fully automate the diagnosis process in a way that the user will need only to provide the image without performing the manual segmentation. The accuracy of the classification was 88% and 90.8% for automated and manual grain identification. With the automated segmented grains, the model performance slightly decreased but remains close to manually segmented grains. We believe this occurs because the segmentation model segment the false positive grains and assigns them to the classification model for differentiation.

We developed a tool that offers a semi-automated differential diagnostic method for mycetoma. It can be used for both manual segmentation and classification. We believe this tool is more reliable for a release than the combined models. This is because that combined model can falsely segment other components as grains leading to an incorrect diagnosis, while the tool guides the differential diagnosis of confirmed mycetoma cases.

7.2 Future perspective

7.2.1 Mycetoma Database

This thesis aims to propose an automated diagnostic method for mycetoma that can be utilised globally (because the global burden is unknown) and in endemic areas especially. However, the database built in this work is attributed to mycetoma species from Sudan and other geographical regions with a similar distribution. As mentioned, this matter might affect the accuracy of our models such that exposing the model to certain species, which were not included in the dataset, could not be correctly classified. Therefore, more samples must be collected to enlarge the existing database with new species and more samples from the existing species. The sample should be collected from different countries and continents as the species' geographic distributions vary widely.

In addition, the ground-truth images of the manually segmented grains required to be updated and include all the grains in each image. Then, the database should be modified accordingly. We observed the necessity of this modification during the evaluation of the segmentation model because the inclusion of all the grains in the ground truth gives different results compared to the single grain.

7.2.2 The Segmentation Model

The GrUnet was trained using the mycetoma database with a single grain per image as a ground truth. As mentioned above, the evaluation demonstrated different performances on the different datasets. For this reason, we believe retraining the model with the updated database could improve the model's capability to segment mycetoma grains. Another possibility is to retrain the model with the predicted mycetoma grains.

To further develop the automated diagnostic method, the presented segmentation model needs to be coupled with a detection technique. This is because we observed a degradation in the accuracy of the combined models which is mostly attributed to the detection and segmentation of false positive grains. This issue is considered a limitation of our proposed automated diagnostic model. To overcome this, we need to propose a detection model to be used for mycetoma grain detection. The model should be the first step in the pipeline of the automated diagnostic method. For this purpose, a dataset of false positive grains is required to develop and train the model.

7.2.3 The Classification Model

The classification of the causative agents' genus and/or species can be explored. Currently, all mycetoma patients are given the same treatment regimen of antifungal or antibacterial regardless of the species. However, there is a correlation between treatment outcomes and species identification. For this reason, classification into species level could help in the follow-up and prognosis.

This classification was examined within the proposed radiomics model. However, we believe that the limited number of images for these classes strongly affects the performance of the extended model. Accordingly, we suggest increasing the number of images of the different classes for the extended model in upcoming works. Also,

another perspective is the development of a grading model that examines the causative agent species.

In addition, particular attention should be given to *Madurella mycetomatis* and *Madurella mycetomatis* negative classification. This classification class is of special interest since *Madurella mycetomatis* is the most common causative organism worldwide, and its treatment is challenging and problematic. Also, most of the affected patients do not respond to medical therapy alone and require surgical intervention. It is interesting to know that histopathology alone cannot make this classification and is only possible through molecular techniques. We tested our radiomics model for this purpose, but the performance was unsatisfactory. Hence, we examine wavelet scatter transforms [165]. The model achieved a classification accuracy of 71%. Extra samples for *Madurella mycetomatis* negative are needed to conclude that this accuracy is reliable. We believe that our *Madurella mycetomatis* negative sample might contain few eumycetoma species compared to the actual 40 reported species [166]. Therefore, more *Madurella mycetomatis* negative samples must be collected considering their species.

Finally, a deep learning model should be considered after enlarging and modifying the database. The model could be able to perform all the tasks of the segmentation and classification of mycetoma grains at once.

List of communications

Communications

- “Mathematical Model for the Diagnosis of the Common Organism Causing Mycetoma”. The Sixth International Conference on Mycetoma, Sudan, Khartoum, February 2019. [Poster]
- “Develop Novel Computational Diagnostic Method of the Organisms Causing Mycetoma Based on Histology: The Prime Diagnostic Method”. Biomedical Research Day, France, Tours, November 2019. [Poster]
- “Develop of Novel Automated Diagnostic Method of the Common Organisms Causing Mycetoma Based on Histology Microscopic Images”. Rwanda, Kigali, November 2021. [Poster]. **Top 20 young women scientists in Sub-Saharan Africa, L’Oréal-UNESCO For Women in Science.**
- “Radiomics Model for Mycetoma Grains Classification from Histopathological Microscopic Images Using Partial Least Squares Discriminant Analysis (PLS-DA)”. Annual research meeting of the Mycetoma Research Center, Sudan, Khartoum, December 2021. [Oral]
- “Computational Diagnostic Method of the Organisms Causing Mycetoma Based on Histology”. Deep Learning Indaba, Tunisia, Tunis, August 2022. [Poster] **Top five posters award.**
- “Computational Diagnostic Method for Mycetoma Causative Agents Using Histopathological Microscopic Images”. Mycetoma Symposium, Sudan, Khartoum, November 2022. [Oral]

Original research paper

- Hyam Omar Ali, Romain Abraham, Guillaume Desoubeaux, Ahmed H. Fahal, Clovis Tauber. “Radiomics model for Mycetoma causative agents identification”. Submitted to Computers in Biology and Medicine.

References

- [1] WHO, "Mycetoma." [Online]. Available: <https://www.who.int/news-room/fact-sheets/detail/mycetoma>.
- [2] W. W. J. Van De Sande, "Global Burden of Human Mycetoma: A Systematic Review and Meta-analysis," *PLoS Negl. Trop. Dis.*, vol. 7, no. 11, 2013.
- [3] W. W. J. van de Sande *et al.*, "The mycetoma knowledge gap: identification of research priorities," *PLoS Negl. Trop. Dis.*, vol. 8, no. 3, p. e2667, 2014.
- [4] L. Y. M. Elkheir, R. Haroun, M. Awadalla, M. Id, and H. F. Id, "Madurella mycetomatis causing eumycetoma medical treatment: The challenges and prospects," pp. 1–17, 2020.
- [5] J. Rippon, *Medical mycology. The pathogenic fungi and the pathogenic actinomycetes*. 1988.
- [6] H. V. Carter, "On a new and striking form of fungus disease principally... - Google Scholar," *Trans Med Phys Soc Bombay*, vol. 6, pp. 104–142, 1860.
- [7] A. J. Chalmers and R. G. Archibald, "A sudanese maduromycosis," *Ann. Trop. Med. Parasitol.*, vol. 10, no. 2, pp. 169–222, Sep. 1916.
- [8] V. Relhan, K. Mahajan, P. Agarwal, and V. K. Garg, "Mycetoma: an update," *Indian J. Dermatol.*, vol. 62, no. 4, p. 332, 2017.
- [9] E. E. Zijlstra, W. W. J. Van De Sande, and A. H. Fahal, "Mycetoma : A Long Journey from Neglect," pp. 3–5, 2016.
- [10] W. Van De Sande *et al.*, "Closing the mycetoma knowledge gap," *Med. Mycol.*, vol. 56, no. suppl_1, pp. S153--S164, 2018.
- [11] R. S. A. Id, M. J. Newport, S. M. Bakhiet, M. E. Ibrahim, and A. H. Fahal, "Host genetic susceptibility to mycetoma," pp. 1–14, 2020.
- [12] A. O. A. A. Ahmed *et al.*, "Mycetoma caused by *Madurella mycetomatis* : a neglected infectious burden," *Lancet Infect. Dis.*, vol. 4, no. September, pp. 566–574, Sep. 2004.
- [13] E. E. Zijlstra, W. W. J. Van De Sande, O. Welsh, E. S. Mahgoub, M. Goodfellow, and A. H. Fahal, "Mycetoma : a unique neglected tropical disease," *Lancet Infect. Dis.*, vol. 16, no. 1, pp. 100–112, 2016.
- [14] A. H. Fahal, "Mycetoma: a thorn in the flesh," *Trans. R. Soc. Trop. Med. Hyg.*, vol. 98, no. 1, pp. 3–11, 2004.

- [15] P. Emmanuel, S. P. Dumre, S. John, J. Karbwang, and K. Hirayama, "Mycetoma : a clinical dilemma in resource limited settings," *Ann. Clin. Microbiol. Antimicrob.*, pp. 1–10, 2018.
- [16] C. M. S. Reis and E. G. de M. Reis-Filho, "Mycetomas: an epidemiological, etiological, clinical, laboratory and therapeutic review," *An. Bras. Dermatol.*, vol. 93, no. 1, pp. 8–18, 2018.
- [17] S. S. AH Fahal, "Clinical presentation of mycetoma," *Sudan Med. J.*, vol. 32, pp. 46–66, 1994.
- [18] A. Fahal, E. L. S. Mahgoub, A. M. E. L. Hassan, and M. E. Abdel-Rahman, "Mycetoma in the Sudan: an update from the mycetoma research centre, University of Khartoum, Sudan," *PLoS Negl. Trop. Dis.*, vol. 9, no. 3, p. e0003679, 2015.
- [19] R. Article, "Eumycetoma and actinomycetoma – an update on causative agents , epidemiology , pathogenesis , diagnostics and therapy," pp. 1873–1883, 2015.
- [20] S. Mattioni, M. Develoux, S. Brun, ... A. M.-M. et maladies, and undefined 2013, "Management of mycetomas in France," *Elsevier*.
- [21] W. W. J. van de Sande *et al.*, "Merits and Pitfalls of Currently Used Diagnostic Tools in Mycetoma," *PLoS Negl. Trop. Dis.*, vol. 8, no. 7, p. e2918, 2014.
- [22] A. A. Ahmed, W. van de Sande, and A. H. Fahal, "Mycetoma laboratory diagnosis," *PLoS Negl. Trop. Dis.*, vol. 11, no. 8, p. e0005638, 2017.
- [23] M. E. Abd El Bagi, "New radiographic classification of bone involvement in pedal mycetoma," *Am. J. Roentgenol.*, vol. 180, no. 3, pp. 665–668, 2003.
- [24] M. E. A. El-Bagi and A. H. Fahal, "Mycetoma revisited," *Saudi Med J*, vol. 30, no. 4, pp. 529–533, 2009.
- [25] B. Journal, A. H. Fahal, H. E. Sheik, M. M. A. Homeida, Y. E. Arabi, and E. S. Mahgoub, "Ultrasonographic imaging of mycetoma," *Br. J. Surg.*, vol. 84, no. 8, pp. 1120–1122, 1997.
- [26] E. K. AM El Hassan, A Fahal, IA El-Hag, "The pathology of mycetoma," *Sudan Med. J. J.*, vol. 32, pp. 23–45, 1994.
- [27] E. Mahgoub and I. Murray, *Mycetoma*. London: William Heinem Medical Books, 1973.
- [28] E. E. Siddig *et al.*, "The Accuracy of Histopathological and Cytopathological Techniques in the Identification of the Mycetoma Causative Agents," *PLoS Negl. Trop. Dis.*, vol. 13, no. 8, p. e0007056, 2019.

- [29] M. Desnos-Ollivier, S. Bretagne, F. Dromer, O. Lortholary, and E. Dannaoui, "Molecular identification of black-grain mycetoma agents," *Am Soc Microbiol*, vol. 44, no. 10, pp. 3517–3523, Oct. 2006.
- [30] E. E. Siddig and A. H. Fahal, "Histopathological Approach in Diagnosis of Mycetoma Causative Agents: A Mini Review," *J Cytol Histol*, vol. 8, p. 466, 2017.
- [31] S. A. Fahal, A.H., El Toum, E.A., El Hassan, A.M., Mahgoub, E.S. and Gumaa, "The host tissue reaction to *Madurella mycetomatis*: new classification," *J. Med. Vet. Mycol.*, vol. 33, no. 1, pp. 15–17, 1995.
- [32] S. Venkatswami, A. Sankarasubramanian, and S. Subramanyam, "The Madura Foot : Looking Deep," no. 14, 2012.
- [33] A. H. Fahal, "Mycetoma—clinicopathological monograph, Khartoum University Press," *Khartoum, Sudan*, 2006.
- [34] A. H. Fahal, "Management of mycetoma," vol. 5, no. 1, pp. 1–7, 2010.
- [35] O. Welsh, L. Vera-Cabrera, E. Welsh, and M. C. Salinas, "Actinomycetoma and advances in its treatment," *Clin. Dermatol.*, vol. 30, no. 4, pp. 372–381, Jul. 2012.
- [36] A. Fahal *et al.*, "A New Model for Management of Mycetoma in the Sudan," vol. 8, no. 10, 2014.
- [37] M. Abbas *et al.*, "The disabling consequences of Mycetoma," *PLoS Negl. Trop. Dis.*, pp. 1–16, 2018.
- [38] CDC, "Fungal diseases: Mycetoma." .
- [39] Samir M Shaheen, "Patients with lower limb amputations for mycetomains the National Center for Prosthetics and Orthotics in the Sudan," *Khartoum Med. J.*, vol. 1, no. 1, pp. 27–29, 2008.
- [40] S. Sridhar, *Digital image processing*. Oxford University Press, 2011.
- [41] R. C. Gonzale and R. E. Woods, *Digital Image Processing*, Third Edit. Pearson Education International.
- [42] O. Sertel, U. V. Catalyurek, H. Shimada, and M. N. Gurcan, "Computer-aided prognosis of neuroblastoma: Detection of mitosis and karyorrhexis cells in digitized histological images," *Proc. 31st Annu. Int. Conf. IEEE Eng. Med. Biol. Soc. Eng. Futur. Biomed. EMBC 2009*, pp. 1433–1436, 2009.
- [43] H. Kong, M. Gurcan, and K. Belkacem-Boussaid, "Partitioning histopathological images: An integrated framework for supervised color-texture segmentation and cell splitting," *IEEE Trans. Med. Imaging*, vol. 30, no. 9, pp. 1661–1677, 2011.

- [44] Y. Wang, D. Crookes, O. S. Eldin, S. Wang, P. Hamilton, and J. Diamond, "Assisted diagnosis of cervical intraepithelial neoplasia (CIN)," *IEEE J. Sel. Top. Signal Process.*, vol. 3, no. 1, pp. 112–121, 2009.
- [45] A. Tabesh *et al.*, "Multifeature prostate cancer diagnosis and gleason grading of histological images," *IEEE Trans. Med. Imaging*, vol. 26, no. 10, pp. 1366–1378, Oct. 2007.
- [46] K. Rodenacker, "a Feature Set for Cytometry on Digitized Microscopic," vol. 25, pp. 1–42, 1992.
- [47] R. Kumar, R. Srivastava, and S. Srivastava, "Detection and Classification of Cancer from Microscopic Biopsy Images Using Clinically Significant and Biologically Interpretable Features," *J. Med. Eng.*, vol. 2015, pp. 1–14, 2015.
- [48] C. Bilgina *et al.*, "Cell-graph mining for breast tissue modeling and classification," in *Engineering in Medicine and Biology Society, 2007. EMBS 2007. 29th Annual International Conference of the IEEE*, 2007, vol. 220, no. 1, pp. 5311–5314.
- [49] N. R. Muhammad Arif, "Detection of Nuclei by unsupervised Manifold Learning," in *11th Medical Image Understanding and Analysis (MIUA)*, 2007.
- [50] S. Waheed, R. A. Moffitt, Q. Chaudry, A. N. Young, and M. D. Wang, "Computer aided histopathological classification of cancer subtypes," *Proc. 7th IEEE Int. Conf. Bioinforma. Bioeng. BIBE*, pp. 503–508, 2007.
- [51] S. Seminowich, A. Sar, S. Yilmaz, and R. M. Rangayyan, "Segmentation of cell nuclei in images of renal biopsy samples," *Can. Conf. Electr. Comput. Eng.*, pp. 1–4, 2010.
- [52] A. S. Jadhav *et al.*, "Quantitative analysis of histopathological features of precancerous lesion and condition using image processing technique," *Proc. - IEEE Symp. Comput. Med. Syst.*, vol. 2006, pp. 231–236, 2006.
- [53] M. N. Babu, V. K. Madasu, M. Hanmandlu, and S. Vasikarla, "Histo-pathological image analysis using OS-FCM and level sets," *Proc. - Appl. Imag. Pattern Recognit. Work.*, 2010.
- [54] A. Chekkoury *et al.*, "Automated malignancy detection in breast histopathological images," *Med. Imaging 2012 Comput. Diagnosis*, vol. 8315, no. May 2014, p. 831515, 2012.
- [55] P. W. Huang and Y. H. Lai, "Effective segmentation and classification for HCC biopsy images," *Pattern Recognit.*, vol. 43, no. 4, pp. 1550–1563, 2010.
- [56] S. K. Dai, Y. C. Wu, Y. J. Jan, and S. C. Lin, "The histological grading of HCC using fusion images," *2009 IEEE Int. Conf. Comput. Intell. Meas. Syst. Appl.*

CIMSA 2009, vol. 1, no. c, pp. 186–189, 2009.

- [57] O. Sertel, J. Kong, U. V. Catalyurek, G. Lozanski, J. H. Saltz, and M. N. Gurcan, “Histopathological image analysis using model-based intermediate representations and color texture: Follicular lymphoma grading,” *J. Signal Process. Syst.*, vol. 55, no. 1–3, pp. 169–183, 2009.
- [58] M. N. Gurcan, T. Pan, H. Shimada, and J. Saltz, “Image analysis for neuroblastoma classification: Segmentation of cell nuclei,” *Annu. Int. Conf. IEEE Eng. Med. Biol. - Proc.*, pp. 4844–4847, 2006.
- [59] O. S. Al-Kadi, “Texture measures combination for improved meningioma classification of histopathological images,” *Pattern Recognit.*, vol. 43, no. 6, pp. 2043–2053, 2010.
- [60] C. Wittke, J. Mayer, and F. Schweiggert, “On the classification of prostate carcinoma with methods from spatial statistics,” *IEEE Trans. Inf. Technol. Biomed.*, vol. 11, no. 4, pp. 406–414, 2007.
- [61] S. Petushi, F. U. Garcia, M. M. Haber, C. Katsinis, and A. Tozeren, “Large-scale computations on histology images reveal grade-differentiating parameters for breast cancer,” *BMC Med. Imaging*, vol. 6, pp. 1–11, 2006.
- [62] K. Belkacem-Boussaid, O. Sertel, G. Lozanski, A. Shana’aah, and M. Gurcan, “Extraction of color features in the spectral domain to recognize centroblasts in histopathology,” *Proc. 31st Annu. Int. Conf. IEEE Eng. Med. Biol. Soc. Eng. Futur. Biomed. EMBC 2009*, pp. 3685–3688, 2009.
- [63] B. Oztan, H. Kong, M. N. Gurcan, and B. Yener, “Follicular lymphoma grading using cell-graphs and multi-scale feature analysis,” *Med. Imaging 2012 Comput. Diagnosis*, vol. 8315, no. 518, p. 831516, 2012.
- [64] C. Demir, S. H. Gultekin, and B. Yener, “Learning the topological properties of brain tumors,” *IEEE/ACM Trans. Comput. Biol. Bioinforma.*, vol. 2, no. 3, pp. 262–270, 2005.
- [65] T. Araujo *et al.*, “Classification of breast cancer histology images using convolutional neural networks,” *PLoS One*, vol. 12, no. 6, Jun. 2017.
- [66] B. E. Bejnordi *et al.*, “Stain specific standardization of whole-slide histopathological images,” *IEEE Trans. Med. Imaging*, vol. 35, no. 2, pp. 404–415, 2016.
- [67] F. Ciompi *et al.*, “The importance of stain normalization in colorectal tissue classification with convolutional networks,” *Proc. - Int. Symp. Biomed. Imaging*, pp. 160–163, 2017.

- [68] A. M. Khan, N. Rajpoot, D. Treanor, and D. Magee, "A nonlinear mapping approach to stain normalization in digital histopathology images using image-specific color deconvolution," *IEEE Trans. Biomed. Eng.*, vol. 61, no. 6, pp. 1729–1738, 2014.
- [69] H. Cho, S. Lim, G. Choi, and H. Min, "Neural Stain-Style Transfer Learning using GAN for Histopathological Images," *arXiv Prepr. arXiv1710.08543*, 2017.
- [70] G. Paschos, "Perceptually uniform color spaces for color texture analysis: An empirical evaluation," *IEEE Trans. Image Process.*, vol. 10, no. 6, pp. 932–937, Jun. 2001.
- [71] M. N. Gurcan *et al.*, "Histopathological Image Analysis: A Review.," *IEEE Rev. Biomed. Eng.*, vol. 2, pp. 147–171, 2009.
- [72] S. Bhattacharjee, "Analysis of Biopsy Tissue Images based on Color Moment Technique and Morphology of Cell Nuclei," pp. 338–342, 1975.
- [73] S. N. Manoli, A. R. Ulle, N. M. Nandini, and T. S. Rekha, "Classification of Breast Lesions using Histopathology Images and Neural Network," *Biomed. Pharmacol. J.*, vol. 3, no. 6, pp. 1745–1748, 2018.
- [74] C. Gunduz, B. Yener, and S. H. Gultekin, "The cell graphs of cancer," *Bioinformatics*, vol. 20, no. SUPPL. 1, pp. 145–151, 2004.
- [75] C. Gunduz-Demir, M. Kandemir, A. B. Tosun, and C. Sokmensuer, "Automatic segmentation of colon glands using object-graphs," *Med. Image Anal.*, vol. 14, no. 1, pp. 1–12, Feb. 2010.
- [76] L. Gorelick *et al.*, "Prostate histopathology: Learning tissue component histograms for cancer detection and classification," *IEEE Trans. Med. Imaging*, vol. 32, no. 10, pp. 1804–1818, 2013.
- [77] C. C. C. Bilgin, P. Bullough, G. E. Plopper, and B. Yener, "ECM-aware cell-graph mining for bone tissue modeling and classification," *Data Min. Knowl. Discov.*, vol. 20, no. 3, pp. 416–438, 2010.
- [78] T. Abeel, T. Helleputte, Y. Van de Peer, P. Dupont, and Y. Saeys, "Robust biomarker identification for cancer diagnosis with ensemble feature selection methods," *Bioinformatics*, vol. 26, no. 3, pp. 392–398, 2009.
- [79] M. Hatt *et al.*, "The first MICCAI challenge on PET tumor segmentation," *Med. image Anal. Elsevier*, vol. 44, pp. 177–195, 2018.
- [80] V. Andrearczyk *et al.*, "Overview of the HECKTOR challenge at MICCAI 2021: automatic head and neck tumor segmentation and outcome prediction in PET/CT images," *Springer*, pp. 1–37, 2021.

- [81] A. Sirinukunwattana, K. Pluim, J.P., Chen, H., Qi, X., Heng, P.A., Guo, Y.B., Wang, L.Y., Matuszewski, B.J., Bruni, E., Sanchez, U. and Böhm, “Gland segmentation in colon histology images: The glas challenge contest,” *Med. image Anal. Elsevier*, vol. 35, pp. 489–502, 2017.
- [82] S. U. Akram, J. Kannala, L. Eklund, and J. Heikkilä, “Cell segmentation proposal network for microscopy image analysis,” *Deep Learn. Data Labeling Med. Appl. Springer*, pp. 21–29, 2016.
- [83] Y. Song *et al.*, “Accurate cervical cell segmentation from overlapping clumps in pap smear images,” *IEEE Trans. Med. Imaging*, vol. 36, no. 1, pp. 288–300, 2017.
- [84] F. Xing, Y. Xie, and L. Yang, “An automatic learning-based framework for robust nucleus segmentation,” *IEEE Trans. Med. Imaging*, vol. 35, no. 2, pp. 550–566, Feb. 2016.
- [85] O. Ronneberger, P. Fischer, and T. Brox, “U-net: Convolutional networks for biomedical image segmentation,” in *International Conference on Medical image computing and computer-assisted intervention*, 2015, vol. 9351, pp. 234–241.
- [86] C. Demir and B. Yener, “Automated cancer diagnosis based on histopathological images: a systematic survey,” 2005.
- [87] Z.-H. H. Zhou, Y. Jiang, Y.-B. Bin Yang, and S.-F. F. Chen, “Lung cancer cell identification based on artificial neural network ensembles,” *Artif. Intell. Med.*, vol. 24, no. 1, pp. 25–36, 2002.
- [88] A. N. Basavanahally *et al.*, “Computerized image-based detection and grading of lymphocytic infiltration in HER2+ breast cancer histopathology,” *IEEE Trans. Biomed. Eng.*, vol. 57, no. 3, pp. 642–653, 2010.
- [89] P. Spyridonos, P. Ravazoula, and D. Cavouras, “Computer-based grading of haematoxylin-eosin stained tissue sections of urinary bladder carcinomas,” *Med. Informatics*, vol. 26, no. 3, pp. 179–190, 2001.
- [90] J. Smolle, “Computer recognition of skin structures using discriminant and cluster analysis,” *Ski. Res. Technol.*, vol. 6, no. 2, pp. 58–63, 2000.
- [91] S. Kothari *et al.*, “Automatic batch-invariant color segmentation of histological cancer images,” *Proc. - Int. Symp. Biomed. Imaging*, pp. 657–660, 2011.
- [92] P. Lambin *et al.*, “Radiomics: Extracting more information from medical images using advanced feature analysis,” *Eur. J. Cancer*, vol. 48, no. 4, pp. 441–446, 2012.
- [93] P. Lambin *et al.*, “Radiomics: The bridge between medical imaging and

- personalized medicine,” *Nat. Rev. Clin. Oncol.*, vol. 14, no. 12, pp. 749–762, 2017.
- [94] V. Kumar *et al.*, “Radiomics: The process and the challenges,” *Magn. Reson. Imaging*, vol. 30, no. 9, pp. 1234–1248, 2012.
- [95] M. Avanzo, J. Stancanello, and I. El Naqa, “Beyond imaging: The promise of radiomics,” *Phys. Medica*, vol. 38, pp. 122–139, 2017.
- [96] E. J. Limkin *et al.*, “Promises and challenges for the implementation of computational medical imaging (radiomics) in oncology,” *Ann. Oncol.*, vol. 28, no. 6, pp. 1191–1206, 2017.
- [97] J. J. M. Van Griethuysen *et al.*, “Computational Radiomics System to Decode the Radiographic Phenotype,” *Cancer Res.*, vol. 77, no. 21, p. e104, Nov. 2017.
- [98] T. Isomura and T. Toyozumi, “Dimensionality reduction to maximize prediction generalization capability,” *Nat. Mach. Intell.* 2021 35, vol. 3, no. 5, pp. 434–446, Apr. 2021.
- [99] G. Chandrashekar and F. Sahin, “A survey on feature selection methods,” *Comput. Electr. Eng.*, vol. 40, no. 1, pp. 16–28, 2014.
- [100] L. I. Kuncheva, “A STABILITY INDEX FOR FEATURE SELECTION,” *Artif. Intell. Appl.*, pp. 421–427, 2007.
- [101] A. C. Haury, P. Gestraud, and J. P. Vert, “The influence of feature selection methods on accuracy, stability and interpretability of molecular signatures,” *PLoS One*, vol. 6, no. 12, pp. 1–12, 2011.
- [102] P. Pudil, F. J. Ferrir, J. Novovičová, and J. Kittler, “Floating search methods for feature selection with nonmonotonic criterion functions,” *Proc. - Int. Conf. Pattern Recognit.*, vol. 2, pp. 279–283, 1994.
- [103] A. Krizhevsky, I. Sutskever, and G. E. Hinton, “ImageNet classification with deep convolutional neural networks,” *Commun. ACM*, vol. 60, no. 6, pp. 84–90, Jun. 2017.
- [104] S. C. B. Lo, S. L. A. Lou, M. V. Chien, and S. K. Mun, “Artificial convolution neural network techniques and applications for lung nodule detection,” *IEEE Trans. Med. Imaging*, vol. 14, no. 4, pp. 711–718, 1995.
- [105] K. Simonyan and A. Zisserman, “Very deep convolutional networks for large-scale image recognition,” *3rd Int. Conf. Learn. Represent. ICLR 2015 - Conf. Track Proc.*, 2015.
- [106] D. Wang, A. Khosla, R. Gargeya, H. Irshad, A. H. Beck, and B. Israel, “Deep

- learning for identifying metastatic breast cancer,” *arXiv Prepr. arXiv1606.05718*, 2016.
- [107] N. Codella *et al.*, “Skin lesion analysis toward melanoma detection 2018: A challenge hosted by the international skin imaging collaboration (isic),” *arXiv Prepr. arXiv1902.03368*, 2019.
- [108] K. He, X. Zhang, S. Ren, and J. Sun, “Deep residual learning for image recognition,” *Proc. IEEE Comput. Soc. Conf. Comput. Vis. Pattern Recognit.*, vol. 2016-December, pp. 770–778, Dec. 2016.
- [109] C. Szegedy *et al.*, “Going deeper with convolutions,” *Proc. IEEE Comput. Soc. Conf. Comput. Vis. Pattern Recognit.*, vol. 07-12-June-2015, pp. 1–9, Oct. 2015.
- [110] G. Huang, Z. Liu, L. Van Der Maaten, and K. Q. Weinberger, “Densely connected convolutional networks,” *Proc. - 30th IEEE Conf. Comput. Vis. Pattern Recognition, CVPR 2017*, vol. 2017-January, pp. 2261–2269, Nov. 2017.
- [111] H. Rezaeilouyeh, A. Mollahosseini, and M. H. Mahoor, “Microscopic medical image classification framework via deep learning and shearlet transform,” *J. Med. Imaging*, vol. 3, no. 4, p. 044501, 2016.
- [112] T. Mitchell, *Machine learning*. New York: McGraw-hill, 1997.
- [113] I. Goodfellow, Y. Bengio, and A. Courville, *Deep Learning*. MIT press, 2016.
- [114] C. M. Bishop, “Pattern Recognition and Machine Learning,” *Inf. Sci. Stat.*, p. 738, 2006.
- [115] R. O. and H. P. . Duda, *Pattern classification*. John Wiley & Sons, 2006.
- [116] F. Rosenblatt, “The perceptron: a probabilistic model for information storage and organization in the brain.,” *Psychol. Rev.*, vol. 6, no. 65, 1958.
- [117] X. Glorot, A. Bordes, Y. B.-P. of the Fourteenth, and U. 2011, “Deep sparse rectifier neural networks,” in *Proceedings of the fourteenth international conference on artificial intelligence and statistics, JMLR Workshop and Conference Proceedings*, 2011, pp. 315–323.
- [118] L. Bottou, “Large-scale machine learning with stochastic gradient descent,” *Proc. COMPSTAT 2010 - 19th Int. Conf. Comput. Stat. Keynote, Invit. Contrib. Pap.*, pp. 177–186, 2010.
- [119] Y. Lecun, P. Haffner, L. Eon Bottou, Y. Bengio, and P. H. Abstract|, “Gradient-based learning applied to document recognition,” *Proc. IEEE*, vol. 11, no. 86, pp. 2278–2324, 1998.

- [120] DNDi, "Mycetoma Facts." [Online]. Available: <https://dndi.org/diseases/mycetoma/facts/>.
- [121] D. Emery and D. W. Denning, "The global distribution of actinomycetoma and eumycetoma," *PLoS Negl. Trop. Dis.*, vol. 14, no. 9, pp. 1–13, 2020.
- [122] L. He, L. R. Long, S. Antani, and G. R. Thoma, "Histology image analysis for carcinoma detection and grading," *Comput. Methods Programs Biomed.*, vol. 107, no. 3, pp. 538–556, 2012.
- [123] K. Suvarna, C. Layton, and J. Bancroft, *Bancroft's theory and practice of histological techniques*, 7th ed. British, Churchill Livingstone Elsevier Ltd, 2013.
- [124] R. Coleman, *Introduction to Histology*. Israel Institute of Technology, 2002.
- [125] H. Fox, "Is H&E morphology coming to an end?," *J. Clin. Pathol.*, vol. 1, no. 53, pp. 38–40, 200AD.
- [126] L. Pantanowitz, A. Sharma, A. B. Carter, T. Kurc, A. Sussman, and J. Saltz, "Twenty Years of Digital Pathology: An Overview of the Road Travelled, What is on the Horizon, and the Emergence of Vendor-Neutral Archives," *J. Pathol. Inform.*, vol. 9, no. 1, p. 40, Jan. 2018.
- [127] F. Ghaznavi, A. Evans, A. Madabhushi, and M. Feldman, "Digital imaging in pathology: whole-slide imaging and beyond," *Annu Rev Pathol*, vol. 1, no. 8, pp. 331–359, 2013.
- [128] M. T. McCann, J. A. Ozolek, C. A. Castro, B. Parvin, and J. Kovačević, "Automated Histology Analysis: Opportunities for signal processing," *IEEE Signal Process. Mag.*, vol. 32, no. 1, pp. 78–87, 2015.
- [129] R. A. van den Berg, H. C. J. Hoefsloot, J. A. Westerhuis, A. K. Smilde, and M. J. van der Werf, "Centering, scaling, and transformations: Improving the biological information content of metabolomics data," *BMC Genomics*, vol. 7, Jun. 2006.
- [130] L. C. Lee, C.-Y. Y. Liang, and A. A. Jemain, "Partial least squares-discriminant analysis (PLS-DA) for classification of high-dimensional (HD) data: A review of contemporary practice strategies and knowledge gaps," *Analyst*, vol. 143, no. 15, pp. 3526–3539, 2018.
- [131] R. G. Brereton and G. R. Lloyd, "Partial least squares discriminant analysis: Taking the magic away," *J. Chemom.*, vol. 28, no. 4, pp. 213–225, 2014.
- [132] O. M. Kvalheim, "Interpretation of partial least squares regression models by means of target projection and selectivity ratio plots," *J. Chemom.*, vol. 24, no. 7–8, pp. 496–504, 2010.

- [133] V. H. J. M. dos Santos *et al.*, “Discriminant analysis of biodiesel fuel blends based on combined data from Fourier Transform Infrared Spectroscopy and stable carbon isotope analysis,” *Chemom. Intell. Lab. Syst.*, vol. 161, pp. 70–78, 2017.
- [134] D. Ballabio and V. Consonni, “Classification tools in chemistry. Part 1: Linear models. PLS-DA,” *Anal. Methods*, vol. 5, no. 16, pp. 3790–3798, 2013.
- [135] P. M. Ramos and I. Ruisánchez, “Data fusion and dual-domain classification analysis of pigments studied in works of art,” *Anal. Chim. Acta*, vol. 558, no. 1–2, pp. 274–282, Feb. 2006.
- [136] N. F. Pérez, J. Ferré, and R. Boqué, “Calculation of the reliability of classification in discriminant partial least-squares binary classification,” *Chemom. Intell. Lab. Syst.*, vol. 95, no. 2, pp. 122–128, Feb. 2009.
- [137] H. Li, Q. Xu, and Y. L. Systems, “libPLS: An integrated library for partial least squares regression and linear discriminant analysis,” *Chemom. Intell. Lab. Elsevier*, 2018.
- [138] K. H. Esbensen and P. Geladi, “Principles of Proper Validation: use and abuse of re-sampling for validation,” *J. Chemom.*, vol. 24, no. 3–4, pp. 168–187, Apr. 2010.
- [139] B. G. Botelho, N. Reis, L. S. Oliveira, and M. M. Sena, “Development and analytical validation of a screening method for simultaneous detection of five adulterants in raw milk using mid-infrared spectroscopy and PLS-DA,” *Food Chem.*, vol. 181, pp. 31–37, 2015.
- [140] L. S. A. Pereira, F. L. C. Lisboa, J. Coelho Neto, F. N. Valladão, and M. M. Sena, “Screening method for rapid classification of psychoactive substances in illicit tablets using mid infrared spectroscopy and PLS-DA,” *Forensic Sci. Int.*, vol. 288, pp. 227–235, 2018.
- [141] J. E. L. Villa, N. R. Quiñones, F. Fantinatti-Garboggini, and R. J. Poppi, “Fast discrimination of bacteria using a filter paper–based SERS platform and PLS-DA with uncertainty estimation,” *Anal. Bioanal. Chem.*, vol. 411, no. 3, pp. 705–713, 2019.
- [142] T. Mehmood, K. H. Liland, L. Snipen, and S. Sæbø, “A review of variable selection methods in Partial Least Squares Regression,” *Chemom. Intell. Lab. Syst.*, vol. 118, pp. 62–69, 2012.
- [143] I.-G. Chong and C.-H. Jun, “Performance of some variable selection methods when multicollinearity is present,” *Chemom. Intell. Lab. Syst.*, vol. 78, no. 1–2, pp. 103–112, 2005.

- [144] S. Boughorbel, F. Jarray, and M. El-Anbari, "Optimal classifier for imbalanced data using Matthews Correlation Coefficient metric," *PLoS One*, vol. 12, no. 6, Jun. 2017.
- [145] D. Chicco and G. Jurman, "The advantages of the Matthews correlation coefficient (MCC) over F1 score and accuracy in binary classification evaluation," *BMC Genomics*, vol. 21, no. 1, Jan. 2020.
- [146] W. van de Sande *et al.*, "Closing the mycetoma knowledge gap," *Med. Mycol.*, vol. 56, no. suppl_1, pp. S153--S164, 2018.
- [147] J. Long, E. Shelhamer, T. D.-P. of the IEEE, and U. 2015, "Fully convolutional networks for semantic segmentation," in *Proceedings of the IEEE conference on computer vision and pattern recognition*, 2015, pp. 3431–3440.
- [148] V. Badrinarayanan, A. Handa, and R. Cipolla, "SegNet: A Deep Convolutional Encoder-Decoder Architecture for Robust Semantic Pixel-Wise Labelling," *arXiv Prepr. arXiv1505.07293*, May 2015.
- [149] F. Mahmood *et al.*, "Deep Adversarial Training for Multi-Organ Nuclei Segmentation in Histopathology Images," *IEEE Trans. Med. Imaging*, vol. 39, no. 11, pp. 3257–3267, 2020.
- [150] K. R. J. Oskal, M. Risdal, E. A. M. Janssen, E. S. Undersrud, and T. O. Gulsrud, "A U-net based approach to epidermal tissue segmentation in whole slide histopathological images," *SN Appl. Sci.*, vol. 1, no. 7, pp. 1–12, Jul. 2019.
- [151] M. Dabass, S. Vashisth, and R. Vig, "Attention-Guided deep atrous-residual U-Net architecture for automated gland segmentation in colon histopathology images," *Informatics Med. Unlocked*, vol. 27, p. 100784, Jan. 2021.
- [152] J. Silva-Rodríguez, E. Payá-Bosch, G. García, A. Colomer, and V. Naranjo, "Prostate Gland Segmentation in Histology Images via Residual and Multi-resolution U-NET," in *International Conference on Intelligent Data Engineering and Automated Learning*, 2020, pp. 1–8.
- [153] A. Kalapahar, J. Silva-Rodriguez, A. Colomer, F. Lopez-Mir, and V. Naranjo, "Gleason Grading of Histology Prostate Images Through Semantic Segmentation via Residual U-Net," *Proc. - Int. Conf. Image Process. ICIP*, vol. 2020-Octob, pp. 2501–2505, 2020.
- [154] Y. Li, Z. Xu, Y. Wang, H. Zhou, and Q. Zhang, "SU-Net and DU-Net Fusion for Tumour Segmentation in Histopathology Images," *Proc. - Int. Symp. Biomed. Imaging*, vol. 2020-April, pp. 461–465, Apr. 2020.
- [155] Y. Park, J. Park, and G. J. Jang, "Efficient Perineural Invasion Detection of

- Histopathological Images Using U-Net,” *Electron.*, vol. 11, no. 10, 2022.
- [156] F. Milletari, N. Navab, and S. A. Ahmadi, “V-Net: Fully convolutional neural networks for volumetric medical image segmentation,” *Proc. - 2016 4th Int. Conf. 3D Vision, 3DV 2016*, pp. 565–571, 2016.
- [157] A. BenTaieb and G. Hamarneh, “Adversarial Stain Transfer for Histopathology Image Analysis,” *IEEE Trans. Med. Imaging*, vol. 37, no. 3, pp. 792–802, 2018.
- [158] A. Riasatian, M. Rasoolijaberi, M. Babaei, and H. R. Tizhoosh, “A Comparative Study of U-Net Topologies for Background Removal in Histopathology Images,” *Proc. Int. Jt. Conf. Neural Networks*, no. 3, 2020.
- [159] X. Xia and B. Kulis, “W-Net: A Deep Model for Fully Unsupervised Image Segmentation,” *arXiv Prepr. arXiv1711.08506*, Nov. 2017.
- [160] J. T. Springenberg, A. Dosovitskiy, T. Brox, and M. Riedmiller, “Striving for simplicity: The all convolutional net,” in *3rd International Conference on Learning Representations, ICLR 2015 - Workshop Track Proceedings*, 2015.
- [161] M. D. Zeiler, “ADADELTA: An Adaptive Learning Rate Method,” *arXiv Prepr. arXiv1212.5701*, Dec. 2012.
- [162] F. and others Chollet, “Keras,” *GitHub*, 2015. [Online]. Available: <https://github.com/fchollet/keras>.
- [163] M. Abadi *et al.*, “Tensorflow: Large-scale machine learning on heterogeneous distributed systems,” *arXiv Prepr. arXiv1603.04467*, 2016.
- [164] M. Wu *et al.*, “DCAN: Deep Contour-Aware Networks for Accurate Gland Segmentation,” *Proc. IEEE Conf. Comput. Vis. Pattern Recognit.*, pp. 2487–2496, 2016.
- [165] J. Bruna and S. Mallat, “Invariant scattering convolution networks,” *IEEE Trans. Pattern Anal. Mach. Intell.*, vol. 35, no. 8, pp. 1872–1886, 2013.
- [166] N. A. Mhmoud *et al.*, “Chaetomium atrobrunneum causing human eumycetoma: The first report,” *PLoS Negl. Trop. Dis.*, vol. 13, no. 5, May 2019.

Méthodes d'Analyse d'Images Histopathologiques pour le Diagnostic Automatique du Mycétome

Résumé

Le mycétome est une maladie infectieuse chronique négligée dans les régions tropicales et subtropicales qui peut entraîner une invalidité grave. En considérant les agents responsables, le mycétome est classé en eumycétome (champignon) et actinomycétome (bactérie). La stratégie diagnostique repose sur la présentation clinique et l'identification des agents responsables du mycétome. L'identification précise des agents responsables est une priorité pour le diagnostic du mycétome. Les outils d'identification actuels comprennent les techniques moléculaires, la cytologie, l'histologie et la culture des grains qui est l'outil de référence. Les techniques moléculaires sont l'outil le plus fiable, mais il est coûteux et donc peu utilisé dans les zones endémiques, tandis que la culture est longue, difficile et nécessite un personnel expert. La cytologie et l'histologie sont des outils simples, rapides et bon marché. Cependant, la cytologie est loin d'être satisfaisante en termes de performances car elle a tendance à donner des résultats faussement positifs. Bien que l'histopathologie soit considérée comme l'outil optimal à utiliser dans les zones endémiques, elle nécessite un pathologiste expert pour une identification concluante qui fait défaut dans les zones rurales endémiques.

Avec l'avènement des approches numériques, des algorithmes automatisés d'analyse d'images peuvent être utilisés comme solution à ce problème. L'objectif principal de cette thèse est de développer une nouvelle méthode diagnostique de calcul pour le diagnostic du mycétome à l'aide d'images microscopiques histopathologiques. Premièrement, nous créons la première base de données d'images microscopiques de mycétomes. Cette contribution découle de la nécessité d'un ensemble de données pour le développement de modèles de calcul. Ensuite, nous présentons une nouvelle méthode de calcul pour discriminer semi-automatiquement les agents responsables du mycétome. La méthode est basée sur l'analyse radiomique de grains de mycétomes segmentés manuellement et l'analyse de discrimination des moindres carrés partiels (PLS-DA). Le modèle présenté peut jouer un rôle fondamental dans un centre clinique non spécialisé car il atteint une précision comparable à celle des pathologistes experts. Enfin, nous introduisons une méthode de segmentation automatisée pour les grains de mycétome. La méthode de segmentation est un modèle de type Convolution Neural Network (CNN) basé sur l'architecture U-net. Il permet l'automatisation et la rapidité des méthodes de discrimination. En conclusion, cette thèse présente à la fois une méthode automatisée de diagnostic des images microscopiques histopathologiques du mycétome et une méthode semi-automatisée de différenciation des grains de mycétome.

Mots-clés: Diagnostic du mycétome, Histopathologie numérique, Images microscopiques, Analyse d'images, Intelligence artificielle et Radiomique.

Computational Approach for the Diagnosis of Mycetoma Causative Agents Using Histopathological Microscopic Images

Abstract:

Mycetoma is a chronic, neglected infectious disease endemic in tropical and subtropical areas that may lead to severe disability. By considering the causative agents, mycetoma is classified into eumycetoma (fungus) and actinomycetoma (bacteria). The diagnosis strategy relies on the clinical presentation and the identification of mycetoma causative agents. Accurate identification of the causative agents is a priority for mycetoma diagnosis.

The current identification tools include molecular techniques, cytology, histology and grain culturing which is the gold standard tool. Molecular techniques are the most reliable tool, but it is expensive to be used in endemic areas, while culture is time-consuming, difficult and requires expert personnel. Cytology and histology are simple, rapid, and cheap tools. However, cytology is far from being satisfactory in terms of performance because it tends to give false positive results. Although histopathology is considered to be the optimal tool to be used in endemic areas, it requires expert pathologists for conclusive identification, which are lacking in endemic rural areas.

With the advent of digital pathology, automated image analysis algorithms can be used to solve this issue. The main aim of this thesis is to develop a novel computational diagnostic method for mycetoma diagnostic using histopathological microscopic images. Firstly, we create the first database for mycetoma microscopic images. This issue arises from the need for a dataset to develop a computation model. Then, we present a novel computation method to semi-automatically discriminate the mycetoma causative agents. The method is based on the radiomics analysis of manually segmented mycetoma grains and Partial Least Square-Discrimination Analysis (PLS-DA). The presented model can play a fundamental role in the non-specialised clinical centres because it reaches an accuracy comparable to expert pathologists. Lastly, we introduce an automated segmentation method for mycetoma grains. The segmentation method is Convolution Neural Network (CNN) model based on U-net architecture. It allows the full automation of the discrimination approach. In conclusion, this thesis presents both automated diagnostic methods for mycetoma histopathological microscopic images and semi-automated differentiate methods for mycetoma grains.

Keywords: Mycetoma diagnosis, Digital Histopathology, Microscopic Images, Image Analysis, Artificial Intelligence and Radiomics.

